Calhoun: The NPS Institutional Archive

DSpace Repository

Theses and Dissertations	1. Thesis and Dissertation Collection, all items

1973-12

The Coanda effect with jet displacement over planar, concave, and convex walls

Baird, Leo James Michael

Monterey, California. Naval Postgraduate School

http://hdl.handle.net/10945/16517

This publication is a work of the U.S. Government as defined in Title 17, United States Code, Section 101. Copyright protection is not available for this work in the United States.

Downloaded from NPS Archive: Calhoun

http://www.nps.edu/library

Calhoun is the Naval Postgraduate School's public access digital repository for research materials and institutional publications created by the NPS community. Calhoun is named for Professor of Mathematics Guy K. Calhoun, NPS's first appointed -- and published -- scholarly author.

Dudley Knox Library / Naval Postgraduate School
411 Dyer Road / 1 University Circle
Monterey, California USA 93943

THE COANDA EFFECT WITH JET DISPLACEMENT OVER PLANAR, CONCAVE, AND CONVEX WALLS

Leo James Michael Baird

Library
Naval Postgraduate School
Monterey, California 93940

NAVAL POSTGRADUATE SCHOOL
Monterey, California

THESIS

THE COANDA EFFECT WITH JET DISPLACEMENT OVER PLANAR, CONCAVE, AND CONVEX WALLS

by

Leo James Michael Baird

Thesis Advisor: G.J. Hokenson

December 1973

T153777

Approved for public release; distribution unlimited.

The Coanda Effect with Jet Displacement Over Planar, Concave, and Convex Walls

by

Leo James Michael Baird
Lieutenant, United States Navy
B.S., United States Naval Academy, 1966

Submitted in partial fulfillment of the
requirements for the degree of

AERONAUTICAL ENGINEER

from the

NAVAL POSTGRADUATE SCHOOL

Library
Naval Postgraduate School
Monterey, California 93940

ABSTRACT

Bourque and Newman presented an extensive paper analyzing the separate effects of deflection angle and offset distance on the reattachment of flow issuing from a two-dimensional incompressible turbulent jet to an adjacent inclined flat plate. Levin and Manion combined the effects of offset distance and vertical wall incidence and derived a set of parametric equations to solve for the attachment distance at a given offset distance and deflection angle. Subsequently, Perry extended the control volume model to account for inaccuracies in defining a base pressure. As part of a general investigation of the Coanda effect, the work of Levin and Manion has been expanded herein to encompass concave and convex surfaces of arbitrary planform. Two methods are outlined for determining the attachment distance for these additional planforms. On the concave wall, agreement averaged within 20% of the experimental data for the range of spread parameters used, and agreement between the two methods as outlined for this surface averaged within 12%. The two methods agree within 10% on the convex wall, and agree within 15% and 12% respectively with the convex wall experimental data, in the range of values of spread parameter used. The planar wall data agree within an average of 12% of theoretical solutions.

The hysteresis of flow attachment is viewed with particular attention focused on the intermediate region in which the flow divides and one portion attaches to the wall, while the remaining portion acts as if issuing from a free jet.

TABLE OF CONTENTS

I. INTRODUCTION ---------- 11

A. PLANAR WALL ---------- 11

B. CONVEX WALL ---------- 15

C. CONCAVE WALL ---------- 21

II. TEST EQUIPMENT AND PROCEDURE ---------- 23

III. TEST RESULTS AND DISCUSSION ---------- 29

A. PLANAR WALL ---------- 29

B. CONVEX WALL ---------- 31

C. CONCAVE WALL ---------- 32

D. COMPARISONS BETWEEN PLANFORMS ---------- 33

E. SURFACE PRESSURE COEFFICIENT ---------- 34

F. DIVISION OF FLOW AND HYSTERESIS ---------- 35

G. CONTROL VOLUME MODEL ---------- 36

H. JET VELOCITY PROFILES ---------- 37

IV. CONCLUSIONS ---------- 38

V. RECOMMENDATIONS FOR FUTURE STUDY ---------- 39

APPENDIX A ---------- 40

APPENDIX B ---------- 49

APPENDIX C ---------- 52

APPENDIX D ---------- 55

APPENDIX E ---------- 58

FIGURES ---------- 60

OUTLINE OF DATA PRESENTATION I. ---------- 70

OUTLINE OF DATA PRESENTATION II. ---------- 85

OUTLINE OF DATA PRESENTATION III. ---------- 100

OUTLINE OF DATA PRESENTATION IV. ---------- 115

OUTLINE OF DATA PRESENTATION V. ---------- 144

LIST OF REFERENCES ---------- 158

INITIAL DISTRIBUTION LIST ---------- 159

FORM DD 1473 ---------- 160

LIST OF FIGURES

FIGURE		Page
1	Planar wall flow model	60
2	Concave wall flow model	60
3	Convex wall flow model	60
4	Planar wall apparatus	61
5	Concave wall apparatus	61
6	Convex wall apparatus	62
7	Concave and convex wall planform	63
8(a)	Pressure port location and vertical wall construction, schematic	64
8(b)	Pressure port location and vertical wall construction, photograph	65
9	Half-jet modification	66
10(a)	Flow constriction device, schematic	67
10(b)	Flow construction device, photograph	68
11	Pitot probe configuration	69
12-14	Theoretical and experimental attachment distance against offset distance, N_{Re} 2.05 x 10^5	71-73
15-17	Theoretical and experimental attachment distance against offset distance, N_{Re} 1.475 x 10^5	74-76
18-19	Attachment distance against offset distance	77-78
20-21	Attachment distance against deflection angle	79-80
22-23	Flow rate against offset distance	81-82
24-25	Flow rate against deflection angle	83-84

Figure		Page
26-28	Theoretical and experimental attachment distance against offset distance for a convex wall, N_{RE} 2.05 x 10^5	86-88
29-31	Theoretical and experimental attachment distance against offset distance for a convex wall, N_{RE} 1.475 x 10^5	89-91
32-33	Attachment distance against offset distance	92-93
34-35	Attachment distance against deflection angle	94-95
36-37	Flow rate against offset distance	96-97
38-39	Flow rate against deflection angle	98-99
40-42	Theoretical and experimental attachment distance against offset distance for a concave wall, N_{RE} 2.05 x 10^5	101-103
43-45	Theoretical and experimental attachment distance against offset distance for a concave wall, N_{RE} 1.475 x 10^5	104-106
46-47	Attachment distance against offset distance	107-108
48-49	Attachment distance against deflection angle	109-110
50-51	Flow rate against offset distance	111-112
52-53	Flow rate against deflection angle	113-114
54-61	Comparison of attachment distance against offset distance for planar, concave, and convex walls	116-123
62-73	Comparison of attachment distance against deflection angle for planar, concave, and convex walls	124-135
74-81	Comparison of flow rate against offset distance for planar, concave, and convex walls	136-143
82	Surface pressure coefficient for planar wall at constant incidence angle	145

Figure Page

83 Surface pressure coefficient for convex wall at constant incidence angle ---------- 146

84 Surface pressure coefficient for concave wall at constant incidence angle ---------- 147

85 Surface pressure coefficient for planar wall at constant offset distance ---------- 148

86 Surface pressure coefficient for convex wall at constant offset distance ---------- 149

87 Surface pressure coefficient for concave wall at constant offset distance ---------- 150

88 Comparison of surface pressure coefficient for planar, concave, and convex walls -------- 151

89 Half-jet velocity profile .5 in. downstream - 152

90 Half-jet velocity profile 1 jet width (1.31 in.) downstream ---------- 153

91 Half-jet velocity profile 2 jet widths (2.62 in.) downstream ---------- 154

92 Half-jet velocity profile 4 jet widths (5.24 in.) downstream ---------- 155

93 Half-jet velocity profile 6 jet widths (7.86 in.) downstream ---------- 156

94 Half-jet velocity profile 9.58 in. downstream ---------- 157

LIST OF SYMBOLS

D	distance from attachment wall to the side of the nozzle (ft)
J	jet momentum flux per unit depth (lbf/ft)
Q	volume flow (ft^3/sec)
Q_e	volume flow at the nozzle exit (ft^3/sec)
Q_T	total volume at a distance s from the nozzle exit (ft^3/sec)
R	radius of a theoretical circular arc described by the jet centerline (ft)
s	arbitrary distance along the jet centerline from the nozzle exit (ft)
s_o	distance from the hypothetical (apparent) origin of the jet to the nozzle exit (ft)
t	dimensionless parameter from Goertler's equation for jet velocity profile
u	jet stream velocity (fps)
u_o	jet stream velocity at the centerline (fps)
u_e	uniform jet stream velocity at the nozzle exit (fps)
w	nozzle width (ft)
y'	distance from the jet centerline to an arbitrary point measured on a line normal to the centerline (ft)
y	distance from the jet centerline that passes through the attachment point to the jet centerline measured on a line normal to the centerline (ft)
x	distance from the attachment point to the offset vertical wall measured along the vertical wall (ft)
α	angle between the jet centerline and the vertical wall (rad or deg)
θ	angle between the jet centerline and the vertical wall (rad or deg)

ρ	density of the fluid (lbm/ft^3)
σ	dimensionless spread parameter for a free jet
g_c	32.2 lbm-ft/sec-lbf
C_{p_s}	pressure coefficient at the vertical wall surface
x_s	distance measured along the vertical wall surface from the jet exit (ft)
L	vertical wall length (ft)
N_{Re}	Reynold's number
p_o	stagnation pressure of the fluid supplied to the jet (lbf/ft^2)
p_B	static pressure of the fluid within the recirculation bubble (lbf/ft^2)
p_∞	static pressure of the fluid medium surrounding the jet (lbf/ft^2)
p_s	static pressure at the wall surface (lbf/ft^2)
a	radius of curvature of the vertical wall (ft)
ϕ	arbitrary angle (rad or deg)

ACKNOWLEDGEMENT

The author expresses his appreciation to Assistant Professor G. J. Hokenson for his counsel and guidance during this investigation. Special appreciation is extended to Mr. Gordan Gulbranson of the Aeronautics Department wood shop and Mr. Glenn Middleton of the Aeronautics Department metal shop for the time and expertise they devoted in assisting with the construction of the apparatus used in this investigation.

I. INTRODUCTION

In 1932 with the establishment of a French patent Henri Coanda became the first to explore the effect of streamline curvature on the deflection of free jets over curved surfaces. Coanda's attention focused primarily on the applications of the effect rather than its detailed understanding. Lighthill, Metral and Zenner, and Yen proposed potential theories for two-dimensional incompressible jets flowing around various shapes with the surrounding fluid at rest [1]. Newman [1] extended these theories to predict the attachment point of the jet flow and its final separation from the surface, for a cylinder and a planar wall. The only perturbation was variation of the vertical wall deflection angle. Borque then teamed with Newman [2] to extend these studies to include offset of the vertical wall from the jet. Levin and Manion [3] furthered the work of Borque and Newman to develop a more general set of expressions for attachment distance as a function of both vertical wall offset and deflection angle. This study seeks to verify the efforts of Levin and Manion and extend it to smoothly curved, concave, and convex surfaces of arbitrary planform.

A. PLANAR WALL

For the planar wall case, Levin and Manion developed a set of expressions from which the attachment distance, for

a given vertical wall offset and angular deflection, could be obtained. This set of expressions was based on the following assumptions.

a. The jet flow is incompressible and two-dimensional.

b. Jet velocity is uniform at the nozzle exit.

c. The jet velocity is independent of the reduced pressure in the separation bubble.

d. The pressure within the separation bubble is uniform.

e. Jet momentum flux is conserved, i.e. drag losses due to channel constraining plates are neglected.

f. The centerline of the jet is a circular arc of radius R.

g. The nozzle width is small compared with R and the attachment wall length is long compared with the jet width.

h. The jet exhibits turbulent flow after emerging from the nozzle, i.e., the Reynolds number is high.

i. Changes in the jet structure due to centrifugal force of curvature are negligible.

j. σ is a floating constant, which accounts for variation of entrainment due to jet curvature. [Figure (1) illustrates this model.]

Assumptions (g) and (h) stem from previous work by Newman [1] and Newman and Borque [2]. In performing a dimensional analysis of the two types of flow, inclined vertical wall without offset and offset vertical wall without deflection, Newman determined that for the former

case the nondimensional surface pressure at any distance x from the sharp corner was

$$C_{p_s} \equiv \frac{p_s - p_\infty}{p_o - p_\infty}$$

and that

$$C_{p_s} = f(\alpha, X/W, L/W, N_{Re})$$

and

$$X/W = f(\alpha, L/W, N_{Re})$$

where w is the jet width, α is the vertical wall deflection angle, L is the vertical wall length, and N_{Re} is the Reynold's number.

Similarly, for the latter problem

$$C_{p_s} = f\{D/W, L/W, X/W, N_{Re}\}$$

$$\frac{X}{W} = f\{D/W, L/W, N_{Re}\}$$

where D is the vertical wall offset distance.

If assumptions (g) and (h) are applied, these functional dependencies reduce to

$$C_{p_s} = f\{\alpha, X/W\}$$

$$X/W = f\{\alpha\}$$

for the inclined wall without offset, and

$$C_{p_s} = f\{D/W, X/W\}$$

$$X/W = f\{D/W\}$$

for the offset wall without deflection.

To develop expressions involving the solution of a vertical wall with both offset and deflection angle Levin and Manion defined a dimensionless parameter t such that

$$t \equiv \tanh\left(\frac{\sigma y}{s + s_o}\right) \qquad (1)$$

where σ is the dimensionless spread parameter for a free turbulent jet streamline that passes through the attachment point to the jet centerline, measured on a line normal to the centerline, s is the distance downstream along the jet centerline from the nozzle exit, and s_o is the distance from the hypothetical (apparent) origin of the jet to the nozzle exit. From this definition they derived an expression for the attaching streamline length to the jet width, w, (Appendix A).

$$\frac{3s}{\sigma W} = \frac{1}{t^2} - 1 \qquad (2)$$

From a force analysis about the attachment point, an expression for the angle at which the attaching streamline intercepts the wall is obtained (Appendix A):

$$\cos\theta = \frac{3}{2}t - \frac{t^3}{3} \qquad \text{(attachment point model)} \qquad (3)$$

$$\cos\theta = \frac{1}{2} + \frac{3}{4}t - \frac{t^3}{4} \qquad \text{(control volume model)} \qquad (4)$$

Further analysis of the geometry of flow attachment (Appendix A) leads to the desired expressions for D/W, X/W:

$$D/W = \left\{\frac{\sigma}{3(\theta+\alpha)}\left(\frac{1}{t^2} - 1\right)\left(1 - \frac{\cos\theta}{\cos\alpha}\right) - \frac{1}{2}\right\} \qquad (5)$$

$$X/W = \left\{\frac{\sigma}{3(\theta+\alpha)}\left(\frac{1}{t^2} - 1\right)(\sin\alpha+\sin\theta) - \frac{\tanh^{-1} t}{3t^2\sin\theta} - \left(\frac{D}{W} + \frac{1}{2}\right)\sin\alpha\right\} \qquad (6)$$

Values for t are found for a range of θ between zero and ninety degrees. When no deflection of the wall occurs ($\alpha = 0$) or no offset is used ($D/W = 0$), the equations reduce to those of Borque [2].

B. THE CONVEX WALL

Newman [1] performed a dimensional analysis for a circular cylinder, similar to that for the planar wall.

From it he deduced that the non-dimensional surface pressure coefficient is given by

$$C_{p_s} = f\{\theta, \frac{W}{a(x)}, N_{Re}\}$$

where a is the radius of the circular cylinder and is the angle between the jet exit and the point of interest on the cylinder's surface, with vertex at the center of the cylinder. At some distance from the jet exit the flow no longer depends on the supply pressure and jet width separately, but on their product.

Therefore

$$C_{p_s} \frac{a(x)}{W} = f\{\theta, N_{Re}\}$$

if a suitable zero is chosen for θ; then for large enough N_{Re}

$$C_{p_s} \frac{a(x)}{W} = f\{\theta\}$$

Applying the similar arguments to the separation angle

$$\theta_{sep} = f\{N_{Re}\}$$

Adapting this to a convex vertical wall with a changing radius of curvature and deflection angle, α, but without vertical wall offset,

$$C_{p_s} \frac{a(x)}{W} = f\{\theta\}$$

where a(x) can be an average radius of curvature over finite segments in the case of an arbitrary planform or a function for a particular planform. Performing a dimensional analysis on the flow

$$\frac{X}{W} = f\{\alpha, \frac{W}{a(x)}, \frac{L}{W}, N_{Re}\}$$

at some distance from the jet exit the flow no longer depends on the attachment distance and jet width separately but on their product.

$$\frac{X}{W} \frac{a(x)}{W} = f\{\alpha, \frac{L}{W}, N_{Re}\}$$

if L is sufficiently large and N_{Re} sufficiently high, then as in the planar wall case,

$$\frac{X}{W} \frac{a(x)}{W} = f\{\alpha\}$$

In the case of an offset vertical wall, without deflection

$$\frac{X}{W} = f\{D/W, L/W, \frac{W}{a(x)}, N_{Re}\}$$

and applying similar arguments as in the previous case,

$$\frac{X}{W}\,\frac{a(x)}{W} = f\{D/W\}$$

Previous investigations reveal that for a convex surface, skin friction is reduced and the displacement thickness is increased as compared with first order solutions [6]. This implies that a surface with convex curvature encourages separation. This would also suggest that a convex surface tested under the same conditions of offset and deflection angle as a planar surface would cause flow separation at a lower deflection angle. Additionally, for a given deflection angle and offset, the convex wall will exhibit a longer reattachment distance, due to curvature. The magnitude of this additional distance may be approximated by the following method with the following assumptions, which are in addition to those specified in the planar wall section:

a. The radius of curvature of the wall is large compared with the radius of curvature of the reattaching streamline.

b. The radius of curvature of the convex wall is constant over the range of possible reattachment distances.

For the coordinate system given in the illustration below, the equation of the planar wall is represented by

$$Y = \text{constant} \qquad (7)$$

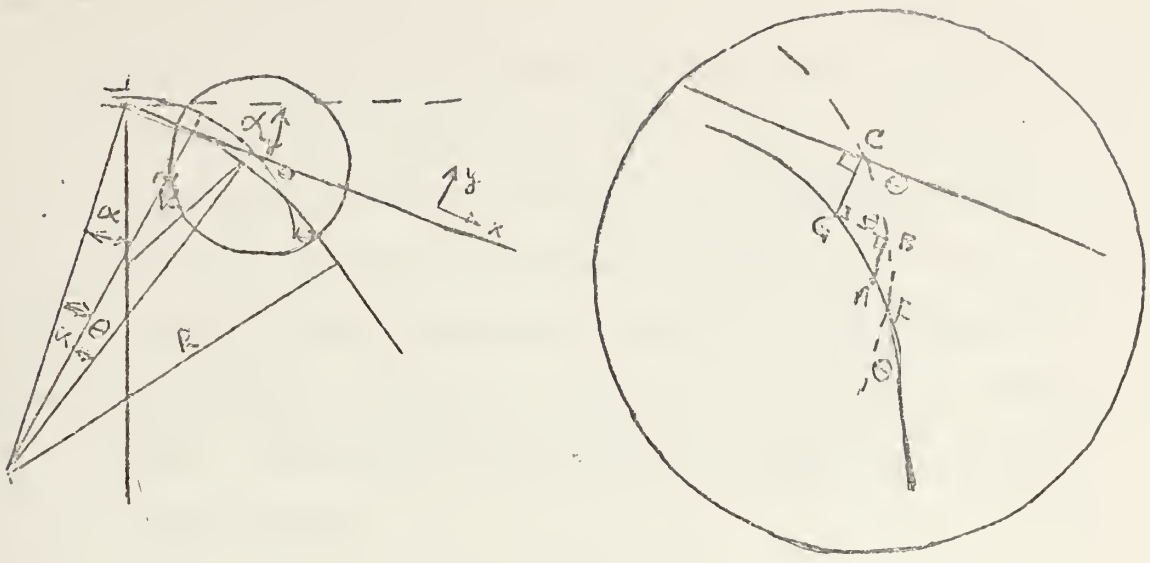

For the region of constant radius of curvature the equation of the convex wall is

$$X^2 + Y^2 = R^2 \tag{8}$$

Solving for Y in the convex wall equation

$$Y = (R^2 - X^2)^{1/2}$$

the approximate magnitude of the divergence of the convex wall is found by solving the equations of Levin and Manion for a planar wall at a given offset and angular deflection. The value of X/W obtained is then used to solve Equation (9) in nondimensional form. This value when subtracted from Equation (7) gives the desired divergence. From this point two methods are available to obtain the new reattachment

distance:

a. The point of reattachment on the convex wall is the same as that experienced by a planar wall at an increased deflection angle and attachment angle. This new deflection angle is equal to the sum of α, the actual deflection angle, and the apparent additional deflection angle due to the wall curvature. This additional angle is found using the relationship

$$s = r\,\phi \tag{10}$$

where s is equal to the magnitude of the wall divergence and r is the value of X/W for the planar wall at the actual deflection angle. The new attachment angle is found by using the new value of deflection angle and resolving the equations of Levin and Manion with an iterative scheme at the constant value of offset distance. Once the attachment angle is found, the attachment distance equation may be solved.

b. The expanded illustration of the reattachment point shows the geometric relationships between the two walls. The arc length GAF is approximately a straight line as is arc GBF, being small compared to the radius of curvature of the convex wall. Using the relationships of the geometry of attachment, the angle with vertex at C is $90 - \theta$. The angle formed by GBC is

θ. Therefore

$$GB = \frac{CG}{\tan \theta}$$

from similar triangle relationships

$$\sin \theta = \frac{GB}{GA}$$

and

$$GA = \frac{GB}{\sin \theta} = \frac{CG}{\sin \theta \tan \theta}$$

$$GF \approx GA = \frac{CG}{\sin \theta \tan \theta}$$

CG is obtained as in the first method. The sum of X/W at the actual deflection angle and GF yields the new X/W value.

C. CONCAVE WALL

The concave wall permits a similar approach as for the convex wall, except that for this type of surface the skin friction is increased and the displacement thickness is decreased as compared with first order solutions. This implies that the concave wall would tend to delay separation as compared with a planar wall tested at similar offset distances and deflection angles. Applying similar arguments as for the convex wall and from the illustration below the

concave wall will behave as a planar wall at a lesser angle of incidence. The same assumptions and methods for the convex wall are applicable to the concave surface.

a. The value of X/W divergence, and angular difference are obtained as in the previous sections. The new deflection angle is the difference between the actual deflection angle, α, and the additional apparent deflection angle. This new value of α is then used to resolve the equations of Levin and Manion for X/W as was done for the convex wall.

b. GF for the concave wall is found as was done for the convex wall. The new value of X/W is equal to the difference between X/W at the angle α and GF.

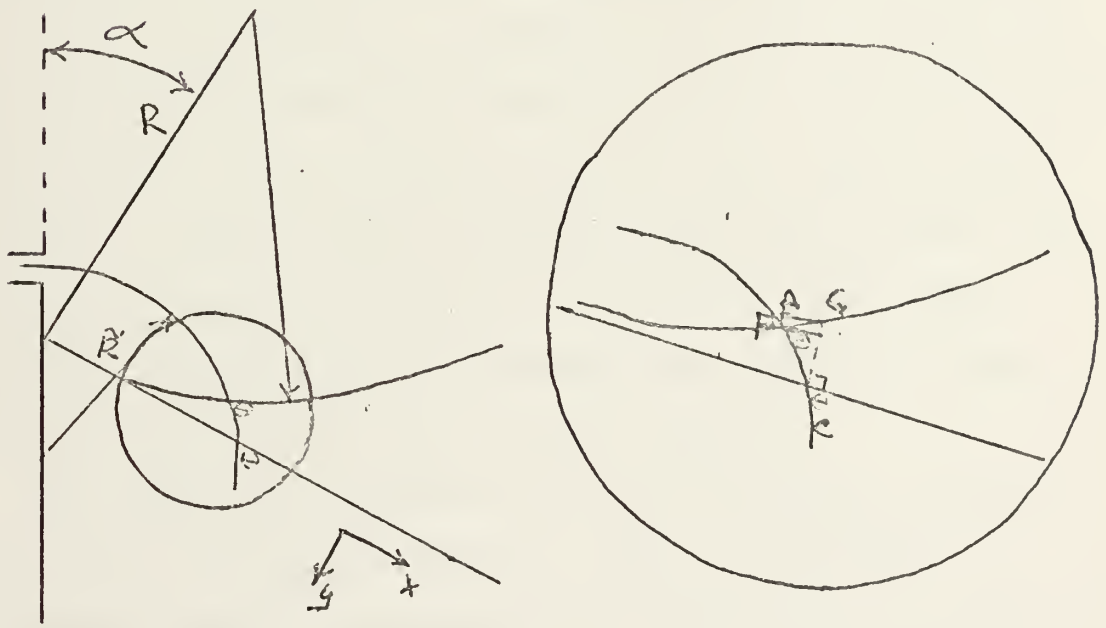

II. TEST EQUIPMENT AND PROCEDURE

The apparatus shown in Figures (4), (5), (6) was designed to produce a two-dimensional, subsonic free air jet of velocity up to 151 feet per second, flowing over a vertical wall. The vertical wall attached to the jet exit was a rectangular section of 0.10 inch thick plexiglass, 69 inches in length, and reinforced with vertical ribs at 15-inch intervals. The wall was flexible axially in order to form a planar, concave, or convex surface.

The vertical wall was attached to the jet exit with a hinge, mounted flush with the jet exit. A 4.75 inch wide by 11-inch high plate extended normal and to the side of the jet exit to provide attachment of the vertical wall at offset distances up to 2.5 inches from the edge of the jet exit, in 0.5 inch increments. To contain the flow laterally as it left the jet when deflecting the various walls, two 3.125 inch wide by 5.75 inch long stainless steel plates were attached to the jet exit, extending into the channels. The plates were strong enough that no observed fluttering occurred to disturb the flow downstream, and thin enough that the flow from the jet was not degraded.

The lateral wall channels for the planar set up were made from 0.25 inch plexiglass. They were attached by lengthwise supports from behind the vertical wall to impose rigidity. The convex and concave channel walls were made

from 0.35 inch plywood with a planform depicted in Figure (7). The channels walls were supported by segmented blocks, contoured to a specific region of the vertical wall. The end of the vertical wall was attached to a castered stand which facilitated angular deflections of the wall.

Static pressure parts were located along the vertical wall as indicated in Figures 8(a) and 8(b). The pressure taps were 1 mm diameter metal tubing, inserted into 3/8 inch diameter pieces of plexiglass and glued into position. The holes in the wall were drilled through the tubing and plexiglass mounts after a 24 hour drying period. Making the holes in this manner allowed for pressure measurement without a large protuberance into the flow.

To record the wall static pressure, the static pressure ports were connected with 1/16-inch Tygon pressure tubing to a forty-eight tube, inclined water manometer bank. Pressure readings within 0.01 inches were possible from the manometer bank.

The jet exit itself was a square 2.62 inches on a side. This was later adapted to a half-jet width by the insertion of a piece of tapered pine wood as shown in Figure (9). The jet was powered by a Wagner Electric, 3 phase, 60 cycle motor attached to an impellar-type blower with a 5000 cubic foot per minute capacity. A flow constriction device, see Figures 10(a) and 10(b) was constructed and attached to the side of the blower unit to permit variation of mass flow rate (Reynold's Number). No reduction of the flow was

observed between the unmodified blower and the modified blower with the constriction device fully opened.

A flow shaper was attached to the blower exit. The shaper was connected to a chamber assembly in which two fine-mesh wire screens were placed on either side of a 6.0 inch by 6.0 inch piece of 1/8 inch honey-combed aluminum. These functioned as flow straighteners. The jet was reduced to its exit dimensions through a tapered design, affixed to the chamber section, see Figure (5). The chamber/jet assembly was mounted on castered steel supports. This allowed freedom to break open a portion of the chamber/jet and make any desired modifications without disassembling the entire apparatus.

To identify regions of separation and reattachment, two-dimensional tufts were made of paper 3/16 inches wide by 6/16 inches long. These were folded back and forth at the half-length to form a flexible hinge. They were placed 1/2 inch above and below the centerline of the channel, i.e. the extended centerline of the jet. The point of reattachment was identified as the point on both sides of which the tufts flapped in opposite directions.

To measure angular displacement, a ninety degree section of 3/16 inch, hard pressed fiberboard, eight inches wide with an outside radius of curvature of 42 inches was utilized. Marks were inscribed at one degree intervals with five degree groupings. A pointer made of 0.25 inch dowling was attached to the wall and the tip colored, affording accurate

angular readings within 0.3 to 0.5 degrees. Movement of the board was precluded by taping it to the floor with mylar tape.

Flow rate and Reynold's number were indicated by a pitot tube connected to a water-filled, u-tube manometer. The pitot probe was mounted as shown in Figure (11). Readings were accomplished by sliding the probe across the flow from the stationary tripod stand. Lateral position of the probe in the channel was determined using a ruler mounted so as to move simultaneously with the probe. Probe position could be extablished within 0.03 to 0.05 inches.

Prior to commencing a run or sequence of runs the equipment was positioned, the manometer bank checked for level readings, a static zero reading taken and tubing was checked for integrity. Position of the angular deflection board was checked and a Reynold's Number check was performed. Free jet flow rates were taken. From the Reynold's number data taken, three were selected and utilized throughout the experimental phase. For the half-jet study only the lowest Reynold's number was used.

After recording the free jet flow rate readings at each Reynold's number, the wall was returned to zero degrees deflection and the flow rate taken 49.3 inches downstream for each wall. The point selected was well downstream of any reattachment points and such that the static pressure was very near ambient pressure. This provided a basis for study of flow rate reduction in the angular deflection for

a given offset, as well as flow rate reduction with offset for a given deflection angle. At zero offset the gap between the wall and the jet edge affected the static pressure and attachment point. For this setting, masking tape was placed over the aperture at the initial separation angle. The tape was smoothed to preclude flow disturbance, and checked for smoothness at each angle change. Tape was not deemed necessary at offsets due to the assumption of uniform pressure within the recirculation region. The particular deflection angles used were not chosen but obtained deflecting the vertical wall until a noticeable change (2-4 inches) in attachment point occurred. The pitot probe, with the static line disconnected, was repositioned to the same relative position in the flow as it had been at zero deflection to measure the maximum flow rate. Static pressure readings were recorded when the shape of the surface pressure profile changed. Reattachment point and flow measurements were recorded and the process repeated until the flow would fully separate from the wall. At this time a hysteresis study was performed to determine the minimum angle at which the flow would reattach and the maximum angle for which the flow would remain attached. Two runs were made for each offset if the reattachment point and flow rate data at the same deflection angles agreed within 0.25 inches. If they did not, an additional run was made. The deflection angle board was repositioned for each offset.

Upon completion of runs for the full jet a half-jet study of attachment distance and flow rate reduction was conducted at the lowest Reynold's number, following the same procedure for each wall type.

III. TEST RESULTS AND DISCUSSION

A. PLANAR WALL

The equations of Levin and Manion were solved on the IBM 360, using a FORTRAN program (Appendix B). The values of attachment distance against offset distance at constant incidence angles were plotted using a program similar to that appearing in Appendix C. Figures 12, 13, 14 depict the results. The spread parameter, σ, increases with offset distance and deflection angle for the range of offset (D/W) values 0.0 to 0.94, using the attachment point model (Equation 11, Appendix A) for values of σ from 7.7 to 15. The results are within 12% of the theoretical values, for the range of spread parameter used.

Variation of X/W with offset distance for constant angles of incidence is presented in Figure 18. For a given value of D/W, X/W increases with incidence angle (see Figure 20), due to the increase in size of the recirculation bubble. At a limiting angle, the flow splits and the bubble size decreases, decreasing X/W. As D/W is increased, the plot of X/W against α becomes more linear (Figure 20). This may be explained in part by the increase in ability of the recirculation zone to become fully established sooner with increased D/W. At zero D/W a much higher incidence angle is necessary to cause flow separation and reattachment because the recirculation zone is not established sufficiently. As

the wall is offset the zone becomes established and becomes more nearly uniform in pressure within the bubble.

Figure 24 shows the decrease in flow rate ($\dot{m}/\dot{m}_o$) with offset due to incidence angle. Each offset exhibits a similar curve which pivots downward from right to left. As the recirculation bubble increases, the rate of flow returning to the wall decreases, being slowed by the quiescent local medium. The reduction of flow rate with D/W at constant α is shown in Figure 22. These values fluctuate about a mean value for each angle. except at the higher angles and offset combinations, such as D greater than 2.0 inches and α greater than 30 degrees where flow split has occurred.

Theoretical values were also obtained and plotted for the half-jet. The data were treated in the same manner to exhibit similarities and differences, and are shown in Figures 15, 16, 17. Increased values of σ (15 and greater) were found to dominate.

Variations such as examined for the full jet case were repeated and are shown in Figures 19, 21, 23 and 25. These variations display results very similar to those of the full jet, but exhibit more stability. This may be due in part to the apparent increase in wall length, since L/W, as shown in the dimensional analysis, can affect the reattachment point for small enough L/W.

B. CONVEX WALL

Theoretical calculations for the convex wall were made using the IBM 360. The FORTRAN program utilized appears in Appendix B. The values of the planar wall solution were computed as before. Then, for the convex wall shape, Method one was first used to compute X/W by solving for the divergence and the new value of α, and then iterating on t, the dimensionless parameter, to find the new value of X/W at the same value of D/W as for the planar wall. X/W from Method two was computed and both methods plotted for various values of σ with the experimental data, (Figures 26, 27, and 28). As the deflection angle and offset distance were increased the value of σ increased as with the planar wall. The two methods agree within 12% of one another and within 15% of the experimental data, for previously specified values of σ.

Plots similar to those for the planar wall were made for the convex wall, Figures 32 to 39. This planform continues to exhibit a hyperbolic plot of X/W against α for the range of D/W used, as opposed to the tendency toward linearity on the planar wall with increasing offset. This is due primarily to the curvature of the wall away from the flow, which forces the flow itself to curve. This increased curvature increases the value of θ, the attachment angle, promoting a lower magnitude of α at separation than for a planar wall at the same offset.

Data for the half-jet agree within 3% of full-jet results. Figures 29, 30, and 31 are theoretical and experimental data for the half-jet. Agreement within 12% is evidenced for the values of σ in the range 7.7 to 15.

C. CONCAVE WALL

The methods used for the convex wall were also applied to the concave wall. Though the two methods used show good agreement between themselves, within 12%, they achieve only fair results, within 20%, at the previously established values of σ, Figures 40 to 45. This may be due to enhancement of the flow through an anti-curvature effect. Instead of increasing and aiding the curvature of the flow as for the convex wall, or having little effect on the flow curvature as for a long, planar wall, the concave wall tends to straighten the flow, as it approaches the wall surface, thereby decreasing θ and yielding higher values of α for which the flow will separate than does a planar wall at the same D/W and α.

Figures 46 to 53 are similar plots as for the planar and convex walls, for both full- and half-jet configurations. For both of these cases the plots of flow rate vs. deflection angle (Figures 52 and 53) reveal a compactness not seen in the previous two cases of planar and convex walls. Over the range of offset distances, the spread in flow rate is reduced. The separation bubble is allowed to form in this case, and due to the wall curvature toward the jet, the

bubble is aided in forming, but this anti-flow curvature also tends to preserve the flow rate as neither of the previous walls did.

D. PLANAR, CONCAVE, AND CONVEX COMPARISONS

Figures 54 through 81 display various comparison plots of the behavior of planar, concave and convex walls for full- and half-jet configurations. They are divided into several subsections as presented below:

(a) Figures 54 through 61 depict attachment distance against offset distance for full- and half-jet setups, at constant α. For both cases, at α of 0 degrees, the walls are very close in behavior but portray independent behavior at higher angles which is preserved as the angle is changed.

(b) Figures 62 through 73 show the change in reattachment distance with deflection angle for the same value of offset (D/W). The order of presentation is the full-jet then half-jet plot, in alternating order. Though the value of D/W is different, except at 0.0, for each jet width, the value of D is the same. Thus as in Figures 63 and 69 the offset distance D of 0.5 inches corresponds to a value of D/W of 0.18 for the full jet, and 0.36 for the half-jet and so on. The peaking-out of these plots is due to flow split.

(c) Figures 74 through 81 are plots of flow rate ($\dot{m}/\dot{m}_o$) against offset distance for constant deflection angles. Again both full- and half-jet data are grouped to show similar and dissimilar tendencies. In previous presentations of flow rate ($\dot{m}/\dot{m}_o$), $\dot{m}_o$ represented the flow rate at zero degrees deflection, measured at a given distance downstream as specified in the discussion of experimental procedure. In this case $\dot{m}_o$ refers to the flow issuing from the free jet at a Reynold's Number of 2.05×10^5.

E. SURFACE PRESSURE COEFFICIENT

Figures 82 through 88 present surface pressure coefficient data as follows:

(a) Figures 82, 83, and 84 give surface pressure coefficient variation against wall position downstream, x_s/W, for planar, convex, and concave walls respectively, at constant values of deflection angle and varied values of offset distance. Similarities are discernible, such as the high-peaked curve prior to separation at low values of α and no offset ($D/W = 0$), and the long flat region of the recirculation bubble after separation. The step in these plots near the jet exit indicates the slight effect of the crevice where the wall/jet interface occurs.

(b) Figures 85, 86, and 87 are similar to those in (a) above except that D/W is held constant and α is

varied. The plots are again similar for the different wall shapes and similar to the plots in (a).

(c) Figure 88 presents a comparison of the planar, concave, and convex planforms. The tendency at higher angles of deflection is to exhibit this similar pattern of curves, especially after the flow divides.

F. DIVISION OF FLOW AND HYSTERESIS

Figures 85, 86, and 87 demonstrate the reduction of pressure within the separation bubble as the size of the bubble increases. For a given offset distance (D/W) a value of α exists for which flow division and hysteresis occur. Newman [1] presents a plot of wall length to slot width against α and describes three regions; one in which the jet flow is attached, one in which the jet flow is both attached and separated, and a region of total separation. This is experimentally verified and does depend on the way the flow is initiated. If the flow is initially detached the attaching portion of the flow will reattach at a lower value of α than that at which the flow will separate if originally attached. The amount of decreased ranged from 1.5 degrees at Reynold's Number of 1.475×10^5 to 0.5 degrees at Reynolds Number 2.05×10^5.

The limiting value of α and X/W are displayed in the peaking of the plots of X/W against α as previously mentioned. Bourque and Newman [2] find this limiting point at which

flow division occurs to exist at about 0.7L. For the model in this investigation this value ranged from 0.36L to 0.47L for the different planforms and a full jet width of 2.62 inches. For the half-jet the width of the range increased, as would be expected from 0.17L to 0.39 L, while the actual magnitudes decreased. This is due to the increase in apparent wall length. The ranges given are valid over the values of D/W and α investigated for each wall type. The reduction in the limiting value for flow division is due to increased values of Reynold's Number (approximately two orders of magnitude) and the resulting increase in turbulence. Additionally, the lower value of the ranges results from the convex wall and the higher value stems from the concave wall.

The decrease in positive surface pressure coefficient in the recirculation bubble beyond the critical value of X/L produces a reduction in X/W. This reduction shows the predominance of pressure reduction over downstream flow rate.

G. CONTROL VOLUME MODEL

All previous theoretical data discussed have been computed using the attachment model. Substitution of Equation (14) vice Equation (11) from Appendix A into the equations of Levin and Manion yield solutions for the control volume model. Despite the espousal of the control volume model by Levin and Manion, no advantage was gained through using this model for the planar wall and concave wall cases. The

convex wall solutions were greatly degraded. A probable cause for this is the low range of offset distances used in this investigation. The effect of the recirculation bubble exists but, as evidenced by the experimental results, its affect at small offset distance is reduced such that for the planar and concave walls either model will suffice, and for the convex wall the attachment model is valid. Because of this the control volume model results are not displayed and it's use is mentioned to provide completeness.

H. JET VELOCITY PROFILES

Velocity profiles were taken for the half-jet configuration using the pitot probe in Figure 11. Plots of the results are presented in Figures 89 to 94. These plots were made using the FORTRAN program in Appendix E. As the distance downstream of the jet exit is increased, the velocity profile transforms from nearly rectangular (Figure 89) to the shape described by the equation

$$u/v = \text{sech}^2 \eta,$$

where $\eta = Y/EX$, as presented by Sawyer [7], Figures 93, 94. E is the entrainment factor defined by the non-dimensionalized equation

$$E \equiv \frac{1}{U}\frac{d}{dx}\int_{-\infty}^{+\infty} u \, dY = \frac{1}{\sigma}$$

and X is $s + s_o$ as defined in Appendix A.

IV. CONCLUSIONS

The experimental results support the methods proposed for the treatment of the concave and convex wall shapes. The high degree of agreement between the two methods for these planforms suggests adoption of the second method as a first approximation. The obvious factor affecting the theoretical results is the value of σ used. Again, experimental results confirm the assumption thatσ is a floating constant. Though Levin and Manion espouse the control volume model because it accounts for the effect of bubble pressure, the attachment point model has been found to agree well with published values of σ and no advantage was gained in using the control volume model for the range of offset distances used. The modification to half-jet width yields close agreement with the unmodified or full-jet results as was expected.

The region of both attached and detached flow invites further investigation. Each wall, within this region of flow, exhibited the same surface pressure profile. The only change in the profile was its reduction in size. No variation in general shape occurs, implying an apparent uniform reduction in the bubble pressure and downstream flow rate.

V. RECOMMENDATIONS FOR FURTHER STUDY

The actual effect of the recirculation bubble during initiation, growth, and apparent shrinkage in the region of divided flow invites further investigation using a hot wire. From such a study contour plots of the bubble pressure could be used to examine the accuracy of assuming a uniform pressure in this region, and to discern when this assumption is valid and when it is not valid. For those areas where it is not valid an estimate of its effect on the flow characteristics might be obtained.

Determination of the reattachment point could also be assisted by using a pitot probe inclined in the direction of flow and used to determine the null position of total dynamic pressure along the surface of the vertical wall. A check against the visual attachment distance provided by the tufts would thus be achieved.

Modifications to the theory of Bourque [4], Bourque and Newman [2] and Levin and Manion [3] were made by Perry [4] and [5]. These references were discovered late in the investigation and are worthy of future investigation.

APPENDIX A

DERIVATION OF LEVIN AND MANION EQUATIONS

The jet stream velocity, u, as a function of the distance s the jet has traveled, the distance y from the jet centerline, and the jet centerline velocity u_o are given by Goertler

$$u = u_o \operatorname{sech}^2\left(\frac{\sigma y'}{s + s_o}\right) \qquad (1)$$

$$u_o = \left[\frac{3 J \sigma g_c}{4 \rho (s + s_o)}\right]^{1/2}$$

where J is the jet momentum flux.

The attaching streamline defines a line of constant volume flow. It lies at a distance W/2 from the jet centerline at the nozzle exit, and a distance y from the centerline at a distance s downstream of the nozzle. The fluid is two dimensional and incompressible by assumption; therefore one-half of the jet volume flow is

$$Q/2 = \int_0^y u \, dy$$

To solve for s_o, one half of the volume flow $Q_2/2$ at the nozzle exit is set equal to one half the volume flow Q/2 at $s > 0$, using Goertler's expression, i.e.

$$Q_e/2 = Q/2 \quad \text{or} \quad u_e \frac{W}{2} = \int_0^y u \, dy \tag{2}$$

where w is the nozzle width and u_e is the velocity at the nozzle exit. Substituting (1) into (2), integrating, noting that tanh (0) = 0, and simplifying

$$u_e \frac{W}{2} = \left[\frac{3}{4} \frac{J(s + s_o)g_c}{\rho \sigma}\right]^{\frac{1}{2}} \tanh\left(\frac{\sigma y}{s + s_o}\right) \tag{3}$$

the expression for half the volume flow at the nozzle exit. The jet momentum flux at the nozzle exit is $J = \frac{\rho U_e^2 W}{g_c}$, and the normalized volume flow for half the stream becomes

$$\left[\frac{3(s + s_o)}{W \sigma}\right]^{\frac{1}{2}} \tanh\left(\frac{\sigma y}{s + s_o}\right) = 1$$

t is then defined as

$$t \equiv \tanh\left(\frac{\sigma y}{s + s_o}\right) \tag{4}$$

$$t^2 = \tanh^2\left(\frac{\sigma y}{s + s_o}\right) = \frac{W \sigma}{3(s + s_o)} \tag{5}$$

which is the equation of the streamline.

Integrating (2), after substitution, between 0 and infinity at the nozzle exit where s = 0 and

$J = \frac{\rho u_e^2 W}{g_c}$, then

$$\left[\frac{3}{4} \frac{\rho u_e^2 u s_o g_c}{4 \rho \sigma}\right]^{\frac{1}{2}} = u_e \frac{W}{2}$$

and

$$s_o = \frac{\sigma W}{3} \tag{6}$$

Substituting (6) into (5) yields

$$\frac{3 s}{\sigma W} = \frac{1}{t^2} - 1 \tag{7}$$

To obtain an expression for the attachment angle θ in terms of t the following procedure is utilized:

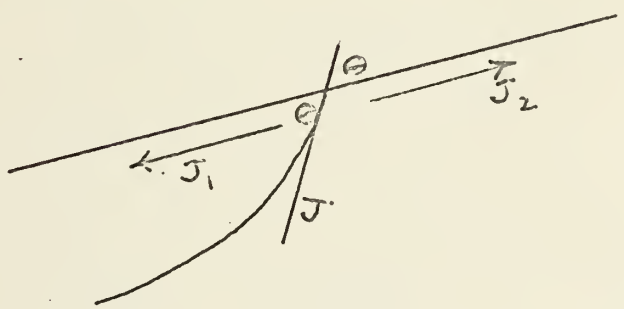

from the above illustration

$$J_1 - J_2 = J \cos \theta \tag{8}$$

the J's can be written as integrals of the form

$$\int \rho\, u^2\, dy$$

Using the Goertler Equation (1), integrating and substituting the value of t from (4)

$$J_2 = \int_y^\infty \rho\, u^2\, dy = \frac{J}{4}(3t - t^3)\Big|_y^\infty$$

since tanh (0) = 0, and tanh (∞) = 1,

$$\begin{aligned} J_2 &= \frac{J}{4}(3 - 1) - \frac{J}{4}(3t - t^3) \\ &= \frac{J}{2} - \frac{J}{4}(3t - t^3) \end{aligned} \tag{9}$$

For J_1

$$J_1 = \int_{-\infty}^y \rho\, u^2\, dy = \int_{-\infty}^0 \rho\, u^2\, dy + \int_0^y \rho\, u^2\, dy$$

but

$$J = \int_{-\infty}^\infty \rho u^2\, dy$$

Therefore

$$\frac{J}{2} = \int_{-\infty}^0 \rho\, u^2\, dy$$

and

$$J_1 = \frac{J}{2} + \int_0^y \rho u^2 \, dy$$

Proceeding as with J_2

$$J_1 = \frac{J}{2} + \frac{J}{4}(3t - t^3) \tag{10}$$

Substituting (9) and (10) into Equation (8) and solving for cos θ for the attachment point model

$$\cos \theta = \frac{3}{2}t - \frac{t^3}{2} \tag{11}$$

The control volume model also yields an expression for the attachment angle as illustrated below.

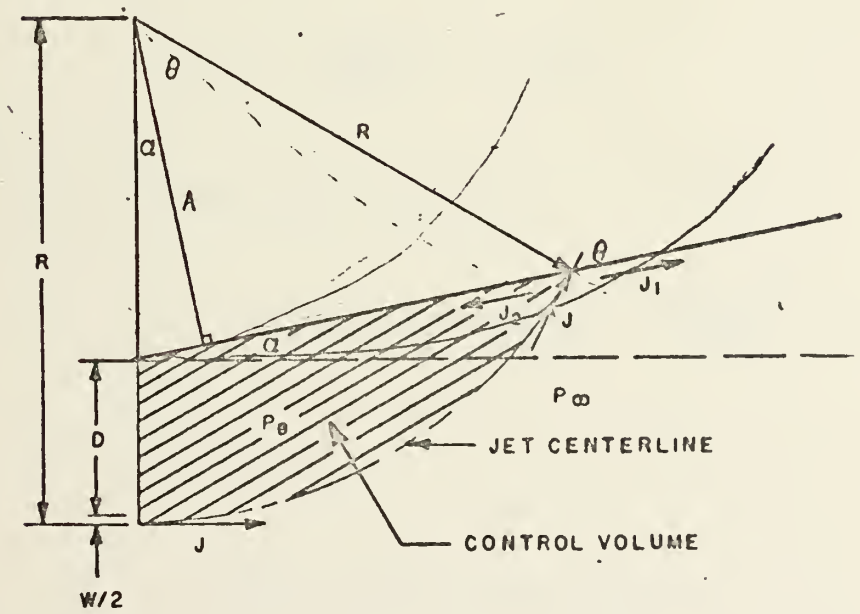

The force equation states that the momentum flux returned to the low pressure region p_B balances the pressure difference times the area normal to the wall. This can be stated

$$J \cos \alpha - J_1 = (p_\infty - p_b)(D + \frac{W}{2}) \cos \alpha \quad (11)$$

where

$$\cos \alpha = \frac{A}{R - D - \frac{W}{2}} \quad \text{and} \quad \cos \theta = \frac{A}{R}$$

therefore

$$R - \frac{A}{\cos \alpha} = D + \frac{W}{2}$$

substituting for $\cos \theta$

$$R(1 - \frac{\cos \theta}{\cos \alpha}) = D + \frac{W}{2}$$

Δp is approximately $\frac{J}{R}$, therefore

$$J \cos \alpha - J_1 = (\frac{J}{R})R(1 - \frac{\cos \theta}{\cos \alpha}) \cos \alpha$$

or

$$\cos \alpha - \frac{J_1}{J} = \cos \alpha - \cos \theta$$

therefore

$$\frac{J_1}{J} = \cos \theta \tag{13}$$

substituting $\frac{J_1}{J}$ in (10)

$$\cos \theta = \frac{1}{2} + \frac{3}{4}t - \frac{t^3}{4} \tag{14}$$

If s is the distance from the nozzle exit to the attachment point (illustration)

$$s = R(\theta + \alpha) \tag{15}$$

combining (7) and (15)

$$\frac{1}{t^2} - 1 = \frac{3R(\theta + \alpha)}{\sigma W}$$

hence

$$R/W = \frac{\sigma}{3(\theta + \alpha)} \left(\frac{1}{t^2} - 1\right) \tag{16}$$

also

$$A = \left(R - D - \frac{W}{2}\right) \cos \alpha = R \cos \theta$$

solving for $\frac{D}{W}$ and substituting for $\frac{R}{W}$ from (16)

$$\frac{D}{W} = \frac{\sigma}{3(\theta + \alpha)}\left(\frac{1}{t^2} - 1\right)\left(1 - \frac{\cos\theta}{\cos\alpha}\right) - \frac{1}{2} \qquad (17)$$

using the following illustration X/W may be found

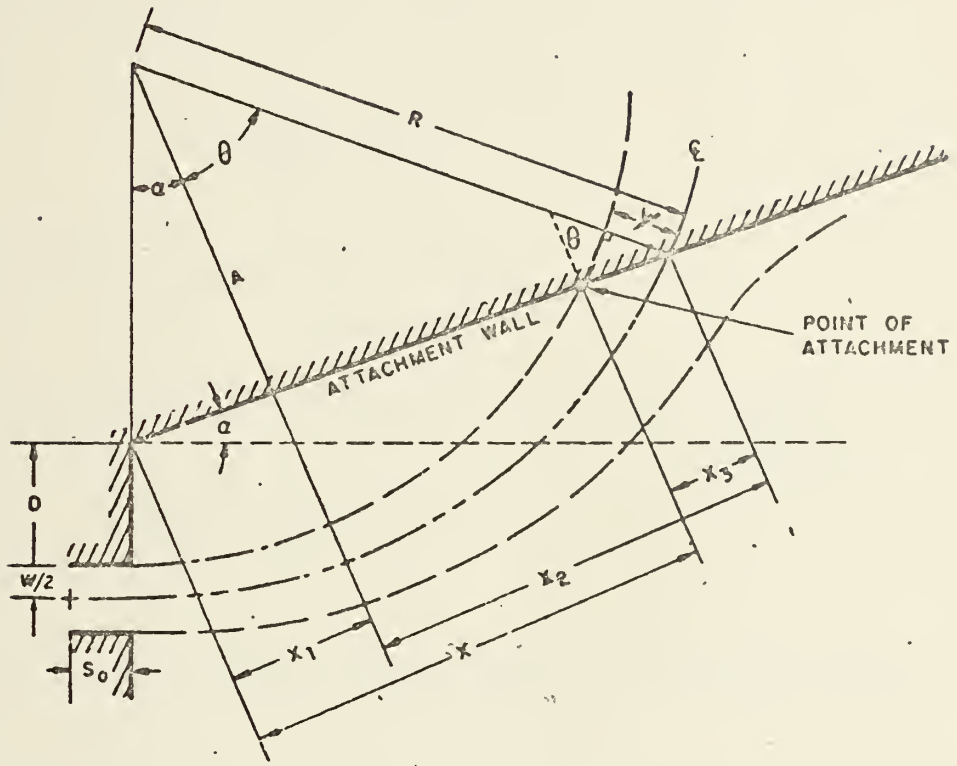

$$X_1 = (R - D - \frac{W}{2}) \sin \alpha$$

$$X_2 = R \sin \theta$$

$$X_3 = Y/\sin \theta$$

$$X = X_1 + X_2 - X_3$$

combining these

$$\frac{X'}{W} = \frac{(R - D - \frac{W}{2})\sin \alpha}{W} + \frac{R}{W} \sin \theta - \frac{y}{W \sin\theta} \quad (18)$$

substituting (6) into (4) and solving for y

$$y = \frac{W}{3t^2} \tanh^{-1} t \quad (19)$$

putting (16) and (19) into (18)

$$\frac{X}{W} = \frac{\sigma}{3(\theta + \alpha)}(\frac{1}{t^2} - 1)(\sin \alpha + \sin \theta) - \frac{\tanh^{-1} t}{3t^2 \sin \theta} - \\ - (\frac{D}{W} + \frac{1}{2}) \sin \alpha \quad (20)$$

at $\alpha = 0$, both (17) and (19) reduces to Borque's equations.

APPENDIX B

THEORETICAL SOLUTION OF ATTACHMENT DISTANCE FOR PLANAR, CONCAVE, AND CONVEX WALLS

```
      SGMA=7.7
      WRITE(6,118) SGMA
      W=2.62
   10 DO 99 J=5,45,5
      ALPHA=FLOAT(J-5)/57.295779
      F=COS(ALPHA)
      H=SIN(ALPHA)
      MM=J-5
      WRITE(6,122) MM
      WRITE(6,131)
      WRITE(6,129)
      DO 75 I=10,99
      T=.01*FLOAT(I)
      Z=ALOG((1.+T)/(1.-T))*.5
      T2=T**2
      CSTTA=(1.5*T-.5*T**3)
      G=CSTTA
      TTA=ARCOS(G)
      P=TTA*57.295779
      C=SIN(TTA)
      Q=SGMA/(3.*(TTA+ALPHA))*(1./T2-1.)
      DW=Q*(1.-G/F)-0.5
      IF(W.GT.2.) GO TO 114
      GO TO 15
  114 IF(DW.GE..00.AND.DW.LE..95) GO TO 8
      GO TO 75
   15 IF(DW.GE.(-.01).AND.DW.LE.1.92) GO TO 8
      GO TO 75

      COMPUTE X/W FOR THE PLANAR WALL

    8 XW=Q*(H+C)-Z/(3.*T2*C)-(DW+.5)*H
```

```
      COMPUTE THE DIVERGENCE AND X/W FOR THE CONVEX WALL BY METHOD 1

      Y2=50./W
      Y1=(Y2**2-XW**2)**0.5
      B=Y2-Y1
      YT=B/XW
      ALPHA1=ALPHA+YT
      H1=SIN(ALPHA1)
      DO 16 ML=200,990
      T1=.001*FLOAT(ML)
      Z1=ALOG((1.+T1)/(1.-T1))*.5
      T21=T1**2
      G1=1.5*T1-.5*T1**3
      TTA1=ARCOS(G1)
      F1=COS(ALPHA1)
      C1=SIN(TTA1)
      Q1=SIGMA/(3.*(ALPHA1+TTA1))*(1./T21-1.)
      DW1=Q1*(1.-G1/F1)-.5
      C=DW1-DW
      IF(0.GE.(-.01).AND.0.LE..01) GO TO 11
   16 CONTINUE
   11 XW1=Q1*(H1+C1)-Z1/(3.*T21*C1)-(DW+.5)*H1

      COMPUTE X/W FOR THE CONVEX WALL BY METHOD 2

      XW2=XW+B/(C*TAN(TTA))
```

```
      CCMPUTE THE DIVERGENCE AND X/W FCR THE CCNCAVE WALL BY METHOD 1

      ALPHA2=ALPHA-YT
      H2=SIN(ALPHA2)
      DC 71 JJ=200,990
      T3=.001*FLOAT(JJ)
      Z2=ALOG((1.+T3)/(1.-T3))*.5
      T22=T3**2
      G2=1.5*T3-.5*T3**3
      TTA2=ARCOS(G2)
      F2=COS(ALPHA2)
      C2=SIN(TTA2)
      Q2=SGMA/(3.*(TTA2+ALPHA2))*(1./T22-1.)
      Dw2=Q2*(1.-G2/F2)-.5
      U=Dw2-DW
      IF(U.GE.(-.01).AND.U.LE..01) GO TC 21
   71 CCNTINUE
   21 Xw3=Q2*(H2+C2)-Z2/(3.*T22*C2)-(DW+.5)*H2

      CCMPUTE X/W FOR THE CONCAVE WALL BY METHOD 2

      Xw4=XW-B/(C*TAN(TTA))
      WRITE(6,130) P,T,DW,XW,XW1,XW2,XW3,XW4
   75 CCNTINUE
   99 CONTINUE
  118 FCRMAT('1',///,5X,'THE VALUE OF SGMA FOR THIS RUN IS  ',F5.2)
  122 FCRMAT('0',/,9X,'VALUES OF DIMENSIONLESS PARAMETERS,CFFSET DISTANC
     1E, AND ATTACHMENT DISTANCE FOR ALPHA =',1X,I2,1X,'DEGREES')
  129 FCRMAT(' ',9X,68('-'))
  130 FORMAT(' ',5X,8(4X,F5.2))
  131 FCRMAT(' ',11X,'P',8X,'T',8X,'DW',7X,'XW',7X,'XW1',6X,'XW2',6X,'XW
     13',6X,'XW4')
   25 STOP
      END
```

APPENDIX C

ATTACHMENT DISTANCE AND FLOW RATE REDUCTION AND PLOTTING

```
      DIMENSION X(20),Y(20),DW(6)
      NAMELIST/DATA1/RE,DW,B
      REAL*8 TITLE(12)
   88 READ(5,DATA1)
      JJ=0
   10 READ(5,100,END=25) TITLE
      MJ=0
      EXSC=.4
      YSCL=2.
      MDXAX=0
      MDYAX=0
      IHIGH=7
      IWIDE=6
    5 READ(5,899) N
      NPTS=N
      READ(5,225) (X(I),I=1,12)
      WRITE(6,226) (X(I),I=1,12)
      READ(5,225) (Y(J),J=1,12)
      WRITE(6,226) (Y(J),J=1,12)
      MJ=MJ+1
      WRITE(6,174) RE,DW(MJ),B
      IF(JJ.GE.19) GO TO 800
   50 WRITE(6,175)
      AGE=Y(1)
      DO 19 J=1,N
      Y(J)=Y(J)/AGE
      WRITE(6,176) X(J),Y(J)
   19 CONTINUE
      GO TO 18
  800 WRITE(6,177)
      IHIGH=8
      DO 81 K=1,N
      Y(K)=Y(K)/B
      WRITE(6,176) X(K),Y(K)
   81 CONTINUE
```

```
 18 IF(MJ.EQ.1) GO TO 7
    IF(MJ.EQ.2) GO TO 8
    IF(MJ.EQ.3) GO TO 9
    IF(MJ.EQ.4) GO TO 113
    IF(MJ.EQ.5) GO TO 777
    IF(MJ.EQ.6) GO TO 778
  7 MC=1
    ITYPE=0
    REAL LABEL/'    '/
    CALL DRAW(NPTS,X,Y,MC,ITYPE,LABEL,TITLE,EXSC,YSCL,IXUP,IYRT,MCXAX,
   1MCYAX,IWIDE,IHIGH,IGRID,LAST)
    MC=2
    ITYPE=1
    REAL*8 AABEL/'        '/
    CALL DRAW(NPTS,X,Y,MC,ITYPE,AABEL,TITLE,EXSC,YSCL,IXUP,IYRT,MCXAX,
   1MCYAX,IWIDE,IHIGH,IGRID,LAST)
    GO TO 5
  8 MC=2
    ITYPE=0
    REAL HABEL/'    '/
    CALL DRAW(NPTS,X,Y,MC,ITYPE,HABEL,TITLE,EXSC,YSCL,IXUP,IYRT,MCXAX,
   1MCYAX,IWIDE,IHIGH,IGRID,LAST)
    MC=2
    ITYPE=2
    REAL*8 CABEL/'        '/
    CALL DRAW(NPTS,X,Y,MC,ITYPE,CABEL,TITLE,EXSC,YSCL,IXUP,IYRT,MCXAX,
   1MCYAX,IWIDE,IHIGH,IGRID,LAST)
    GO TO 5
  9 MC=2
    ITYPE=0
    REAL MABEL/'    '/
    CALL DRAW(NPTS,X,Y,MC,ITYPE,MABEL,TITLE,EXSC,YSCL,IXUP,IYRT,MCXAX,
   1MCYAX,IWIDE,IHIGH,IGRID,LAST)
    MC=2
    ITYPE=3
    REAL*8 RABEL/'        '/
    CALL DRAW(NPTS,X,Y,MC,ITYPE,RABEL,TITLE,EXSC,YSCL,IXUP,IYRT,MCXAX,
   1MCYAX,IWIDE,IHIGH,IGRID,LAST)
    GO TO 5
113 MC=2
    ITYPE=0
    REAL PABEL/'    '/
    CALL DRAW(NPTS,X,Y,MC,ITYPE,PABEL,TITLE,EXSC,YSCL,IXUP,IYRT,MCXAX,
   1MCYAX,IWIDE,IHIGH,IGRID,LAST)
```

```
      MC=2
      ITYPE=4
      REAL*8 GABEL/'          '/
      CALL DRAW(NPTS,X,Y,MC,ITYPE,GABEL,TITLE,EXSC,YSCL,IXUP,IYRT,MCXAX,
     1MCYAX,IWIDE,IHIGH,IGRID,LAST)
      GO TO 5
  777 MC=2
      ITYPE=0
      REAL SABEL/'    '/
      CALL DRAW(NPTS,X,Y,MC,ITYPE,SABEL,TITLE,EXSC,YSCL,IXUP,IYRT,MCXAX,
     1MCYAX,IWIDE,IHIGH,IGRID,LAST)
      MC=2
      ITYPE=5
      REAL*8 DABEL/'          '/
      CALL DRAW(NPTS,X,Y,MC,ITYPE,DABEL,TITLE,EXSC,YSCL,IXUP,IYRT,MCXAX,
     1MCYAX,IWIDE,IHIGH,IGRID,LAST)
      GO TO 5
  778 MC=2
      ITYPE=0
      REAL BABEL/'    '/
      CALL DRAW(NPTS,X,Y,MC,ITYPE,BABEL,TITLE,EXSC,YSCL,IXUP,IYRT,MCXAX,
     1MCYAX,IWIDE,IHIGH,IGRID,LAST)
      MC=3
      ITYPE=1
      REAL*8 FABEL/'          '/
      CALL DRAW(NPTS,X,Y,MC,ITYPE,FABEL,TITLE,EXSC,YSCL,IXUP,IYRT,MCXAX,
     1MCYAX,IWIDE,IHIGH,IGRID,LAST)
      GO TO 10
  100 FORMAT(6A8)
  174 FORMAT('0',5X,'THE FOLLOWING REDUCED DATA IS FOR REYNOLDS NUMBER',
     11X,F10.2,2X,'OFFSET DISTANCE',1X,F5.3,1X,' , AND JET WIDTH',1X,F5.
     23)
  175 FORMAT(' ',///,30X,'WALL DEFLECTION',12X,'FLOW RATE')
  176 FORMAT(' ',16X,2(18X,F6.3))
  177 FORMAT(' ',///,30X,'WALL DEFLECTION',12X,'ATTACH DIST')
  225 FORMAT(12F5.2)
  226 FORMAT(' ',//,3X,12(3X,F5.2))
  300 FORMAT(' ',10X,'THE SUCCESS OF THE DRAW IS',I2)
  899 FORMAT(I2)
   25 STOP
      END
```

APPENDIX D

SURFACE PRESSURE COEFFICIENT COMPUTATION AND PLOTTING

```
      DIMENSION X(40),Y(40),YUN(40),RE(2),HO(3),Z(40)
      NAMELIST/DATA2/HO,RE,SNTHTA,WL
      REAL*8 TITLE(12)
      READ(5,225) (Z(I),I=1,35)
      WRITE(6,226) (Z(J),J=1,35)
      B=2.62
      DO 21 M=1,35
   21 Z(M)=Z(M)/B
      JJ=0
   10 READ(5,DATA2)
      MJ=0
      EXSC=3.
      YSCL=.3
      MDXAX=2
      IXUP=2
      MDYAX=0
      IWIDE=6
      IHIGH=8
      JJ=JJ+1
      READ(5,100,END=25) TITLE
    5 READ(5,899) N
      NPTS=N
      DO 707 I=1,35
  707 X(I)=Z(I)
      READ(5,225) (YUN(J),J=1,N)
      WRITE(6,226) (YUN(I),I=1,N)
      MJ=MJ+1
      IF(JJ.EQ.1) WRITE(6,174) RE(1)
      WRITE(6,175)
      DO 18 K=1,N
      YUN(K)=(YUN(K)-HO(MJ))*SNTHTA
      Y(K)=YUN(K)/RE(2)
      WRITE(6,176) Y(K),X(K)
   18 CONTINUE
   33 IF(MJ.EQ.1) GO TO 12
      IF(MJ.EQ.2) GO TO 13
      IF(MJ.EQ.3) GO TO 14
```

```
 12 MC=1
    ITYPE=0
    REAL ZABEL/'     '/
    CALL DRAW(NPTS,X,Y,MC,ITYPE,ZABEL,TITLE,EXSC,YSCL,IXUP,IYRT,MDXAX,
   1MDYAX,IWIDE,IHIGH,IGRID,LAST)
    IF(NPTS.GT.30) GO TO 909
111 MC=2
    ITYPE=1
    REAL*8 LABEL/'          '/
    CALL DRAW(NPTS,X,Y,MC,ITYPE,LABEL,TITLE,EXSC,YSCL,IXUP,IYRT,MDXAX,
   1MDYAX,IWIDE,IHIGH,IGRID,LAST)
    GO TO 5
 13 MC=2
    ITYPE=0
    REAL AABEL/'     '/
    CALL DRAW(NPTS,X,Y,MC,ITYPE,AABEL,TITLE,EXSC,YSCL,IXUP,IYRT,MDXAX,
   1MDYAX,IWIDE,IHIGH,IGRID,LAST)
    IF(NPTS.GT.30) GO TO 909
112 MC=2
    ITYPE=2
      REAL*8 CABEL/'          '/
    CALL DRAW(NPTS,X,Y,MC,ITYPE,CABEL,TITLE,EXSC,YSCL,IXUP,IYRT,MDXAX,
   1MDYAX,IWIDE,IHIGH,IGRID,LAST)
    GO TO 5
 14 MC=2
    ITYPE=0
    REAL PABEL/'     '/
    CALL DRAW(NPTS,X,Y,MC,ITYPE,PABEL,TITLE,EXSC,YSCL,IXUP,IYRT,MDXAX,
   1MDYAX,IWIDE,IHIGH,IGRID,LAST)
    IF(NPTS.GT.30) GO TO 909
```

```
113 MC=3
    ITYPE=3
    REAL*8 DABEL/'          '/
    CALL DRAW(NPTS,X,Y,MC,ITYPE,DABEL,TITLE,EXSC,YSCL,IXUP,IYRT,MCXAX,
   1MCYAX,IWIDE,IHIGH,IGRID,LAST)
    WRITE(6,300) LAST
    GO TO 10
505 WRITE(6,175)
    NPTS=NPTS/2
    DO 101 MK=2,NPTS
    Y(MK)=Y(2*MK+1)
    X(MK)=X(2*MK+1)
    WRITE(6,176) Y(MK),X(MK)
101 CONTINUE
    IF(MJ.EQ.1) GO TO 111
    IF(MJ.EQ.2) GO TO 112
    IF(MJ.EQ.3) GO TO 113
100 FORMAT(6A8)
174 FORMAT('0',5X,' THE FOLLOWING REDUCED DATA IS FOR REYNOLDS NUMBER'
   1,1X,F10.2,2X,'AND A CONVEX WALL')
175 FORMAT(' ',///,30X,'SURFACE PRESSURE',12X,'WALL POSITION')
176 FORMAT(' ',16X,2(18X,F6.3))
177 FORMAT(' ',///,30X,'WALL DEFLECTION',12X,'ATTACH DIST')
225 FORMAT(12F5.2)
226 FORMAT(' ',//,3X,12(3X,F5.2))
300 FORMAT(' ',10X,'THE SUCCESS OF THE DRAW IS',I2)
899 FORMAT(I2)
 25 STOP
    END
```

APPENDIX E

VELOCITY PROFILE PLOT

```
      DIMENSION X(50),Y(50)
      REAL*8 TITLE(12)
      READ(5,188) JJ
      DO 66 I=1,JJ
      READ(5,100) TITLE
      READ(5,188) N
      READ(5,12) (Y(K),K=1,N)
      DO 99 L=2,N
   99  X(L)=0.1*FLOAT(L-1)
      X(1)=0.0
      NPTS=N
      EXSC=0
      YSCL=0
      MDXAX=0
      MDYAX=0
      IWIDE=6
      IHIGH=8
      MC=1
      ITYPE=0
```

```
      REAL LABEL/'    '/
      CALL DRAW(NPTS,X,Y,MC,ITYPE,LABEL,TITLE,EXSC,YSCL,IXUP,IYRT,MDXAX,
     1MDYAX,IWIDE,IHIGH,IGRID,LAST)
      WRITE(6,300) LAST
      IF(I.GE.4) GO TO 77
   55 MC=3
      ITYPE=1
      REAL*8 CABEL/'        '/
      CALL DRAW(NPTS,X,Y,MC,ITYPE,CABEL,TITLE,EXSC,YSCL,IXUP,IYRT,MDXAX,
     1MDYAX,IWIDE,IHIGH,IGRID,LAST)
      WRITE(6,300) LAST
      GO TO 66
   77 NPTS=NPTS/2
      DO 101 MK=2,NPTS
      Y(MK)=Y(2*MK+1)
      X(MK)=X(MK*2+1)
  101 CONTINUE
      GO TO 55
   66 CONTINUE
   12 FORMAT(10F7.4)
  100 FORMAT(6A8)
  188 FORMAT(I2)
  300 FORMAT(///,10X,'THE SUCCESS OF THE DRAW IS',I2)
  106 STOP
      END
```

Figure 1. Flow Model for Planar Wall

Figure 2. Flow Model for Concave Wall

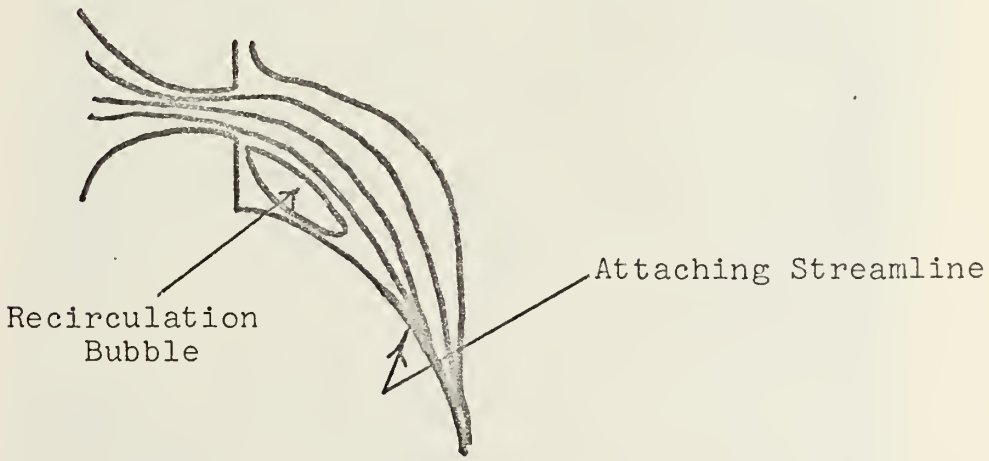

Figure 3. Flow Model for Convex Wall

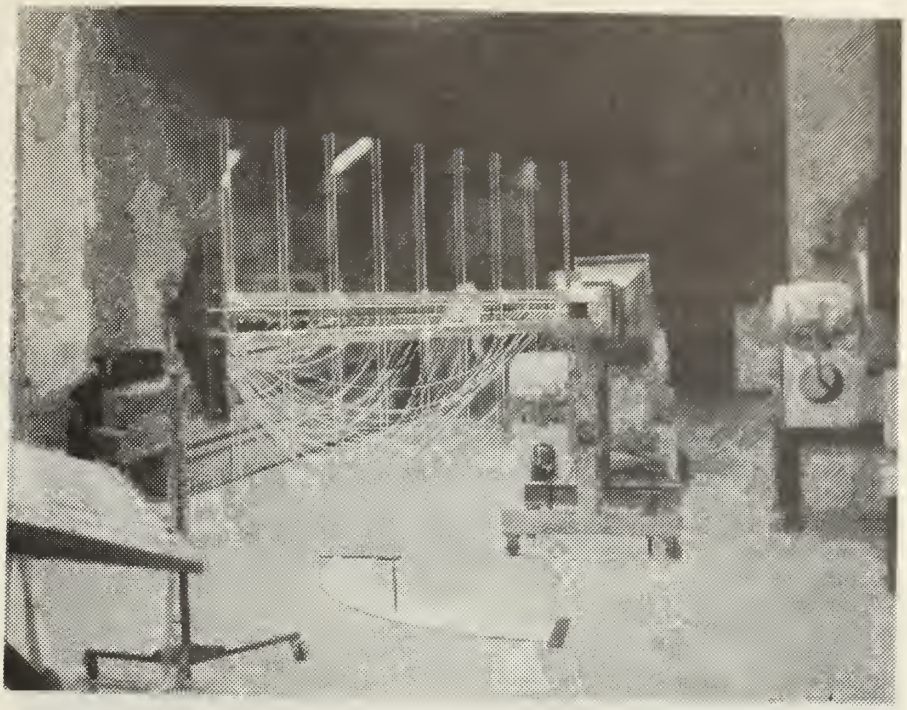

Figure 4. Planar Wall

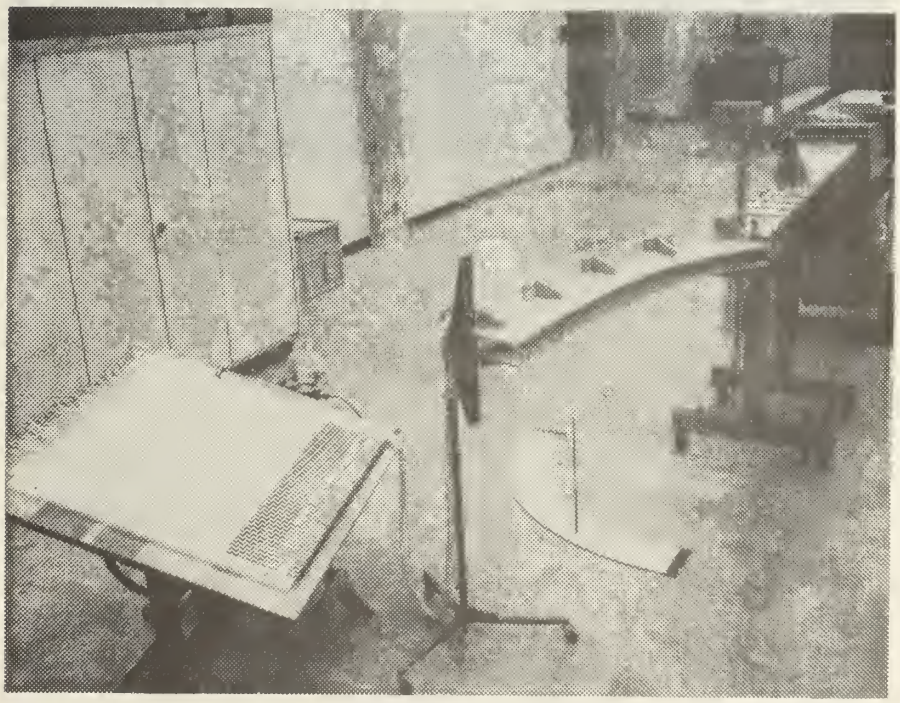

Figure 5. Concave Wall

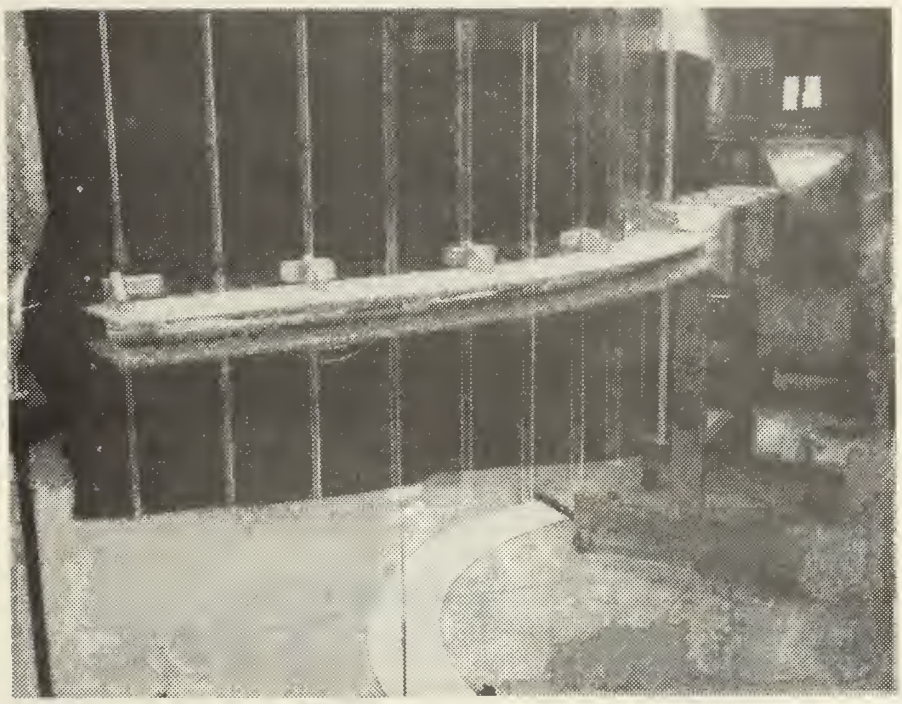

Figure 6. Convex Wall

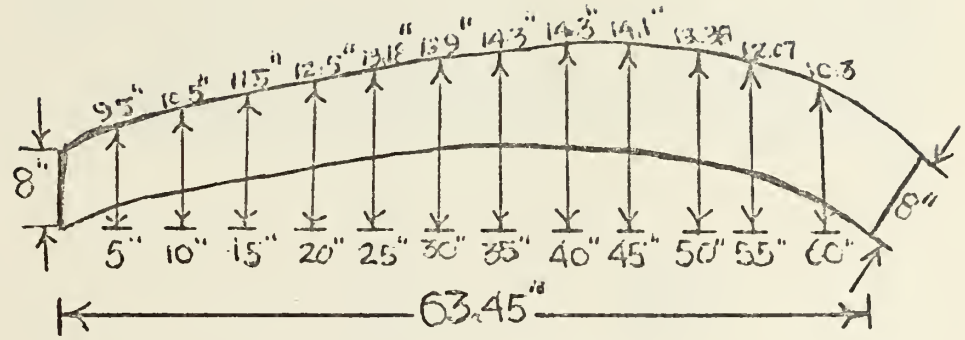

Figure 7. Convex and Concave Wall Planform

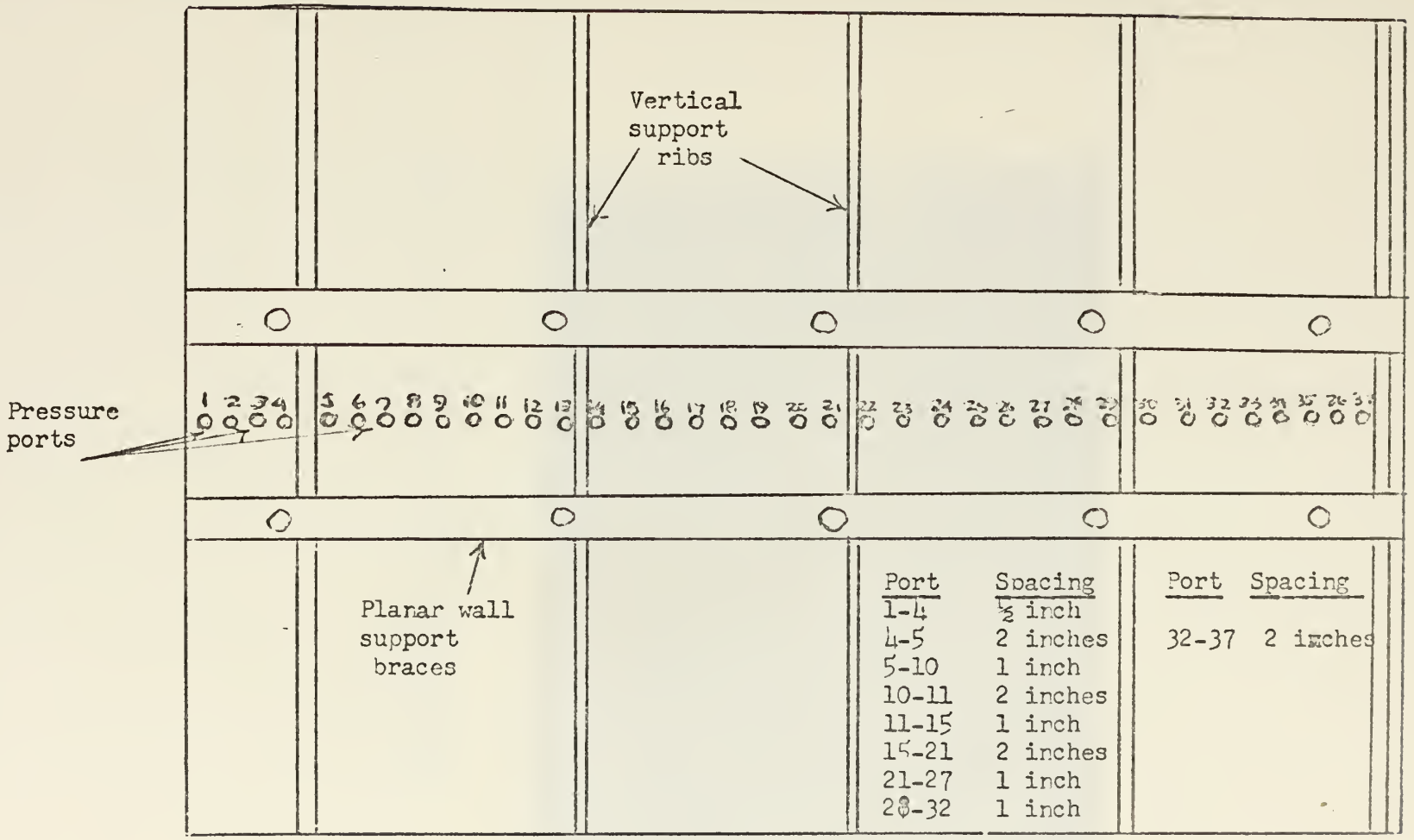

Figure 8. Pressure port location and vertical wall construction

Figure 8.b. Pressure Port Location and Vertical Wall Construction

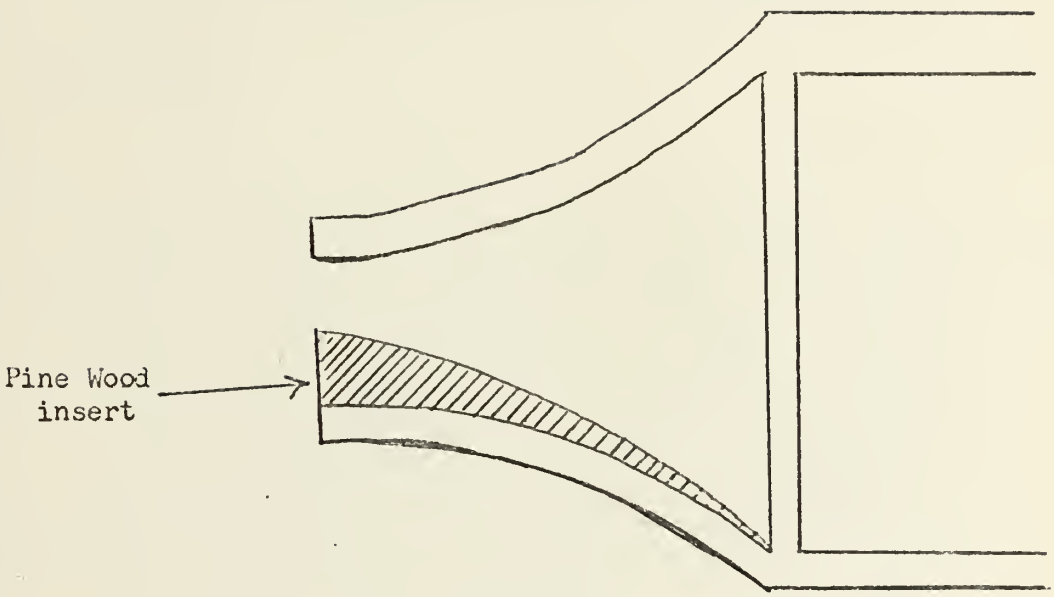

Figure 9. Half-jet Modification

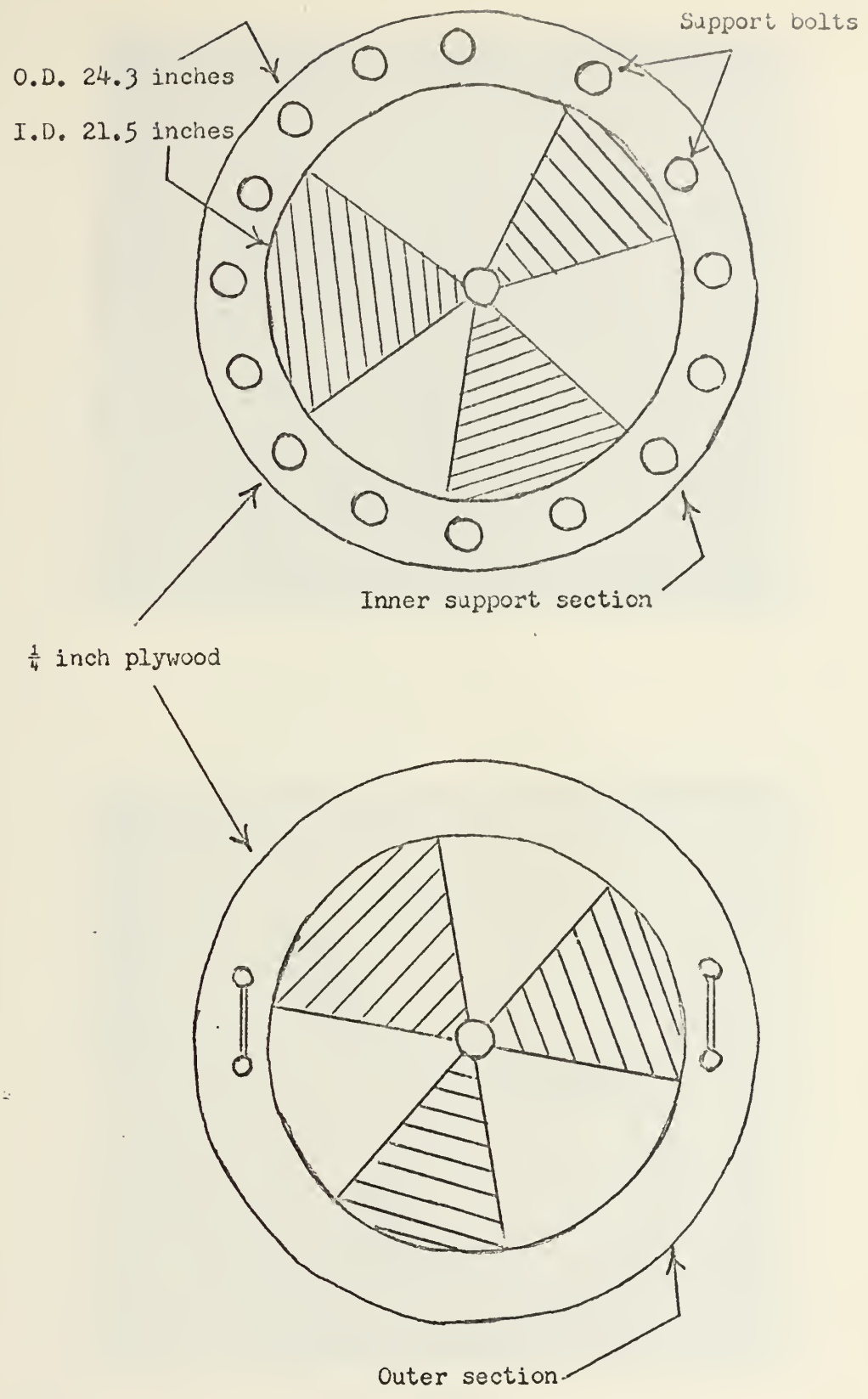

Figure 10.a. Flow Constriction Device

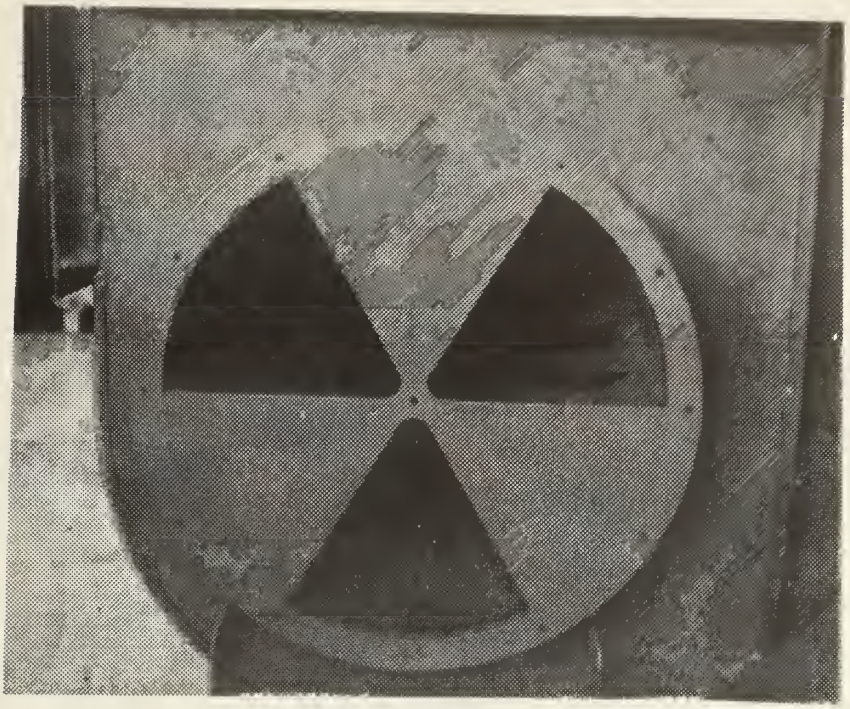

Inner Support Section

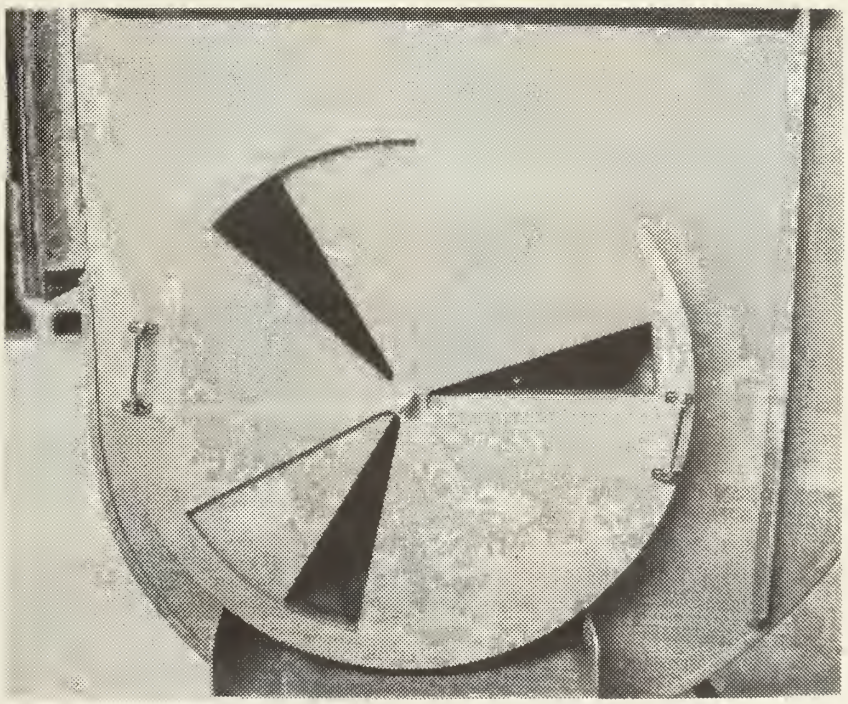

Outer Section

Figure 10.b. Flow Constriction Device

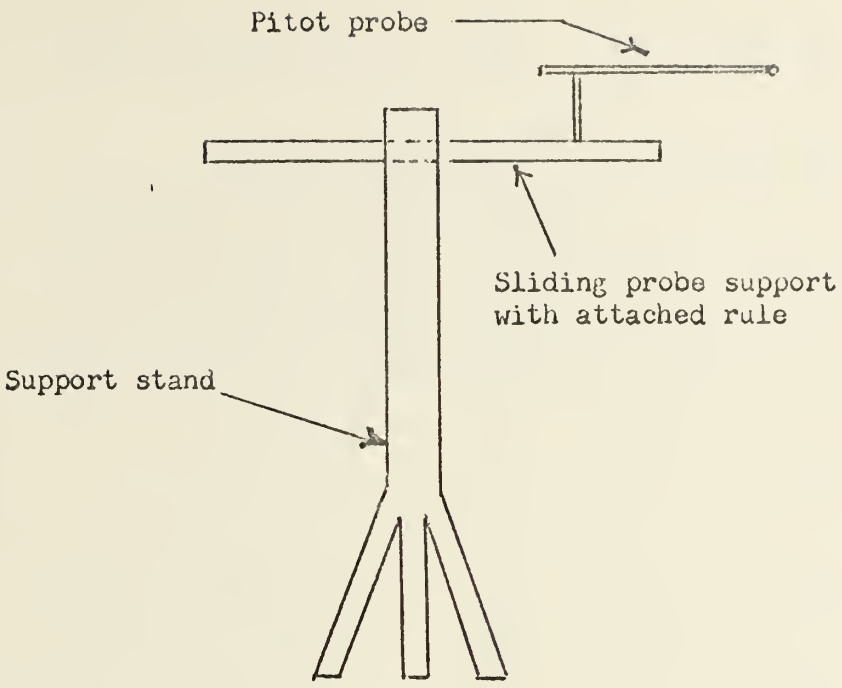

SIDE VIEW

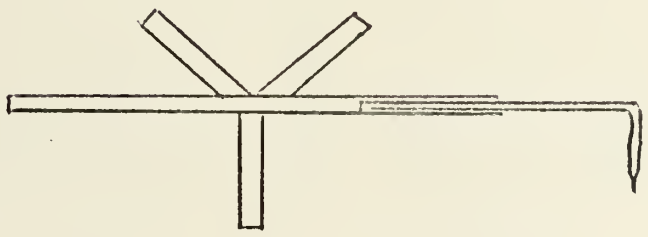

TOP VIEW

Figure 11. Pitot Probe Configuration

OUTLINE OF DATA PRESENATION I.

A. Planar Wall

1. Comparison with theoretical calculations

a.	X/W vs. D/W	jet width = 2.62 in.	$N_{Re} = 2.05 \times 10^5$	α = 15,20,25 deg.	Fig. 12-14
b.	X/W vs. D/W	jet width = 1.31 in.	$N_{Re} = 1.475 \times 10^5$	α = 15,20,25 deg.	Fig. 15-17

2.

a.	X/W vs. D/W	jet width = 2.62 in.	$N_{Re} = 2.05 \times 10^5$	α = 15,20,25,30 deg.	Fig. 18
b.	X/W vs. D/W	jet width = 1.31 in.	$N_{Re} = 1.475 \times 10^5$	α = 15,20,25,30 deg.	Fig. 19

3.

a.	X/W vs. α	jet width = 2.62 in.	$N_{Re} = 2.05 \times 10^5$	D/W = 00=0.0, 01=.18, 02=.36, 03=.56, 04=.74, 05=.94	Fig. 20
b.	X/W vs. α	jet width = 1.31 in.	$N_{Re} = 1.475 \times 10^5$	D/W = 00=0.0, 01=.36, 02=.74, 03=1.12, 04=1.48, 05=1.88	Fig. 21

4.

a.	$\dot{m}/\dot{m}_o$ vs. D/W	jet width = 2.62 in.	$N_{Re} = 2.05 \times 10^5$	α as in 2.a. above	Fig. 22
b.	$\dot{m}/\dot{m}_o$ vs. D/W	jet width = 1.31 in.	$N_{Re} = 1.475 \times 10^5$	α as in 2.b. above	Fig. 23

5.

a.	$\dot{m}/\dot{m}_o$ vs. α	jet width = 2.62 in.	$N_{Re} = 2.05 \times 10^5$	D/W as in 3.a. above	Fig. 24
b.	$\dot{m}/\dot{m}_o$ vs. α	jet width = 1.31 in.	$N_{Re} = 2.05 \times 10^5$	D/W as in 3.b. above	Fig. 25

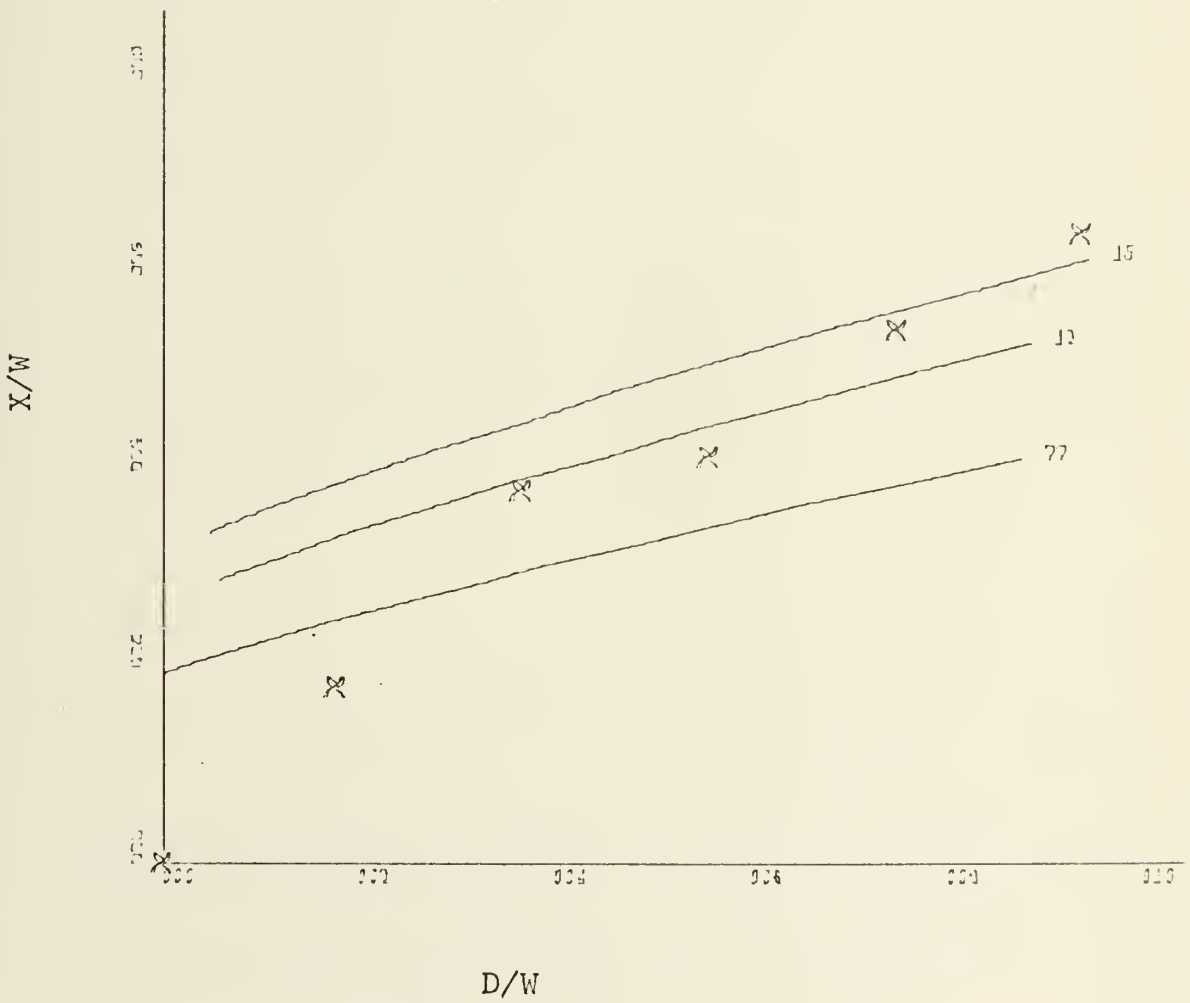

Figure 12. Attachment Distance vs. Offset Distance for Planar Wall at 15 Degrees Incidence for Theoretical and Experimental Data, Jet width 2.62 inches, Re = 2.05×10^5, σ = 7.7, 12, 15.

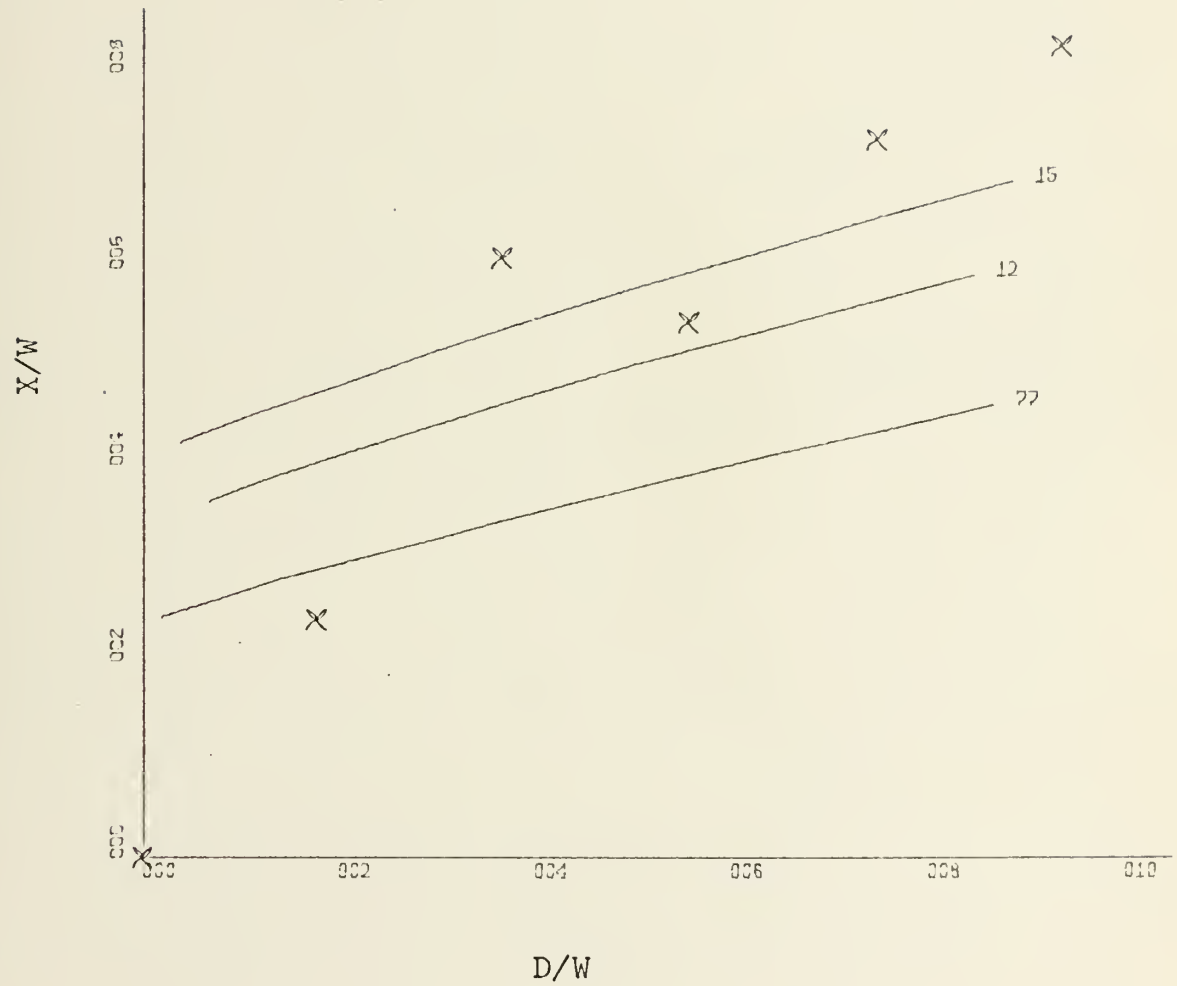

Figure 13. Attachment Distance vs. Offset Distance for Planar Wall at 20 Degrees Incidence for Theoretical and Experimental Data, Jet Width 2.62 inches, Re = 20.5 x 10^5, σ = 7.7, 12, 15.

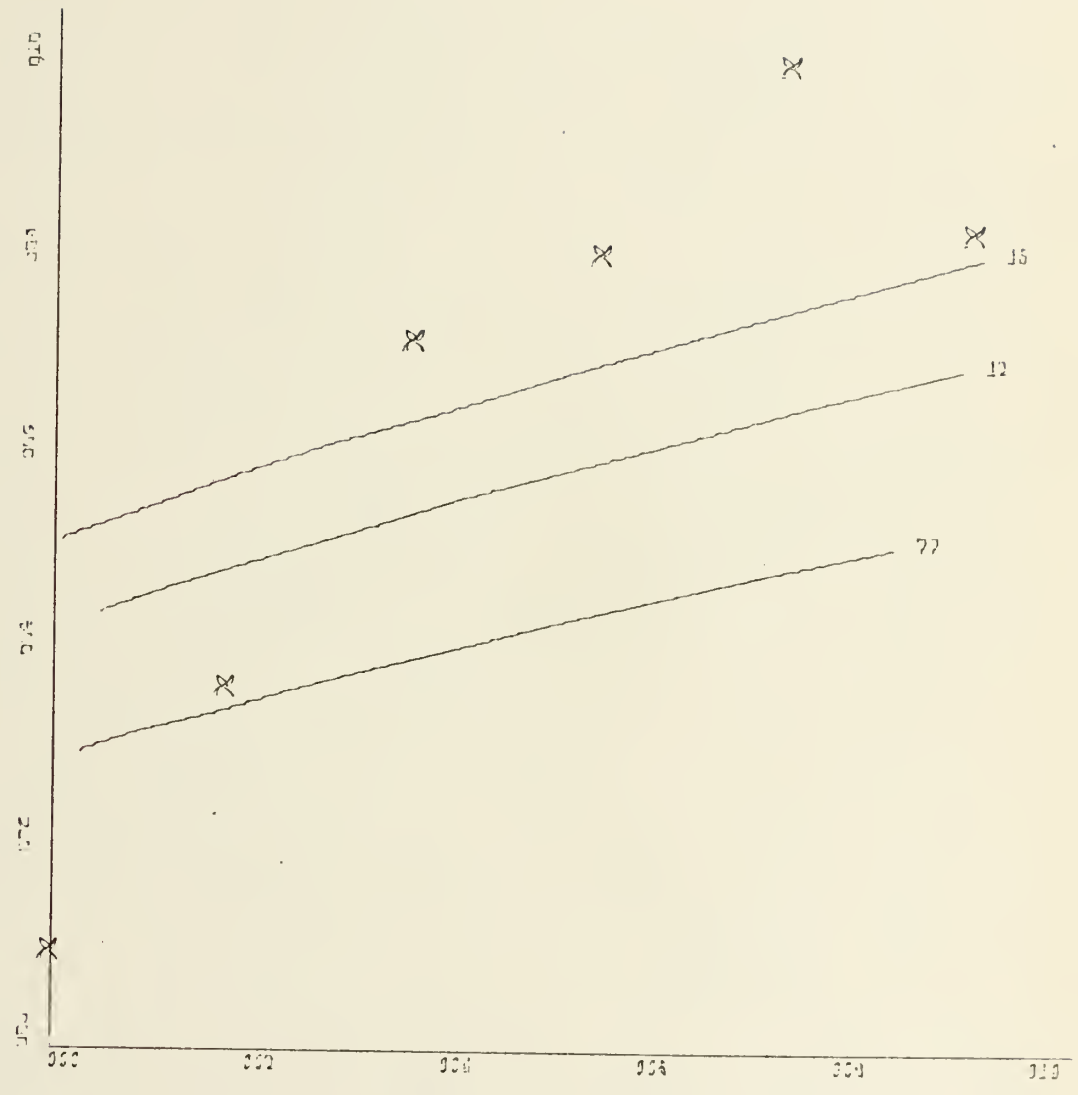

Figure 14. Attachment Distance vs. Offset Distance for Planar Wall at 25 Degrees Incidence for Theoretical and Experimental Values, Jet Width 2.62 inches, Re = 20.5 x 10^5, σ = 7.7, 12, 15.

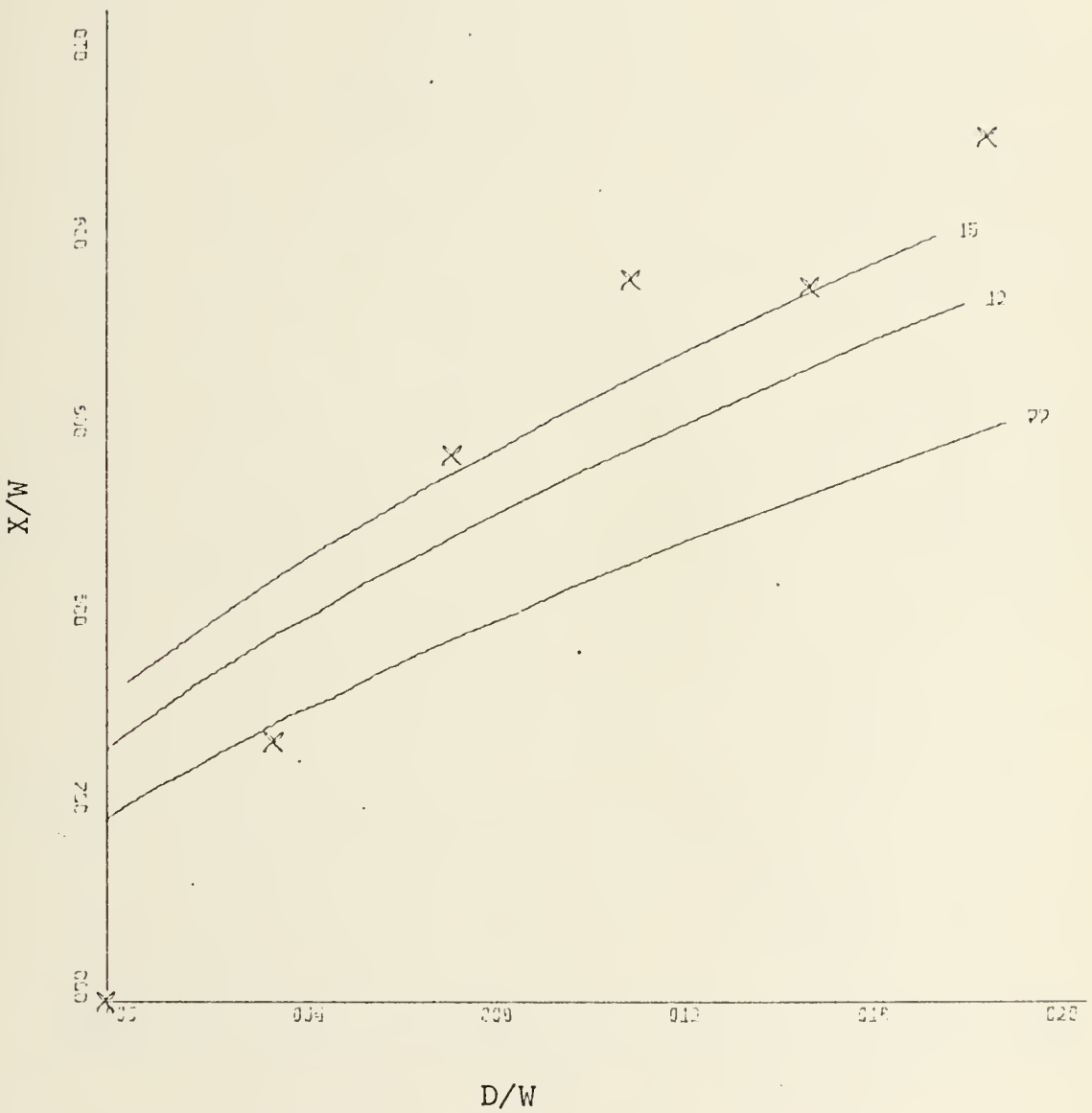

Figure 15. Attachment Distance vs. Offset Distance for a Planar Wall at 15 Degrees Incidence for Theoretical and Experimental Data, Jet Width 1.31 inches, Re = 147500, σ = 7.7, 12, 15.

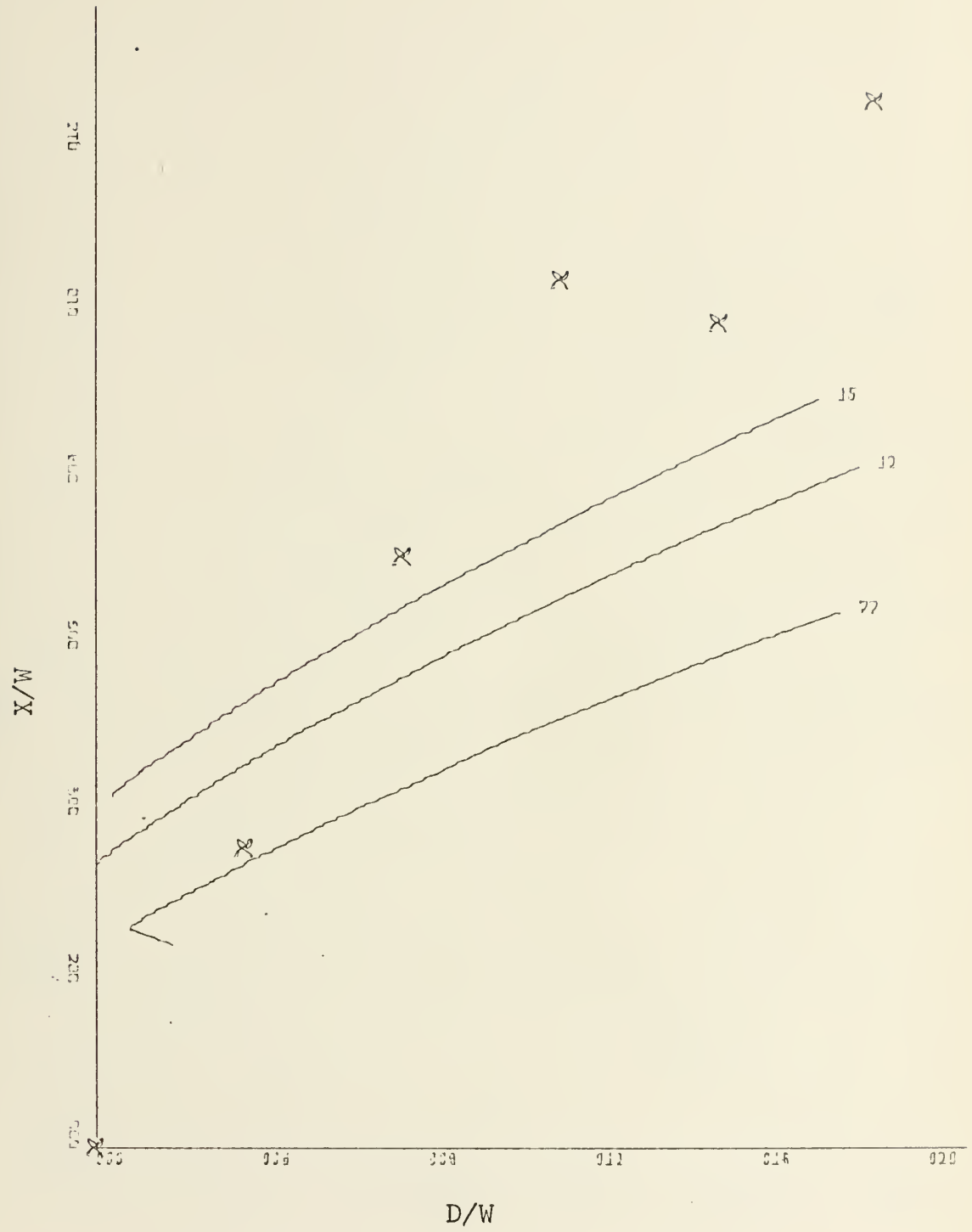

Figure 16. Attachment Distance vs. Offset Distance for a Planar Wall at 20 Degrees Incidence for Theoretical and Experimental Data, Jet Width 1.31 inches, Re = 147500, σ = 7.7, 12, 15.

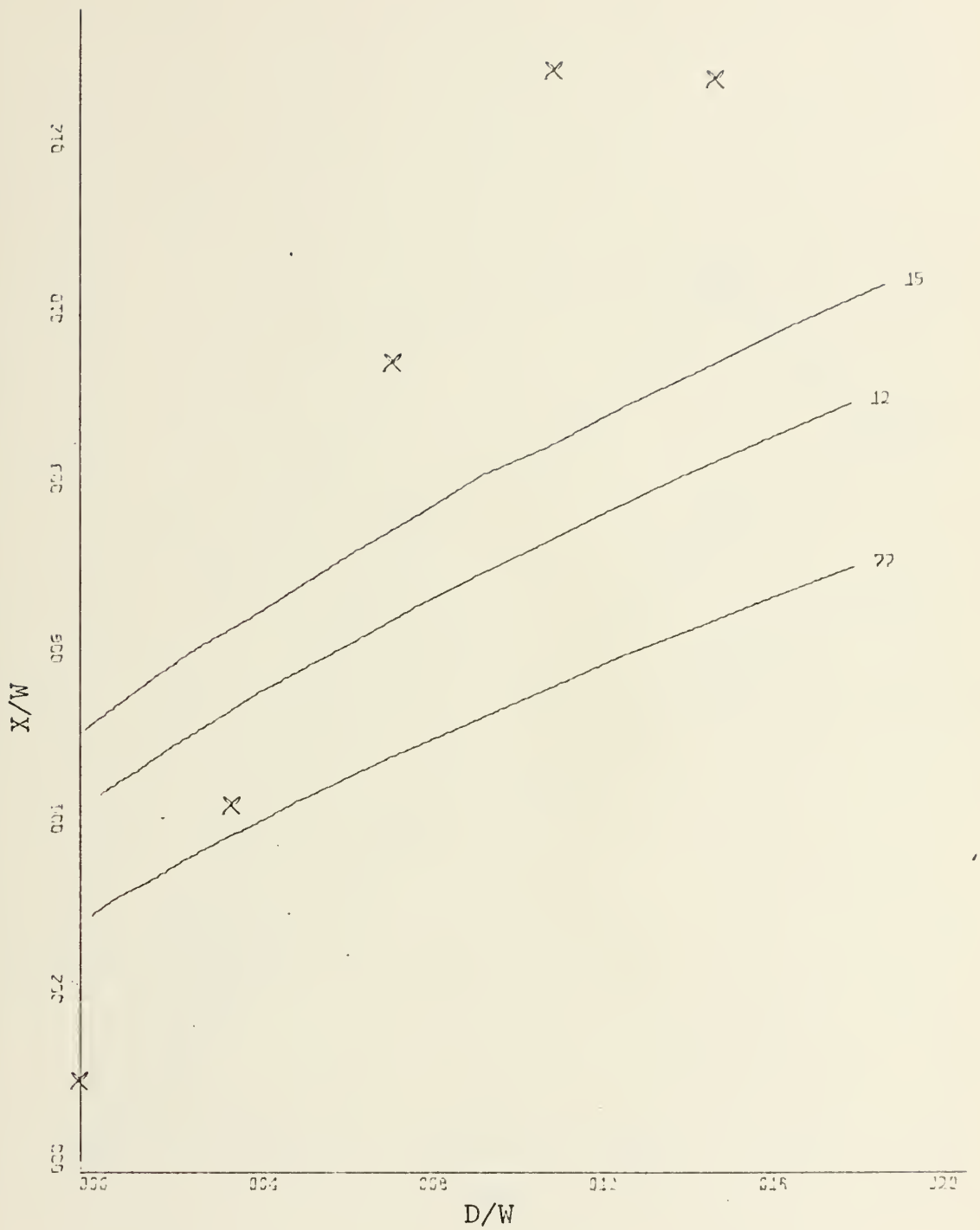

Figure 17. Attachment Distance vs. Offset Distance for a Planar Wall at 25 Degrees Incidence for Theoretical and Experimental Data, Jet Width 1.31, Re = 147500, σ = 7.7, 12, 15.

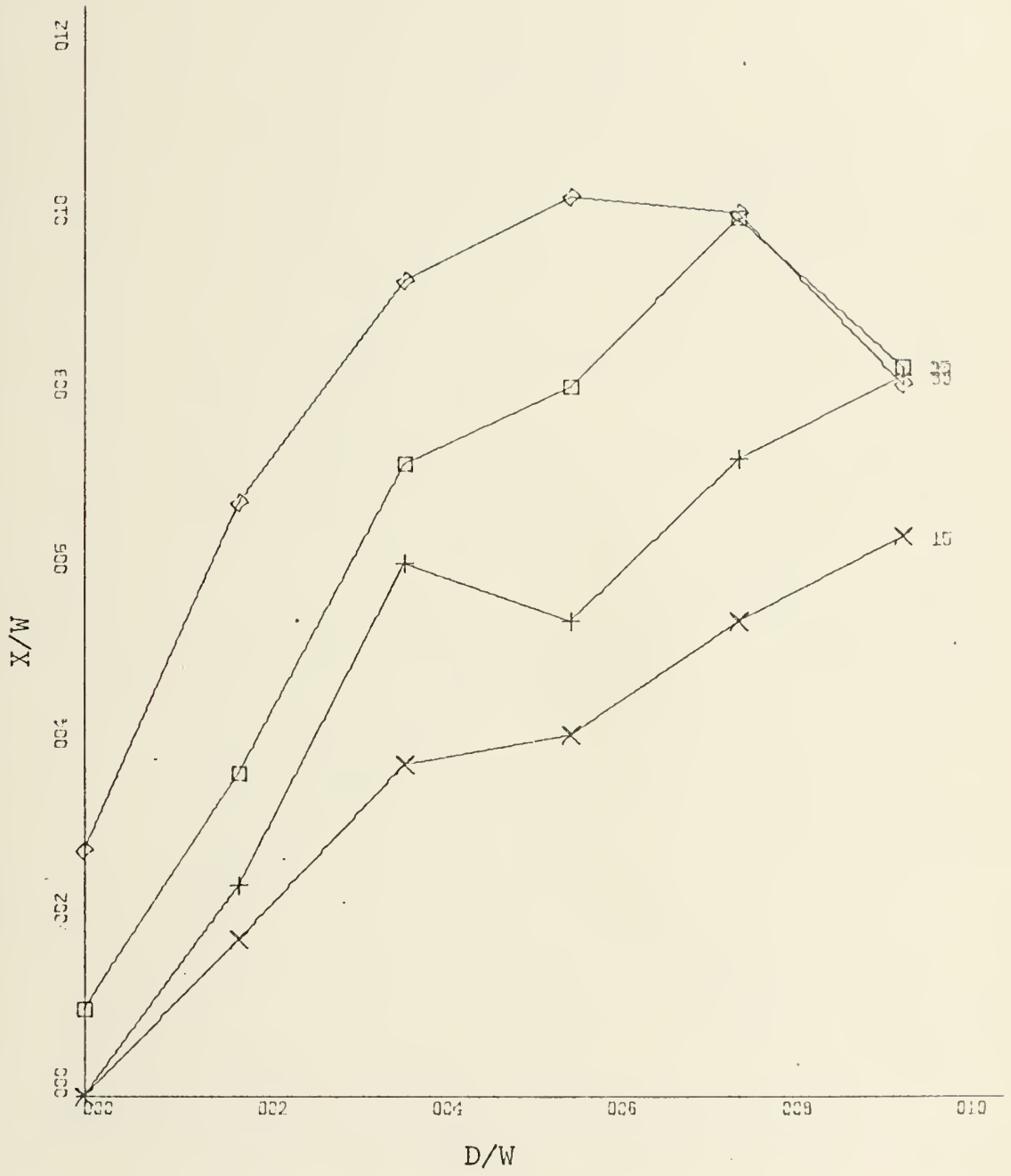

Figure 18. Attachment Distance vs. Offset Distance for Planar Wall, Re = 2.05 x 10^5, Constant Deflection Angles of 15, 20, 25, and 30 Degrees and Jet Width of 2.62 inches.

Figure 19. Attachment Distance vs. Offset Distance for Planar Wall, Re = 1.475 x 10^5 Constant Deflection Angles of 15, 20, 25, 30 and Jet Width of 1.31 Inches.

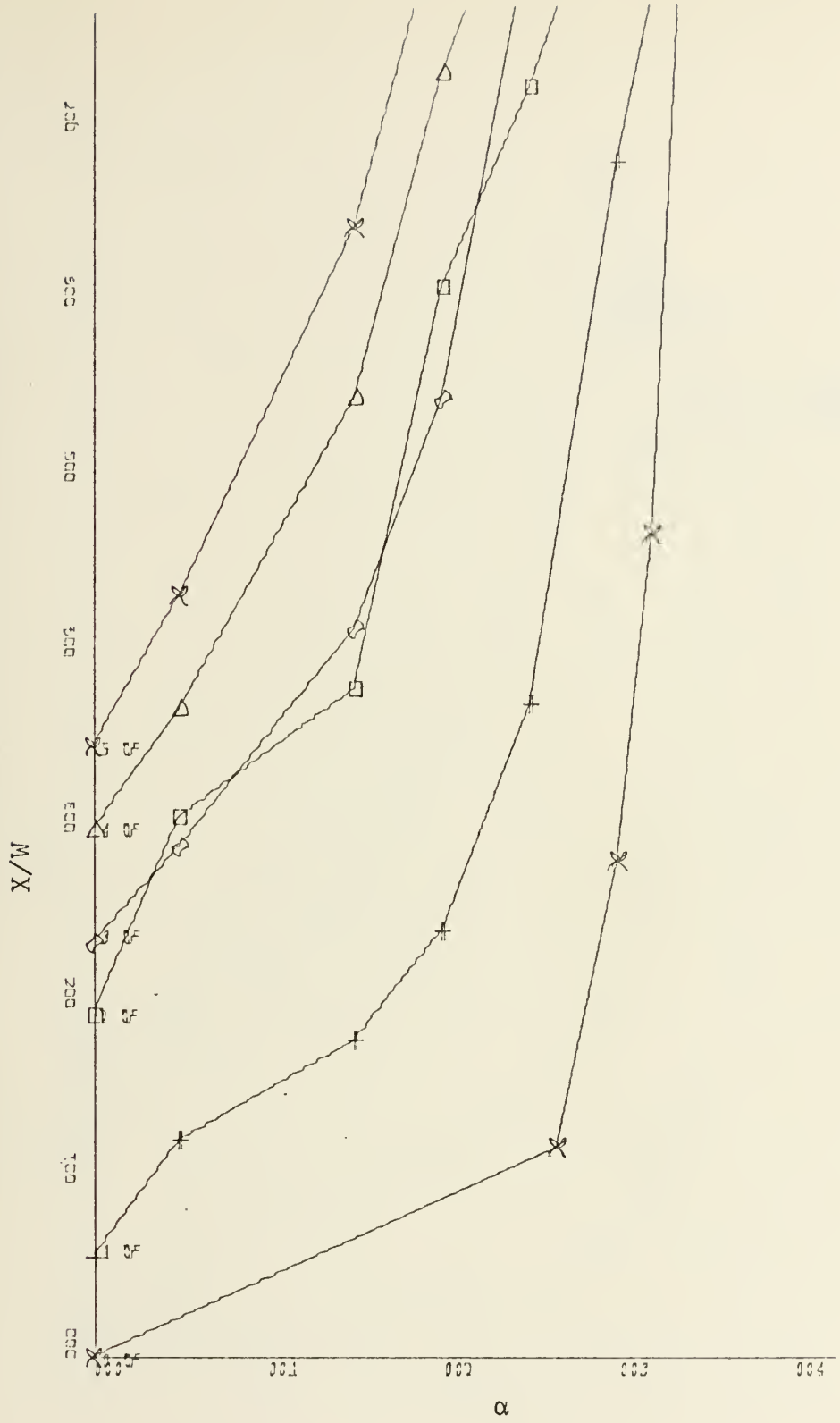

Figure 20. Attachment Distance vs. Deflection Angle for Various Offset Distances, Jet Width 2.62 inches, Planar Wall, Re of 2.05 x 10^5.

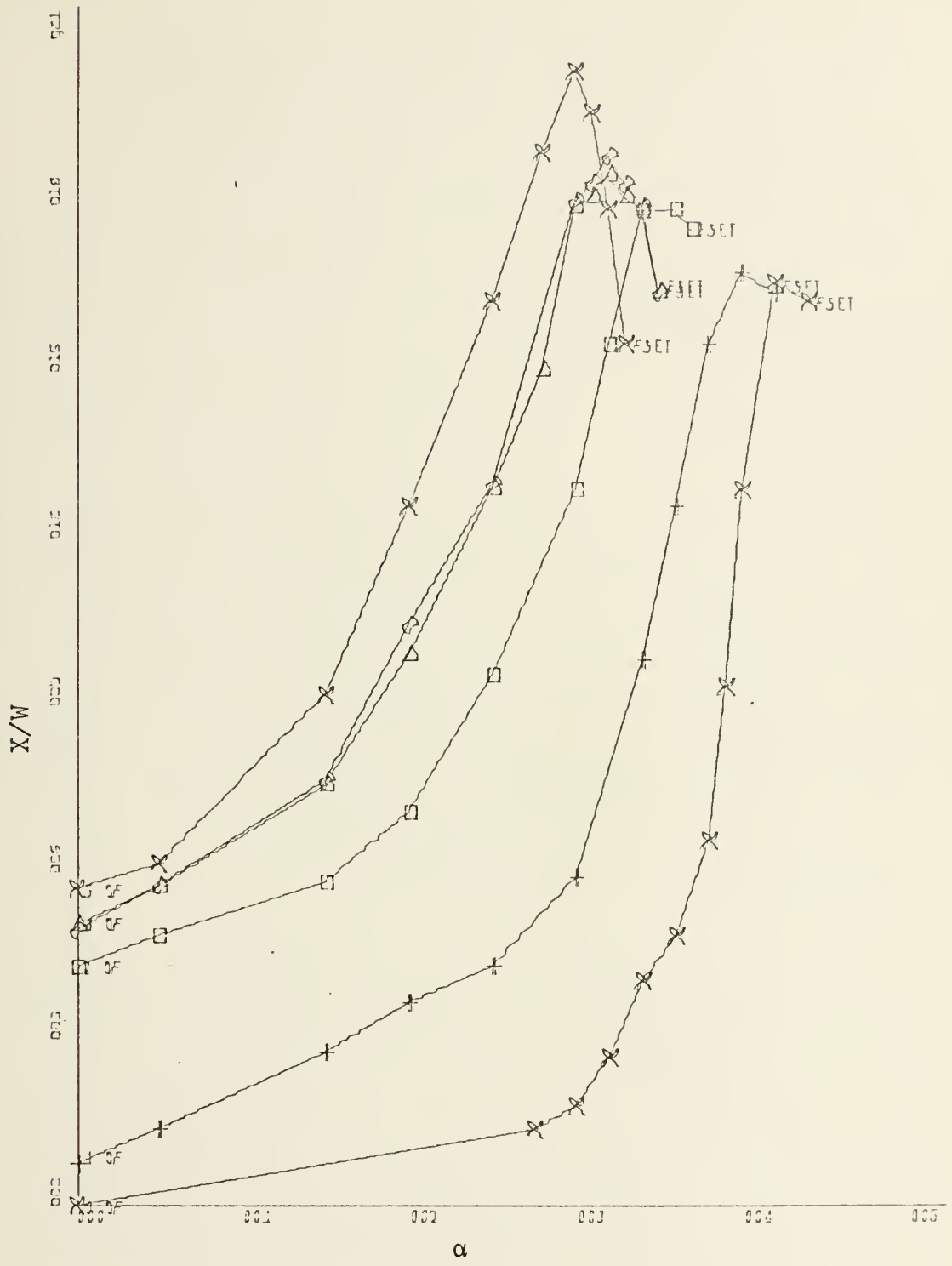

Figure 21. Attachment Distance vs. Deflection Angle for Various Offset Distances, Jet Width of 1.31 Inches, Planar Wall, Re of 1.475×10^5.

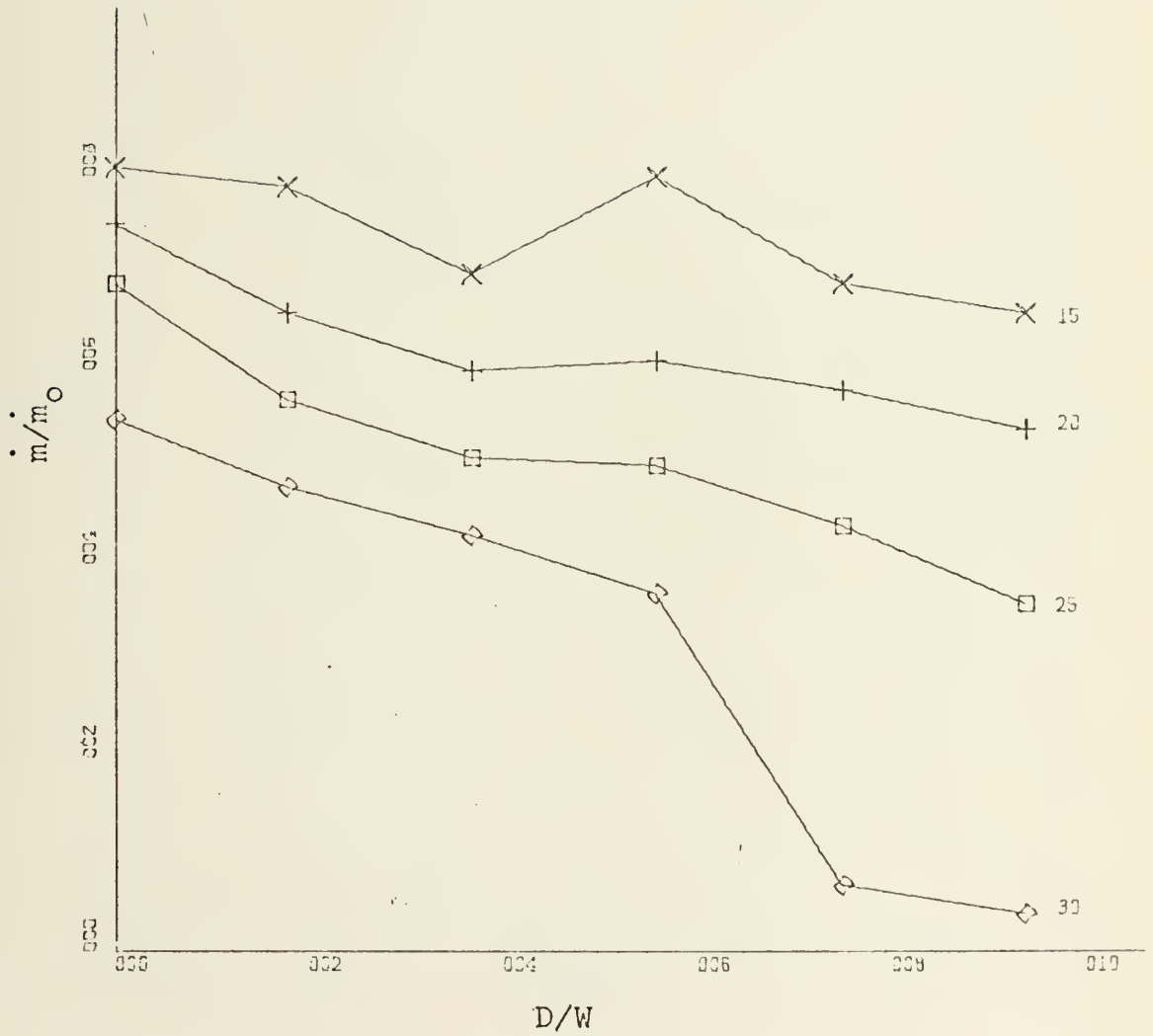

Figure 22. Flow Rate vs. Offset Distance for Planar Wall at Constant Deflection Angles, Jet Width of 2.62 inches, Re = 2.05 x 10^5 , α = 15, 20, 25, 30 Degrees

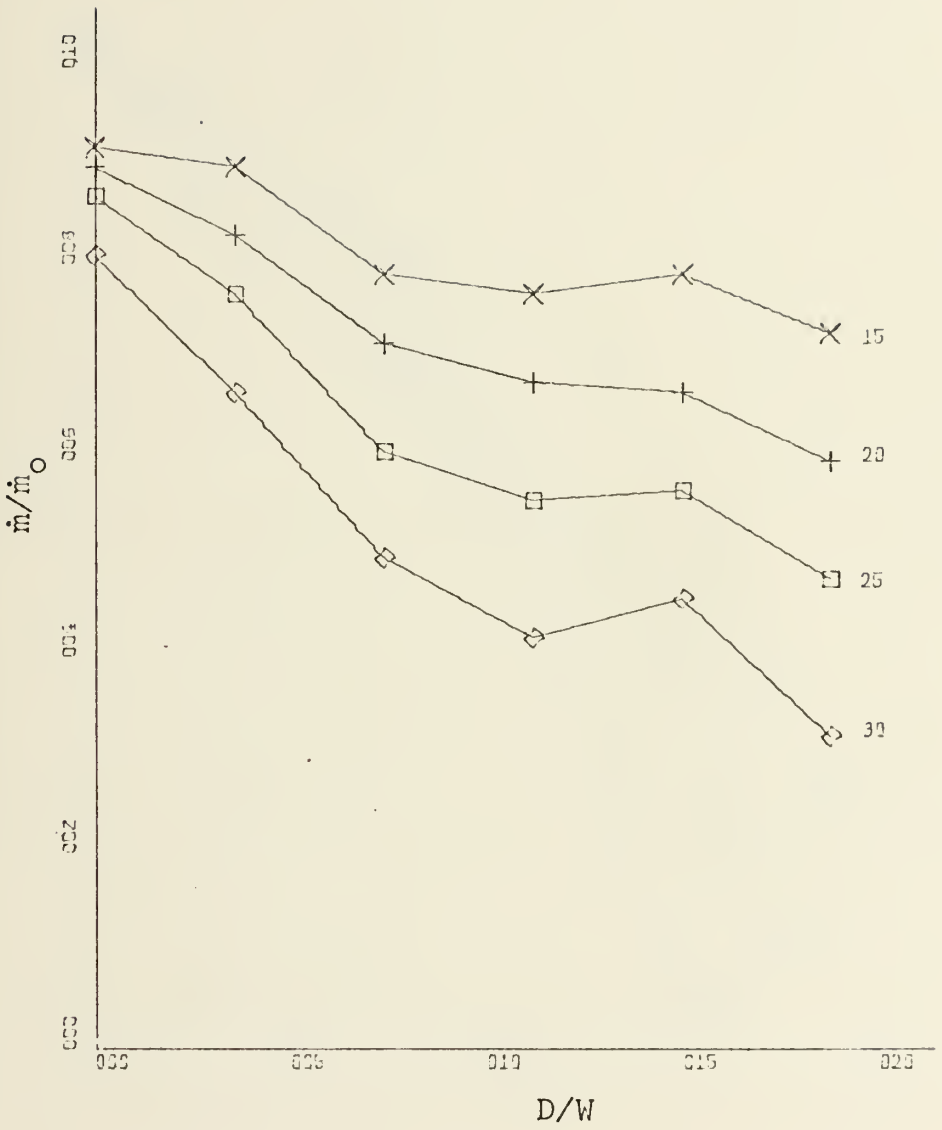

Figure 23. Flow Rate vs. Offset Distance for Planar Wall at Constant Deflection Angles, Jet Width of 1.31 inches, Re = 1.475×10^5, α = 15, 20, 25, 30 degrees.

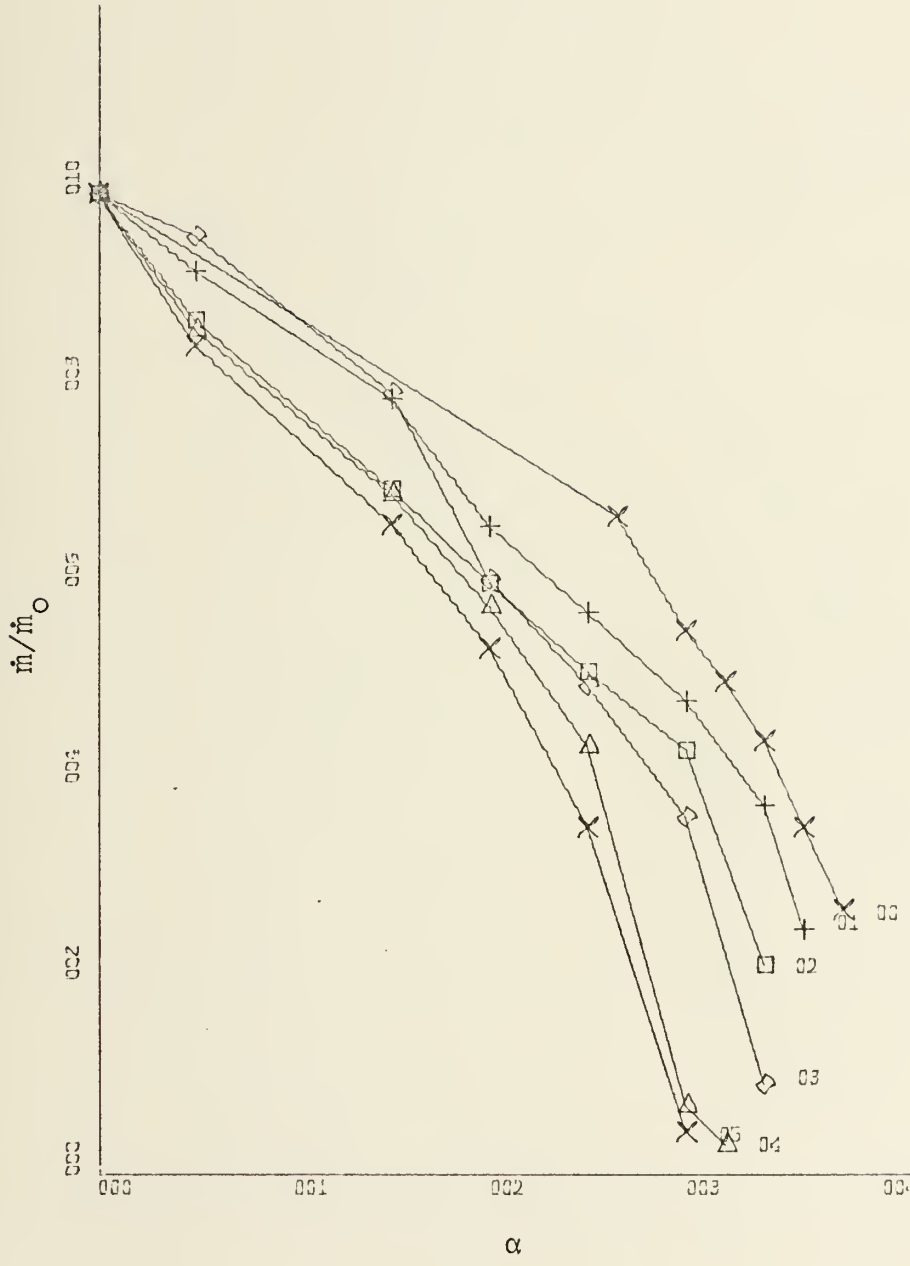

Figure 24. Flow Rate vs. Deflection Angle at Various Offset Distances for Planar Wall, Re = 2.05 x 10^5, Jet Width of 2.62 Inches, Offset Distance Numbers 00, 01, 02, 03, 04, 05.

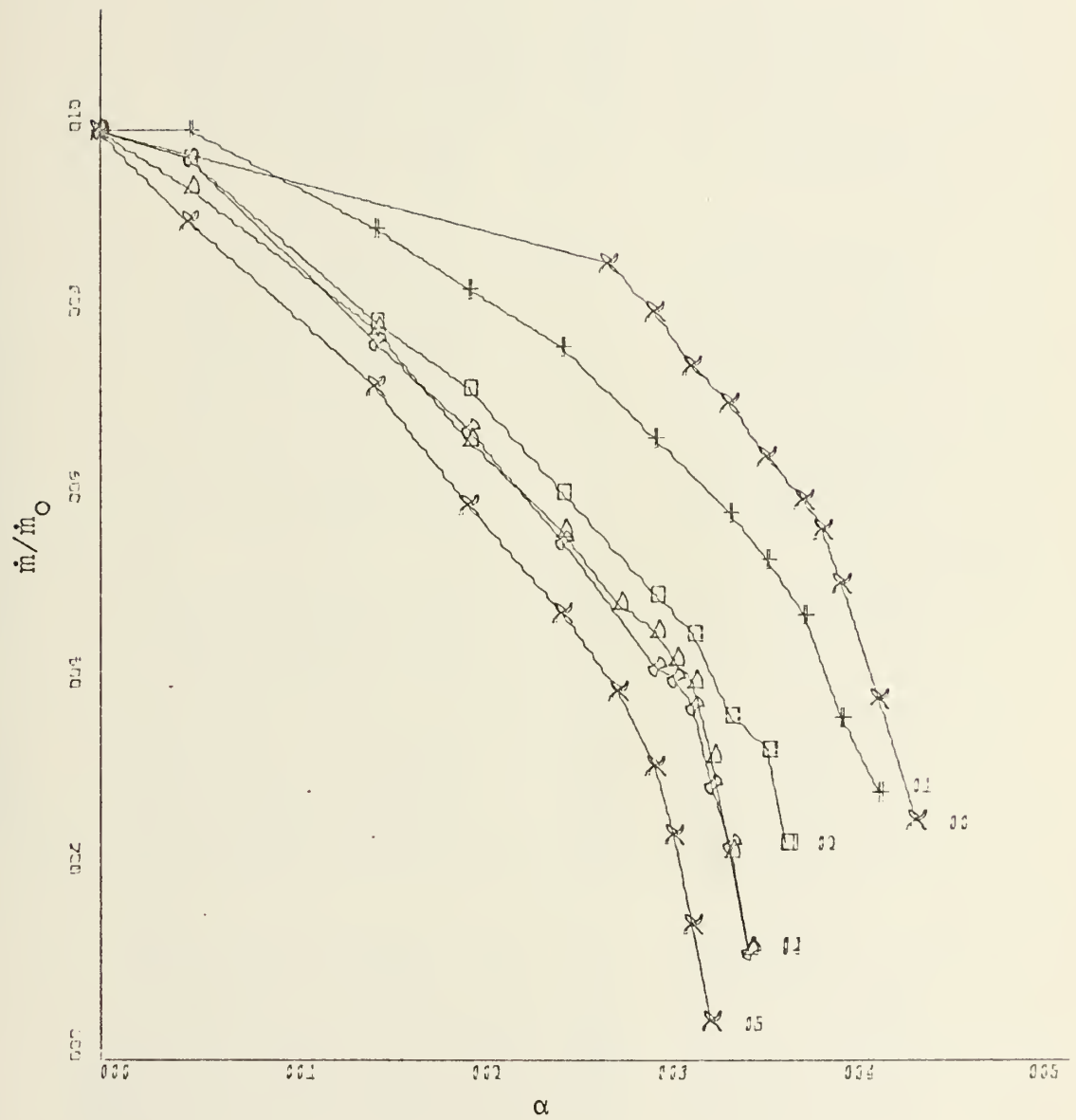

Figure 25. Flow Rate vs. Deflection Angle at Various Offset Distances, for Planar Wall, Re = 1.475×10^5, Jet Width of 1.31 Inches, Offset Distance Numbers 00, 01, 02, 03, 04, 05.

OUTLINE OF DATA PRESENTATION II.

A. Convex Wall

1. Comparison with theoretical calculations

a.	X/W vs. D/W	jet width = 2.62 in.	$N_{Re} = 2.05 \times 10^5$	α = 15,20,25 deg.		Fig. 26-28
b.	X/W vs. D/W	jet width = 1.31 in.	$N_{Re} = 1.475 \times 10^5$	α = 15,20,25 deg.		Fig. 29-31

2.

a.	X/W vs. D/W	jet width = 2.62 in.	$N_{Re} = 2.05 \times 10^5$	α = 15,20,25 deg.		Fig. 32
b.	X/W vs. D/W	jet width = 1.31 in.	$N_{Re} = 1.475 \times 10^5$	α = 15,20,25 deg.		Fig. 33

3.

a.	X/W vs. α	jet width = 2.62 in.	$N_{Re} = 2.05 \times 10^5$	D/W =	00=0.0, 01=.18, 02=.36, 03=.56, 04=.74, 05=.94	Fig. 34
b.	X/W vs. α	jet width = 1.31 in.	$N_{Re} = 1.475 \times 10^5$	D/W =	00=0.0, 01=.36, 02=.74, 03=1.12, 04=1.48, 05=1.94	Fig. 35

4.

a.	$\dot{m}/\dot{m}_o$ vs. D/W	jet width = 2.62 in.	$N_{Re} = 2.05 \times 10^5$	α	as in 2.a. above	Fig. 36
b.	$\dot{m}/\dot{m}_o$ vs. D/W	jet width = 1.31 in.	$N_{Re} = 1.475 \times 10^5$	α	as in 2.b. above	Fig. 37

5.

a.	$\dot{m}/\dot{m}_o$ vs. α	jet width = 2.62 in.	$N_{Re} = 2.05 \times 10^5$	D/W	as in 3.a. above	Fig. 38
b.	$\dot{m}/\dot{m}_o$ vs. α	jet width = 1.31 in.	$N_{Re} = 1.475 \times 10^5$	D/W	as in 3.b. above	Fig. 39

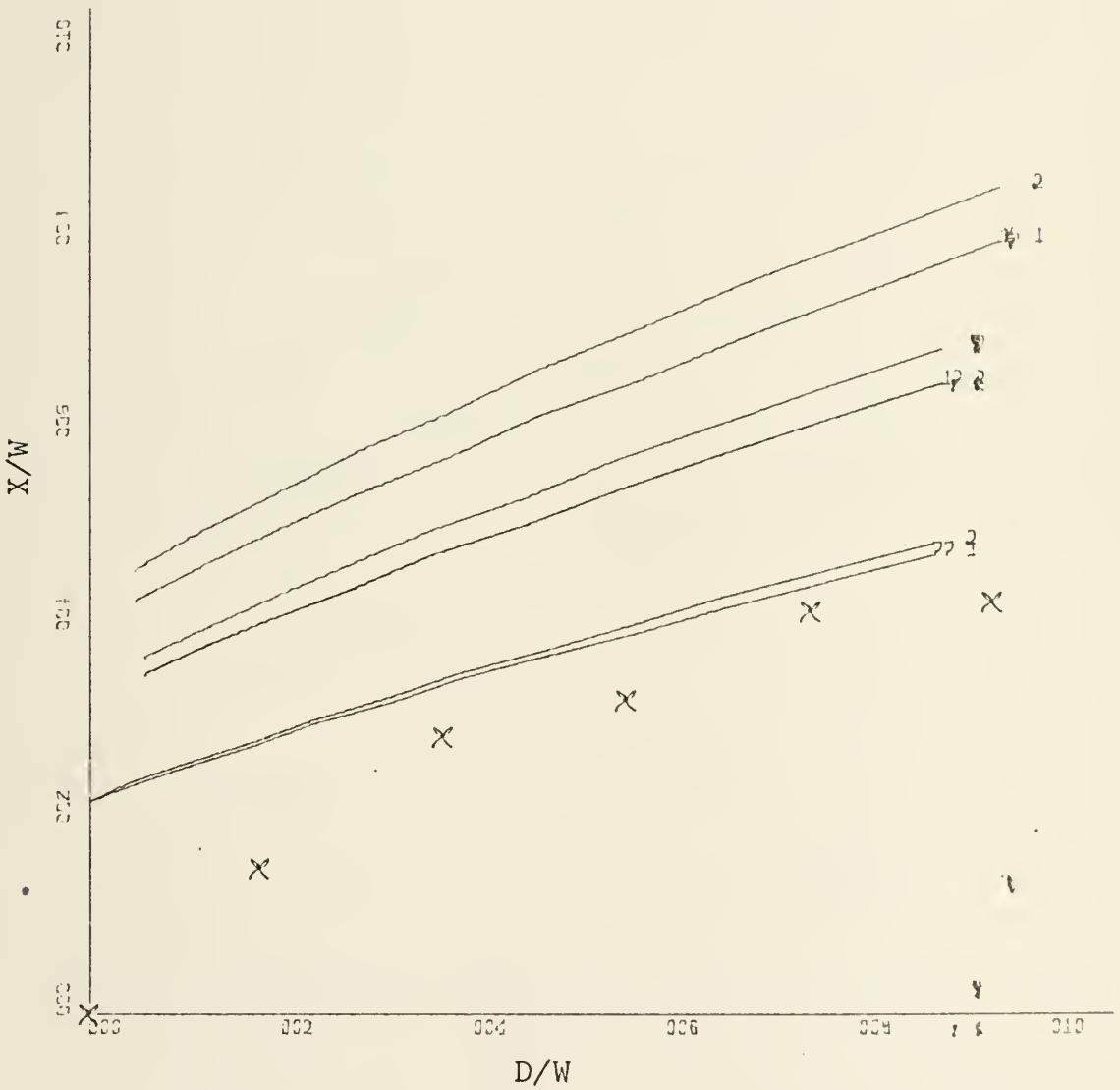

Figure 26. Attachment Distance vs. Offset Distance for a Convex Wall at 15 Degrees Incidence using Methods One(1) and Two(2) and Comparing With Experimental Data, Jet Width 2.62 inches, Re = 2.05×10^5, σ = 7.7, 12, 15.

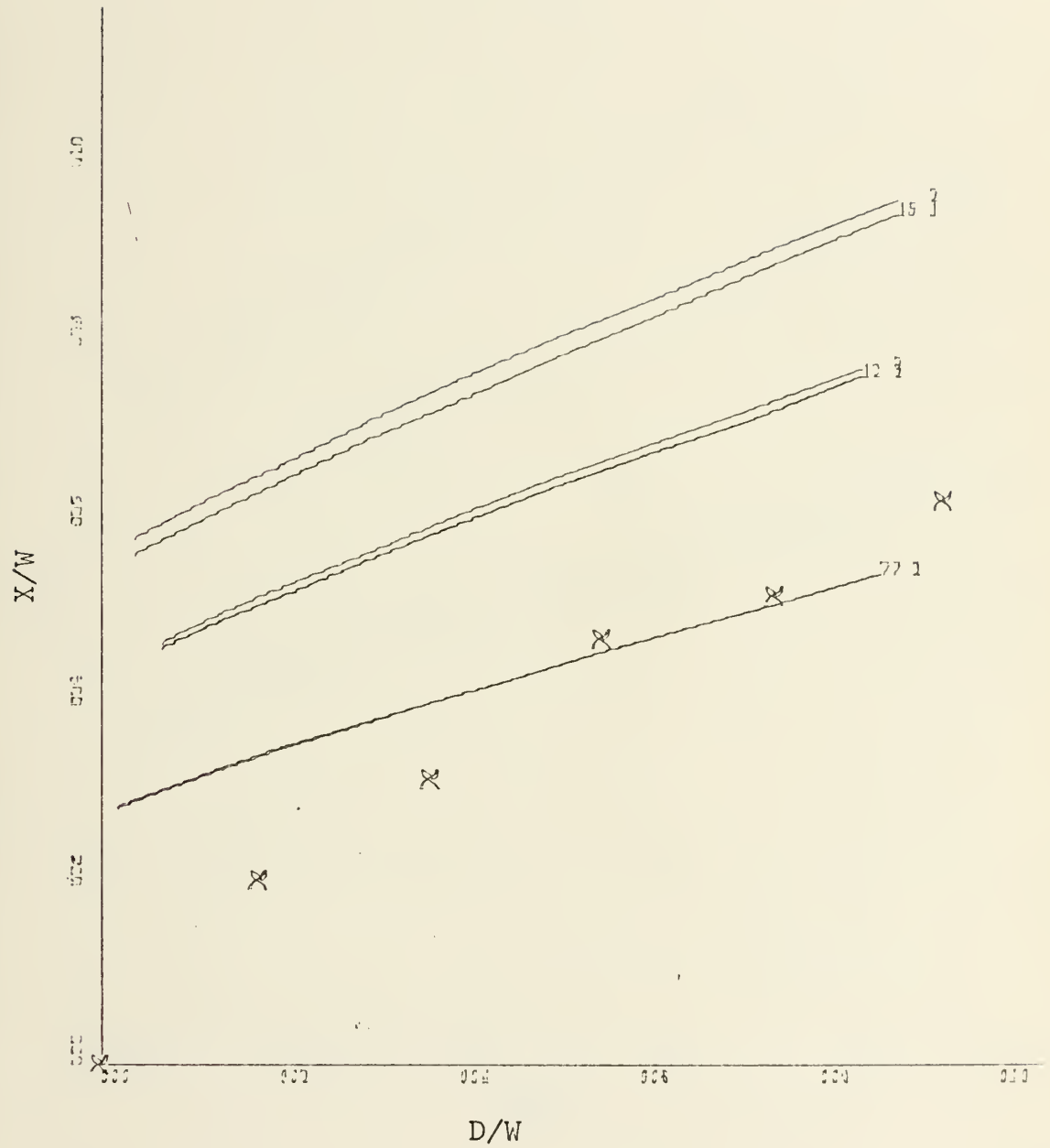

Figure 27. Attachment Distance vs. Offset Distance for a Convex Wall at 20 Degrees Incidence using Methods One(1) and Two(2) and Comparing with Experimental Data, Jet Width 2.62 inches, Re = 2.05 x 10^5, σ = 7.7, 12, 15.

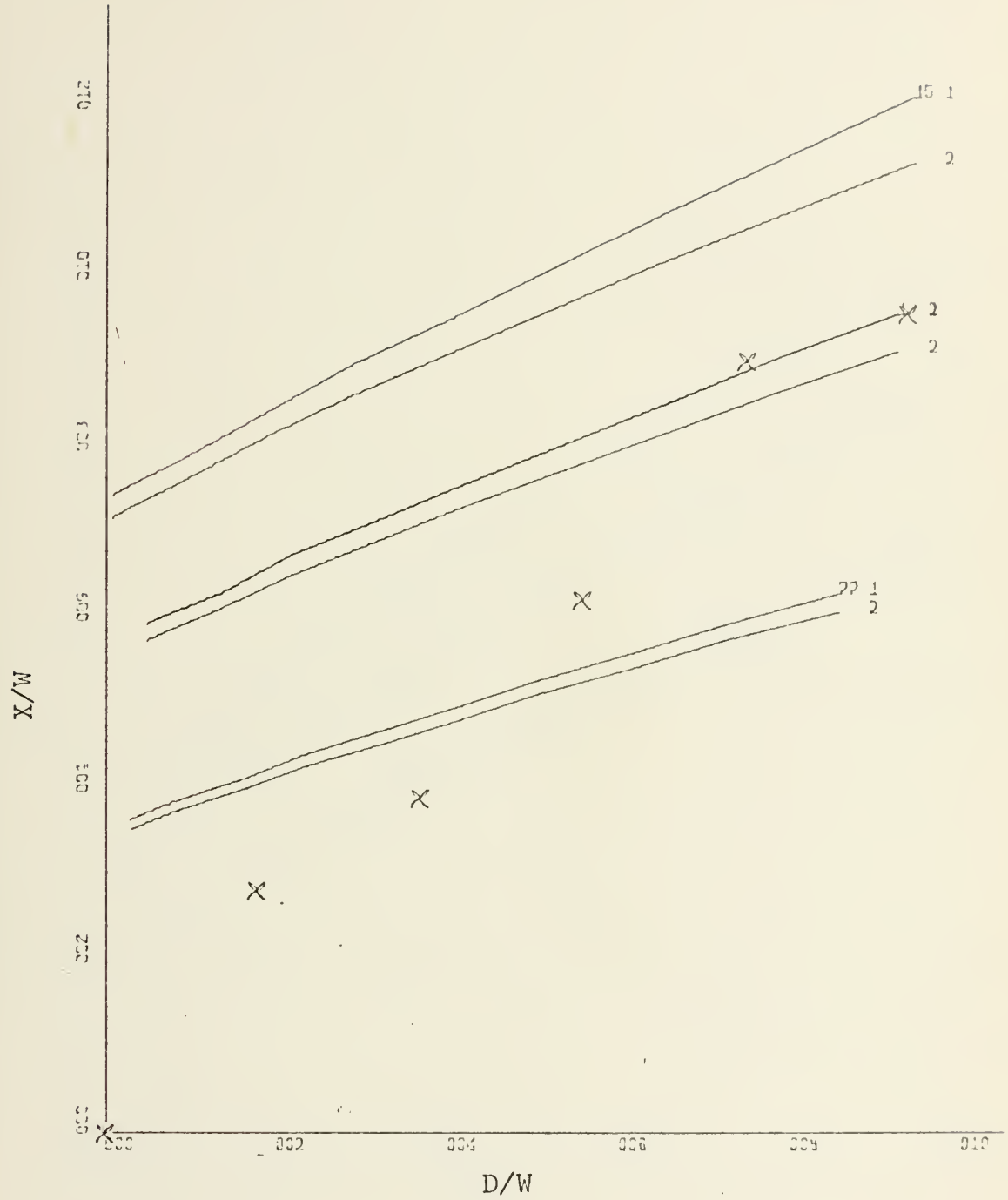

Figure 28. Attachment Distance vs. Offset Distance for a Convex Wall at 25 Degrees Incidence using Methods One(1) and Two (2) and Comparing with Experimental Data, Jet Width 2.62 inches, Re = 2.05 x 10^5, σ = 7.7, 12, 15.

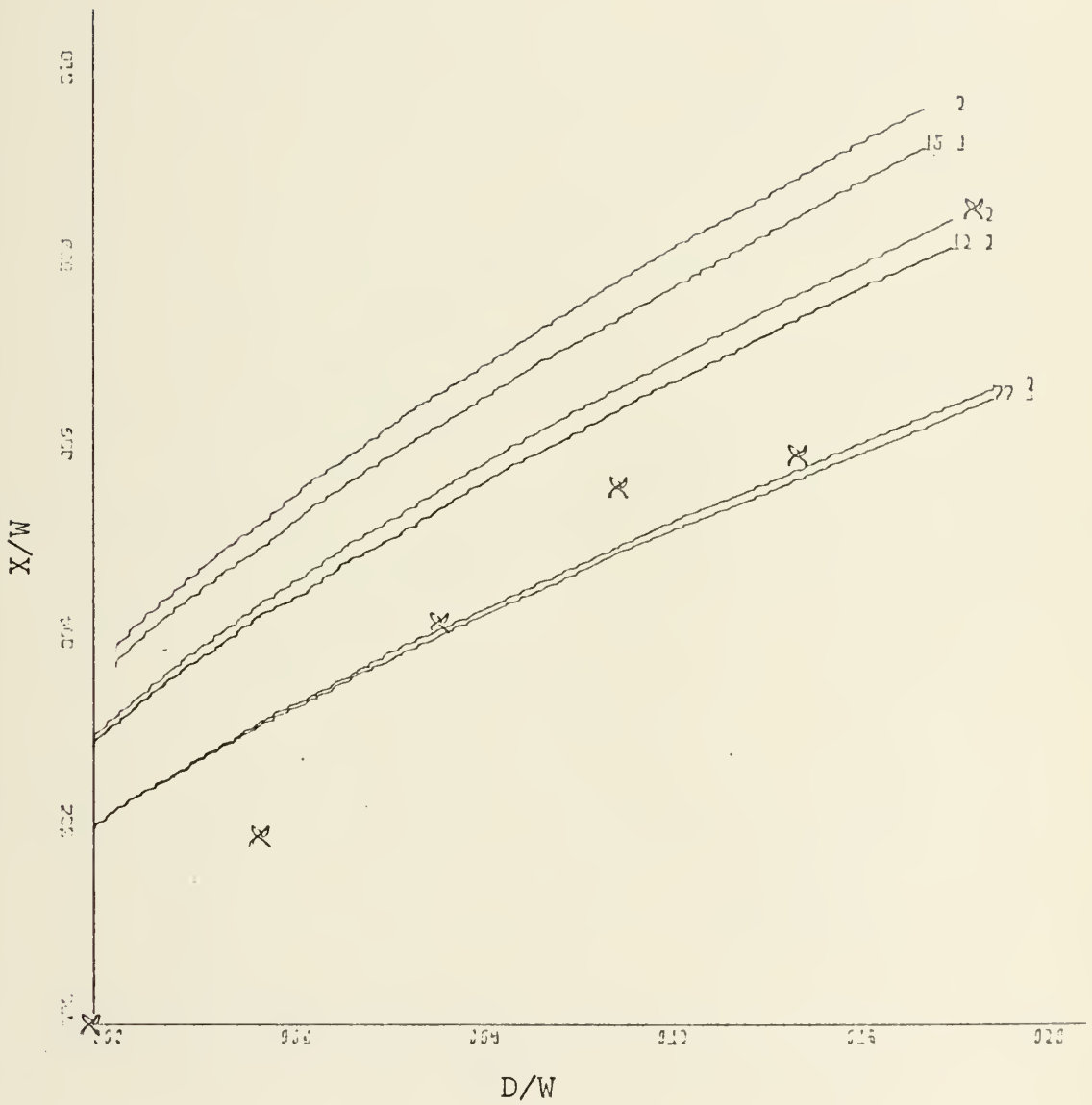

Figure 29. Attachment Distance vs. Offset Distance for a Convex Wall at 15 Degrees Incidence using Methods One(1) and Two(2) and Comparing with Experimental Data, Jet Width 1.31, Re = 1.475×10^5, σ = 7.7, 12, 15.

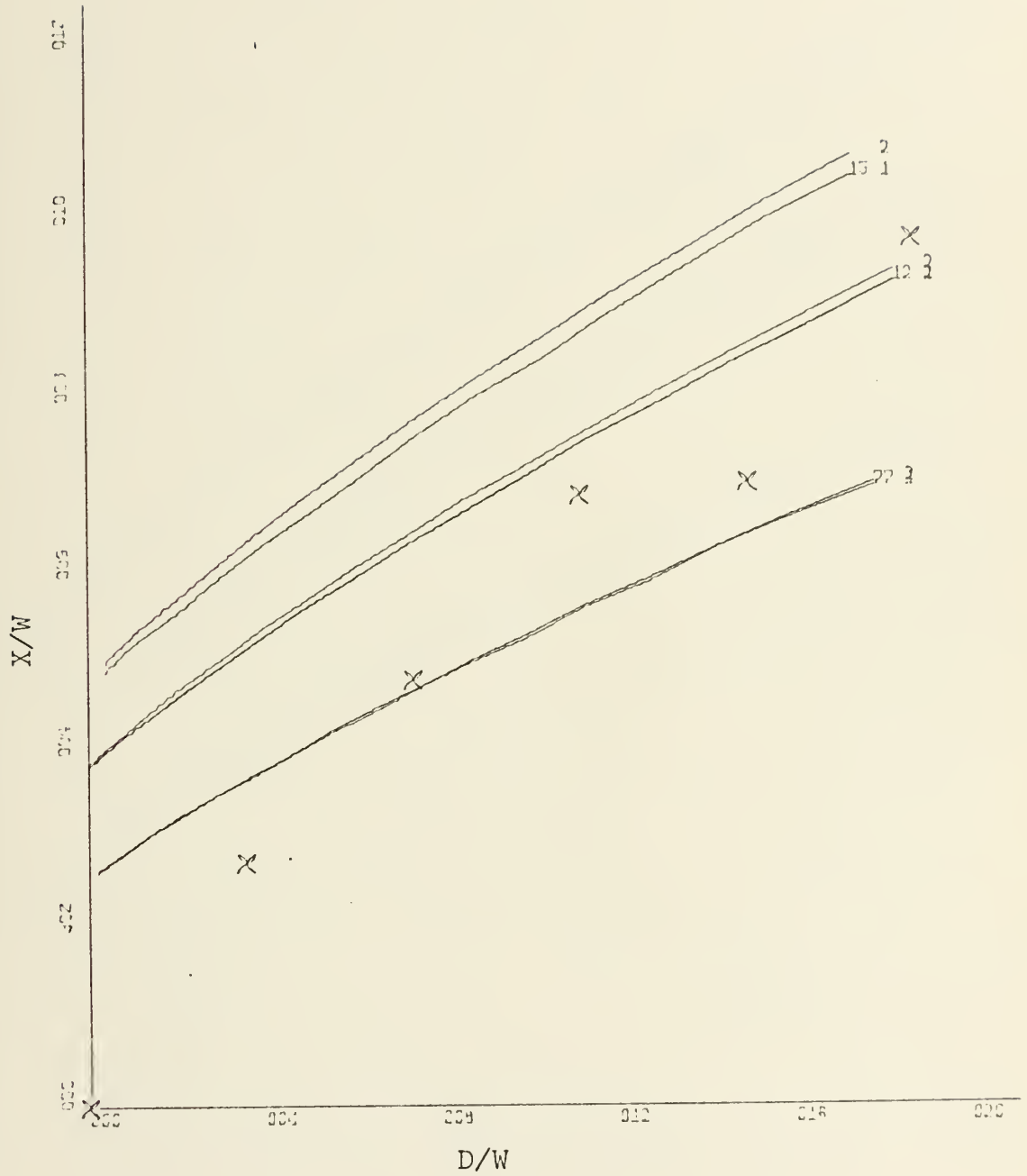

Figure 30. Attachment Distance vs. Offset Distance for a Convex Wall at 20 Degrees Incidence uisng Methods One(1) and Two(2), and Comparing with Experimental Data, Jet Width 1.31, Re = 1.475×10^5, σ = 7.7, 12, 15.

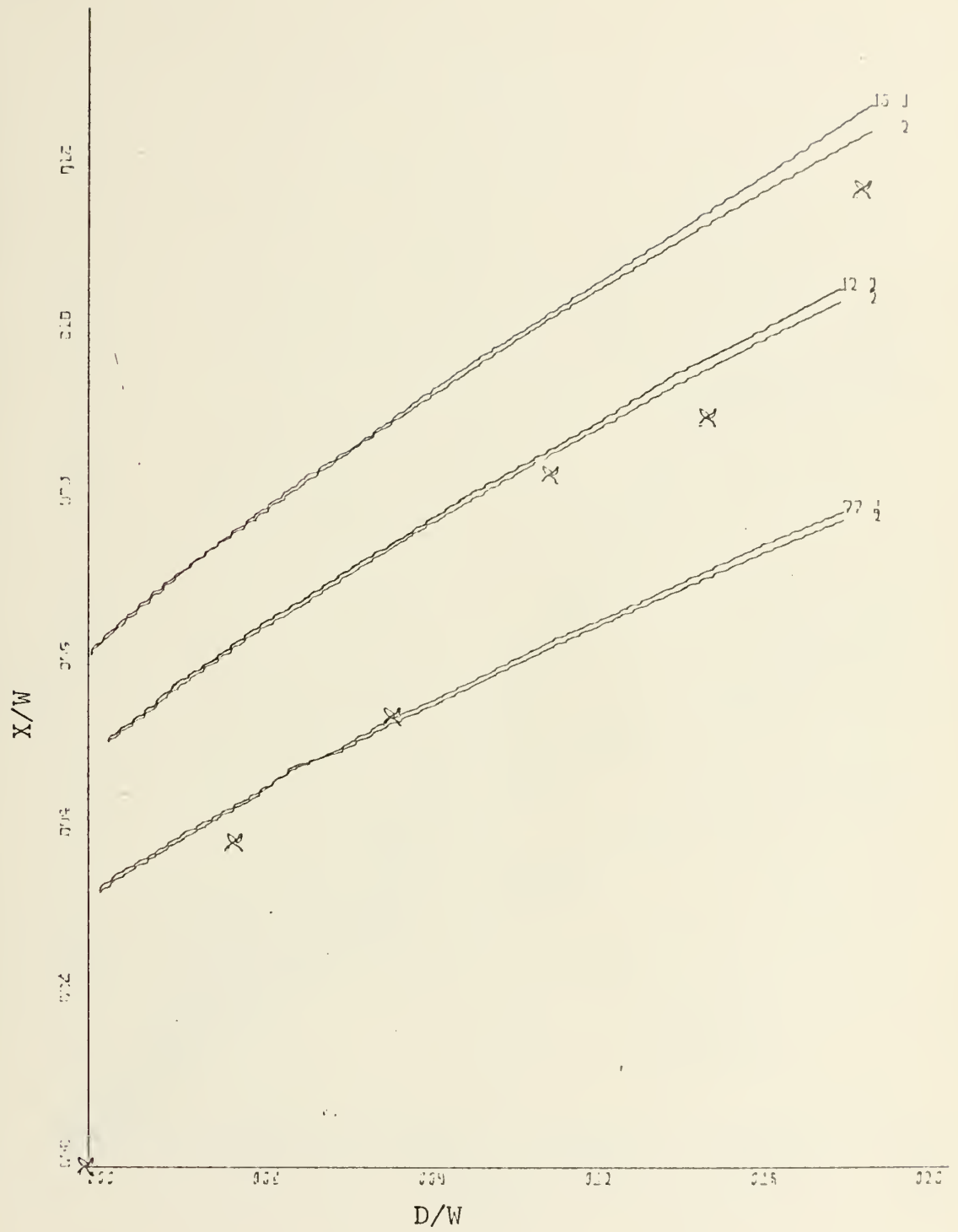

Figure 31. Attachment Distance vs. Offset Distance for a Convex Wall, at 25 Degrees Incidence using Methods One(1) and Two(2), and Comparing with Experimental data, Jet Width 1.31, Re = 1.475×10^5, σ = 7.7, 12, 15.

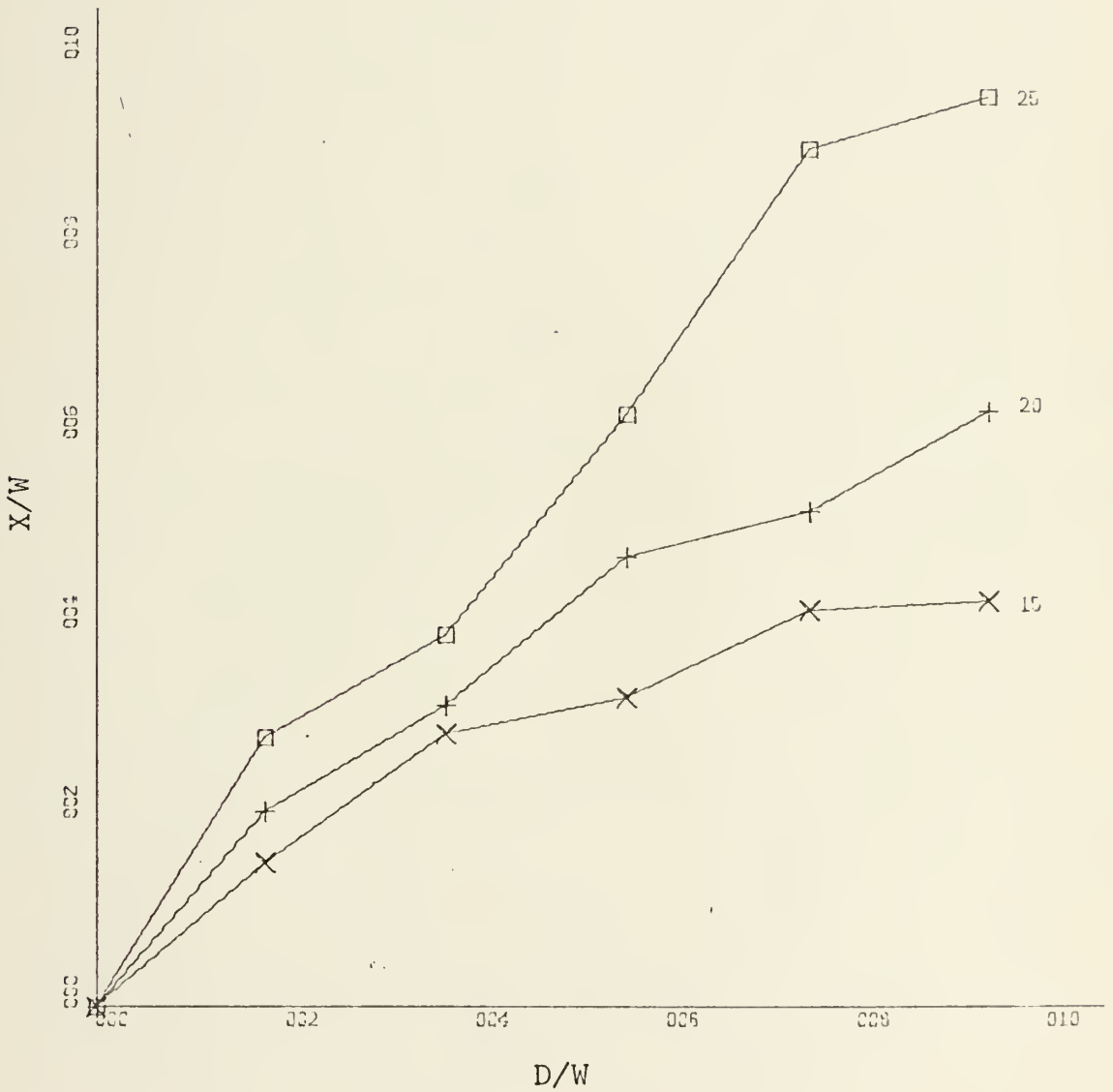

Figure 32. Attachment Distance vs. Offset Distance for Convex Wall, Re = 2.05 x 10^5, Constant Deflection Angles, and Jet Width of 2.62 inches, α = 15, 20, 25 degrees.

Figure 33. Attachment Distance vs. Offset Distance for Convex Wall, Re = 1.475×10^5, Consant Deflection Angles, and Jet Width of 1.31 inches, α = 15, 20, 25 degrees.

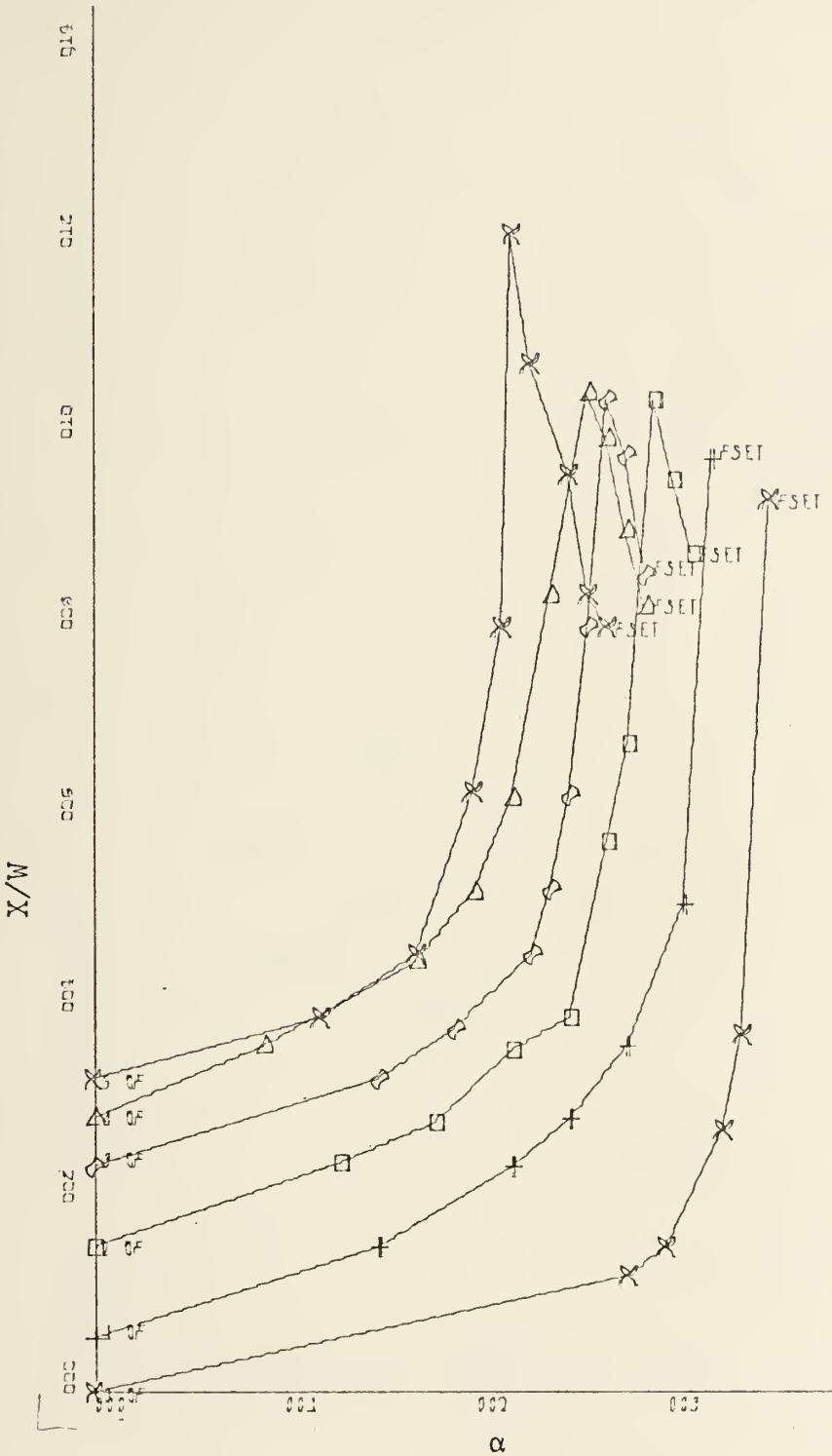

Figure 34. Attachment Distance vs. Deflection Angle for Various Offset Distances, Jet Width of 2.62 inches, Convex Wall, Re = 2.05 x 10^5, D/W of 00, 01, 02, 03, 04, 05.

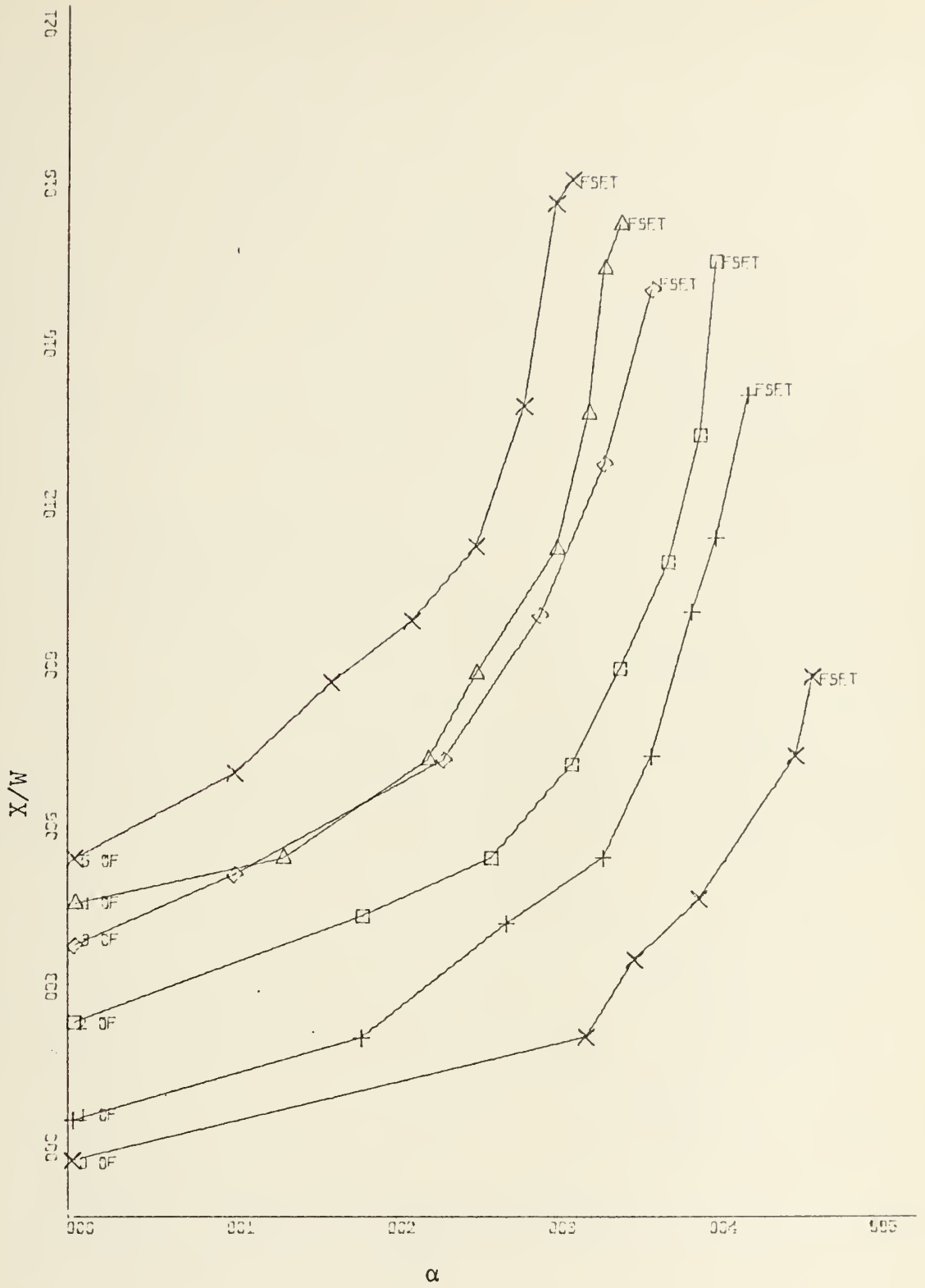

Figure 35. Attachment Distance vs. Deflection Angle for Jet Width of 1.31 inches, Convex Wall, Re = 1.475×10^5, D/W of 00, 01, 02, 03, 04, 05.

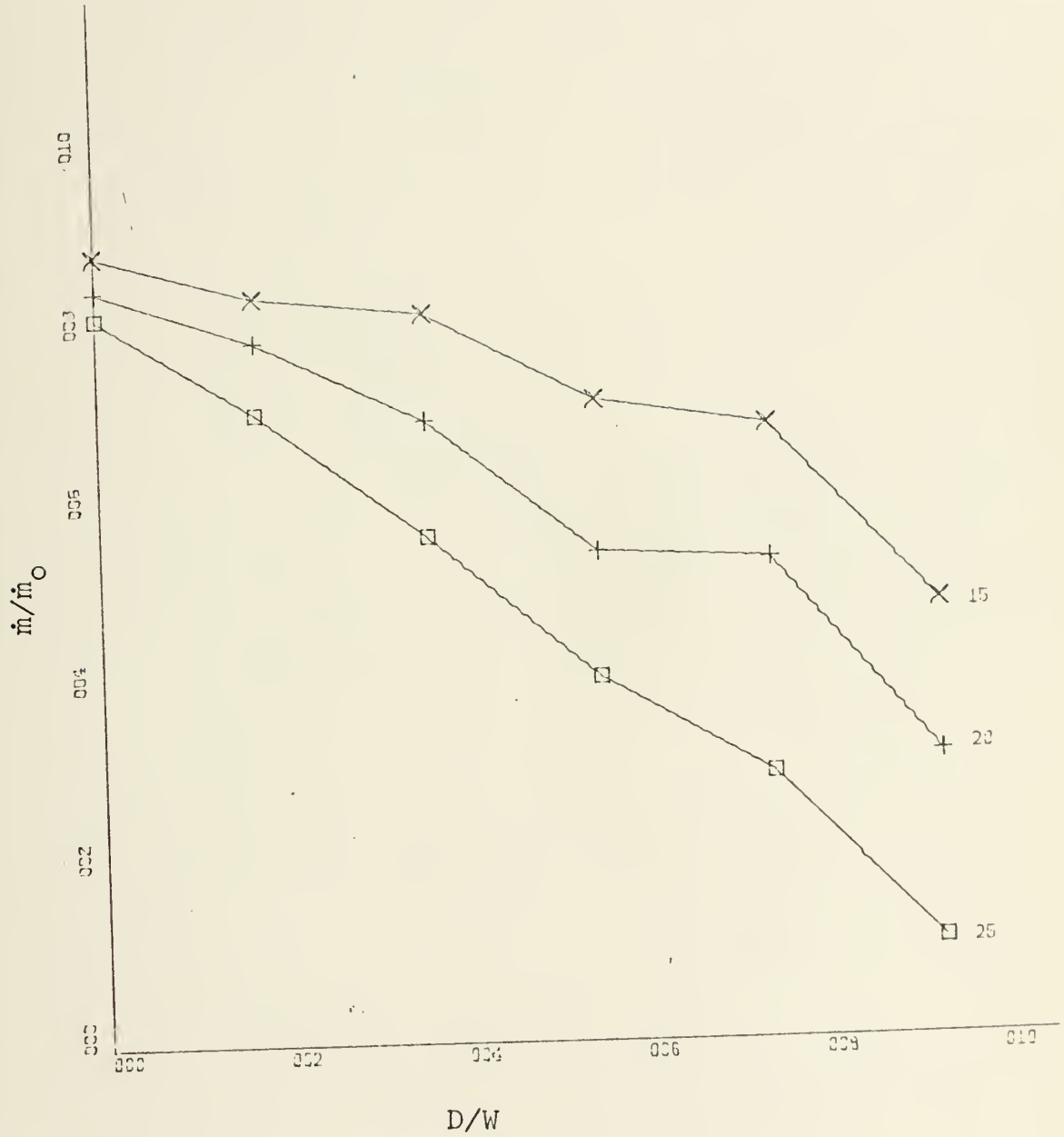

Figure 36. Flow Rate vs. Offset Distance for Convex Wall at Constant Deflection Angles, Jet Width = 2.62 inches, Re = 2.05 x 10^5, α = 15, 20, 25 degrees.

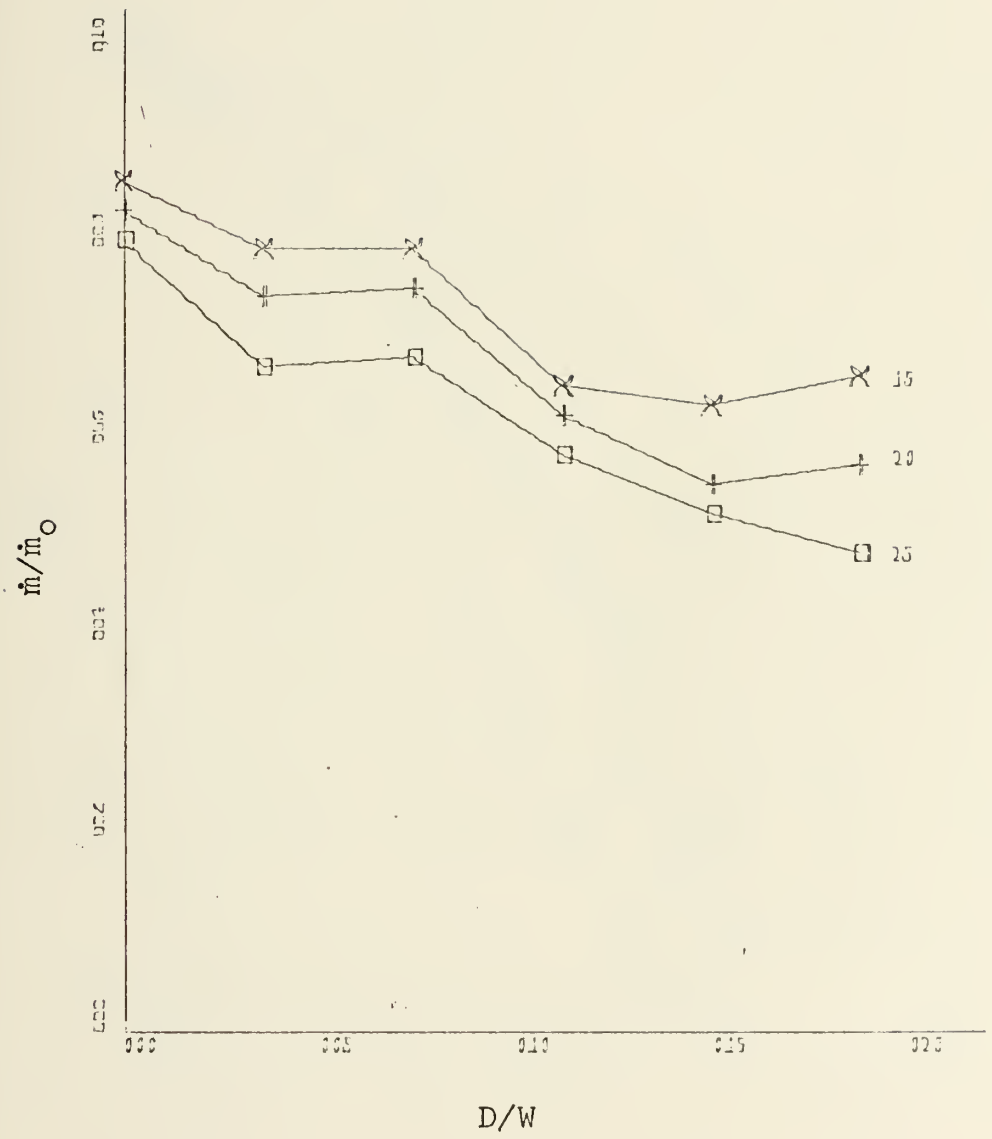

Figure 37. Flow Rate vs. Offset Distance for Convex Wall at Constant Deflection Angles, Jet Width = 1.31 inches, Re = 1.475×10^5, α = 15, 20, 25 degrees.

Figure 38. Flow Rate vs. Deflection Angle at Various Offset Distances for Convex Wall, Re = 2.05 x 10^5, Jet Width = 2.62 inches, D/W of 00, 01, 02, 03, 04, 05.

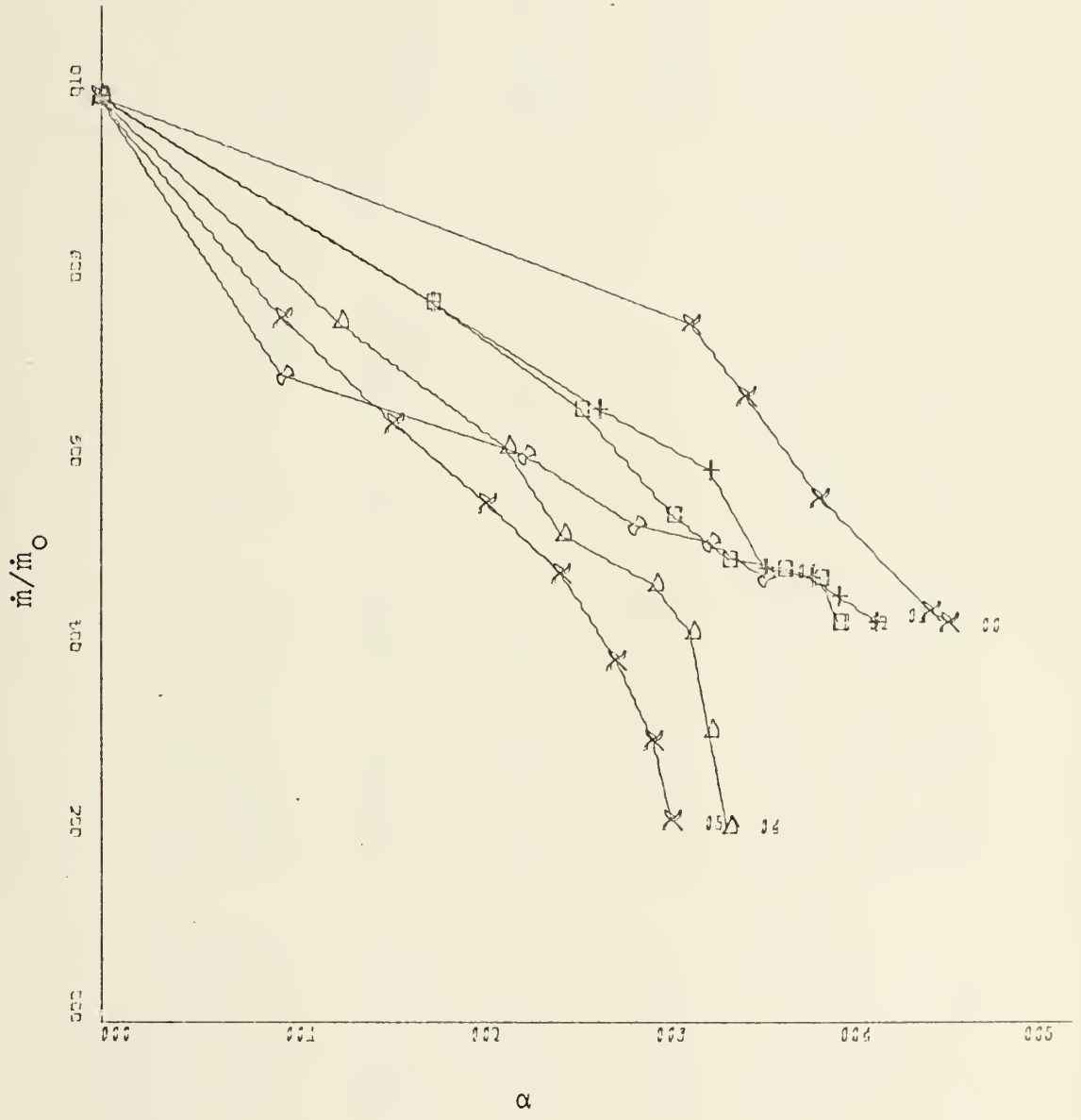

Figure 39. Flow Rate vs. Deflection Angle at Various Offset Distances for Convex Wall, Re = 14.75 x 10^5, Jet Width of 1.31 inches, D/W of 00, 01, 02, 03, 04, 05.

OUTLINE OF DATA PRESENTATION III.

A. Concave Wall.

1. Comparison with theoretical calculations

a.	X/W vs. D/W	jet width = 2.62 in.	$N_{Re} = 2.05 \times 10^5$	α = 15,20,25 deg.		Fig. 40-42
b.	X/W vs. D/W	jet width = 1.31 in.	$N_{Re} = 1.475 \times 10^5$	α = 15,20,25 deg.		Fig. 43-45

2.

a.	X/W vs. D/W	jet width = 2.62 in.	$N_{Re} = 2.05 \times 10^5$	D/W = 15,20,25,30 deg.		Fig. 46
b.	X/W vs. D/W	jet width = 1.31 in.	$N_{Re} = 1.475 \times 10^5$	α = 15,20,25,30 deg.		Fig. 47

3.

a.	X/W vs. α	jet width = 2.62 in.	$N_{Re} = 2.05 \times 10^5$	D/W =	00=0.0, 01=0.18, 02=0.36, 03=0.56, 04=0.74, 05=0.94	Fig. 48
b.	X/W vs. α	jet width = 1.31 in.	$N_{Re} = 1.475 \times 10^5$	D/W =	00=0.0, 01=.36, 02=.74, 03=1.12, 04=1.48, 05=1.88	Fig. 49

4.

a.	$\dot{m}/\dot{m}_o$ vs. D/W	jet width = 2.62 in.	$N_{Re} = 2.05 \times 10^5$	α	as in 2.a. above	Fig. 50
b.	$\dot{m}/\dot{m}_o$ vs. D/W	jet width = 1.31 in.	$N_{Re} = 1.475 \times 10^5$	α	as in 2.b. above	Fig. 51

5.

a.	$\dot{m}/\dot{m}_o$ vs. α	jet width = 2.62 in.	$N_{Re} = 2.05 \times 10^5$	D/W	as in 3.a. above	Fig. 52
b.	$\dot{m}/\dot{m}_o$ vs. α	jet width = 1.31 in.	$N_{Re} = 1.475 \times 10^5$	D/W	as in 3.b. above	Fig. 53

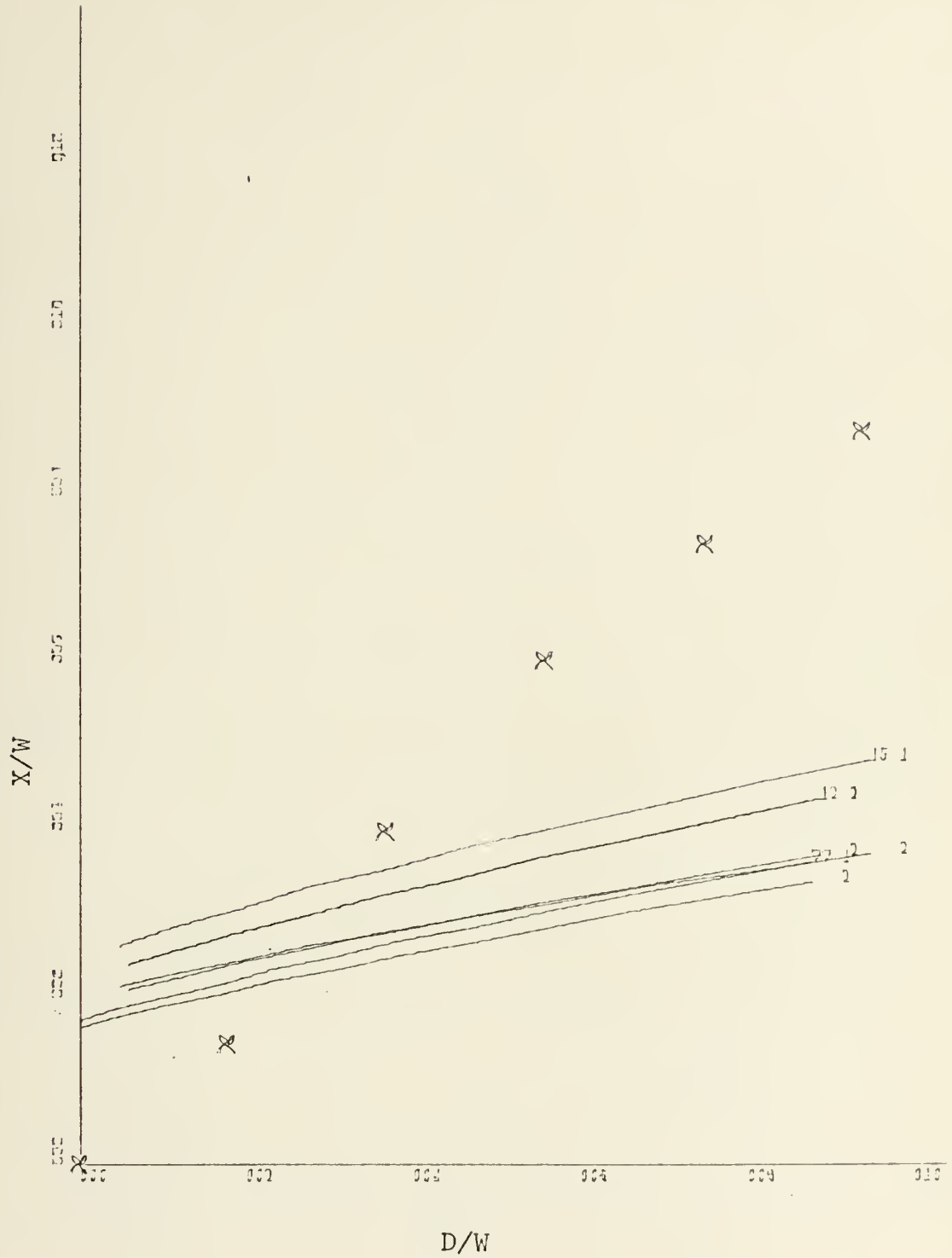

Figure 40. Attachment Distance vs. Offset Distance for a Concave Wall at 15 Degrees Incidence using Methods One(1) and Two(2) and Comparing with Experimental Data, Jet Width 2.62 inches, Re = 2.05×10^5, σ = 7.7, 12, 15.

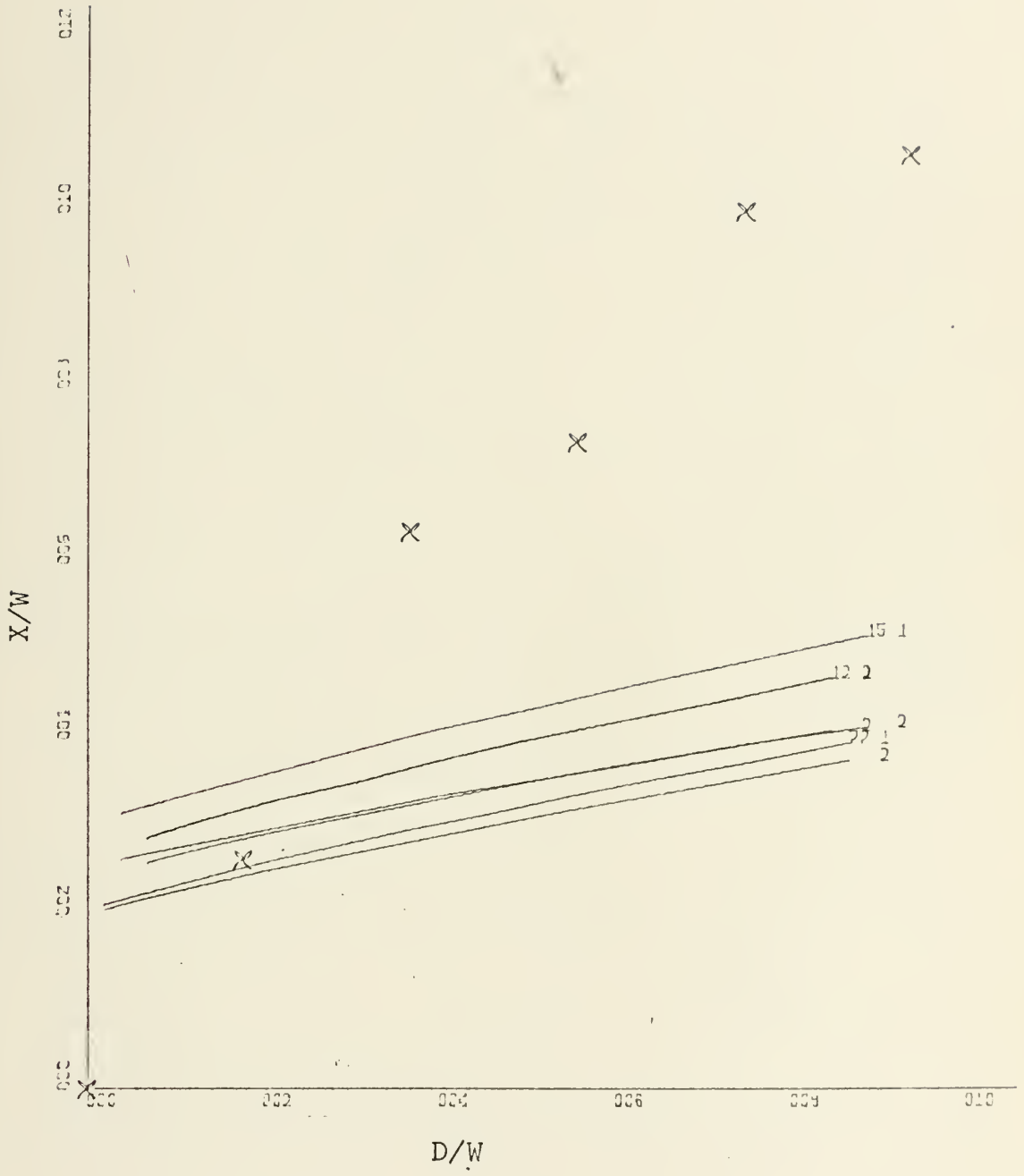

Figure 41. Attachment Distance vs. Offset Distance for a Concave Wall at 20 Degrees Incidence using Methods One(1) and Two(2) and Comparing with Experimental Data, Jet Width 2.62, Re = 2.05×10^5, σ = 7.7, 12, 15.

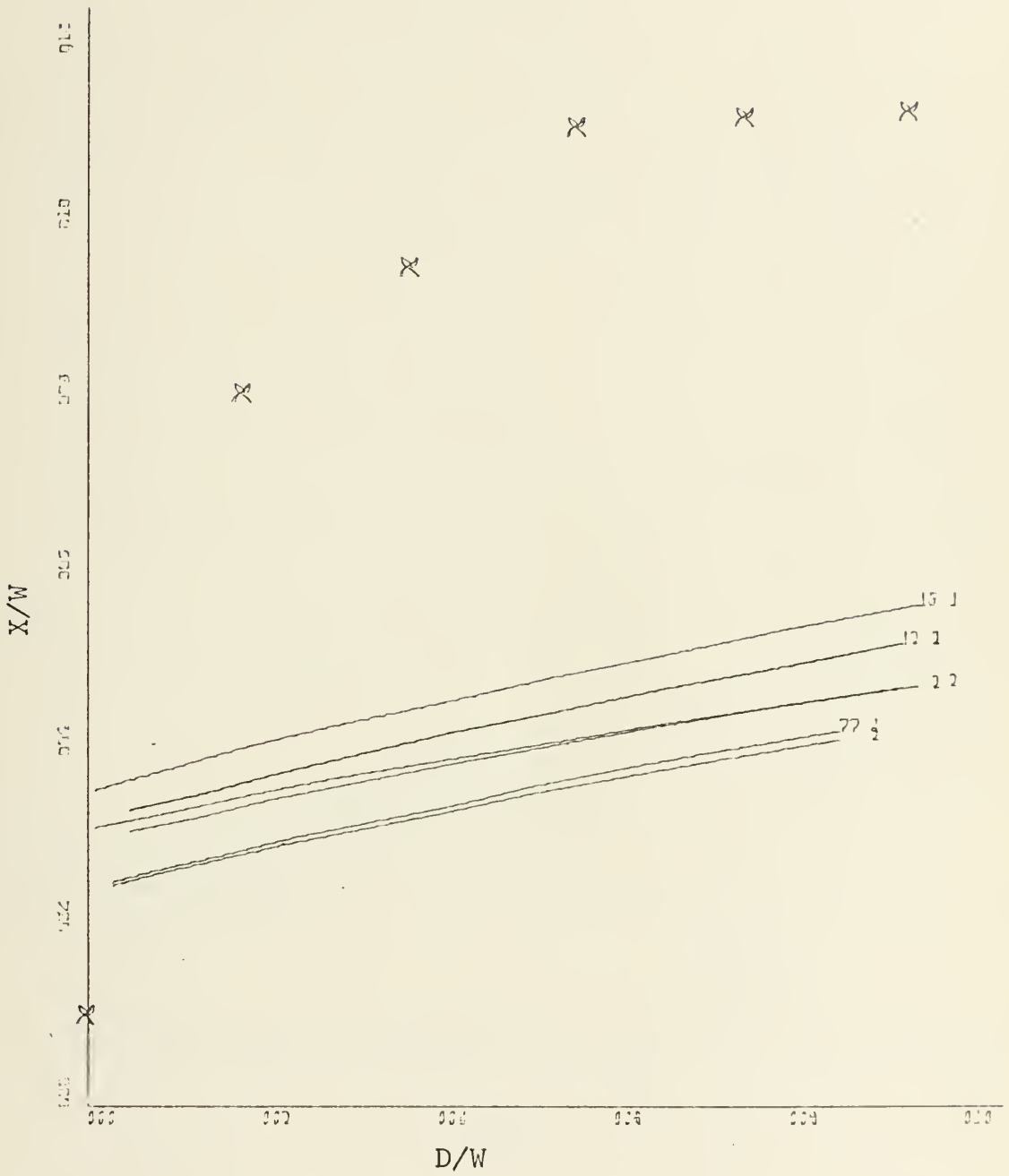

Figure 42. Attachment Distance vs. Offset Distance for a Concave Wall at 25 Degrees Incidence Using Methods One(1) and Two(2) and Comparing With Experimental Data, Jet Width 2.62 Inches, Re = 2.05×10^5, σ = 7.7, 12, 15.

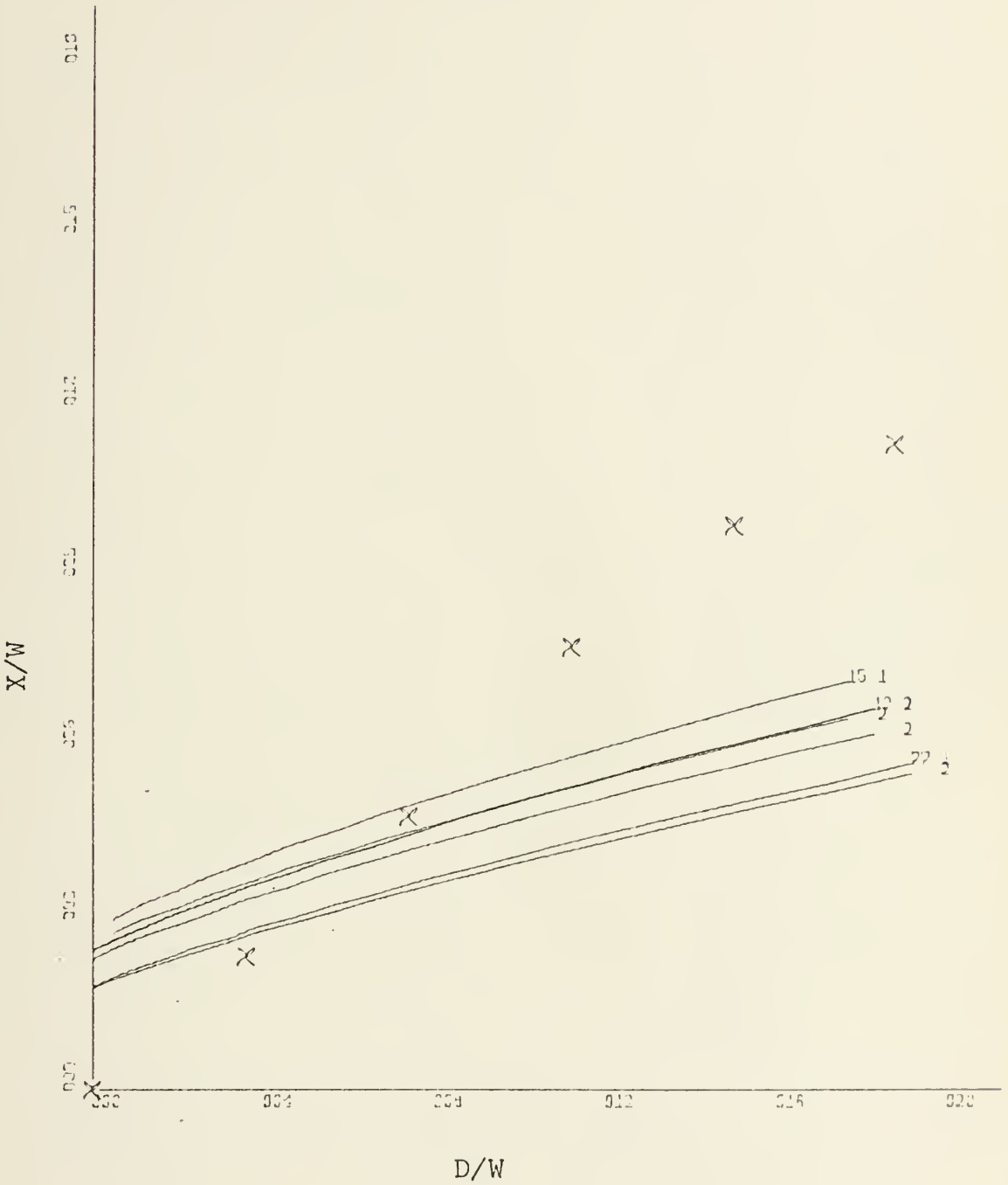

Figure 43. Attachment Distance vs. Offset Distance for a Concave Wall at 15 Degrees Incidence Using Methods One(1) and Two(2) and Comparing With Experimental Data, Jet Width of 1.31 inches, Re = 1.47×10^5, σ = 7.7, 12, 15.

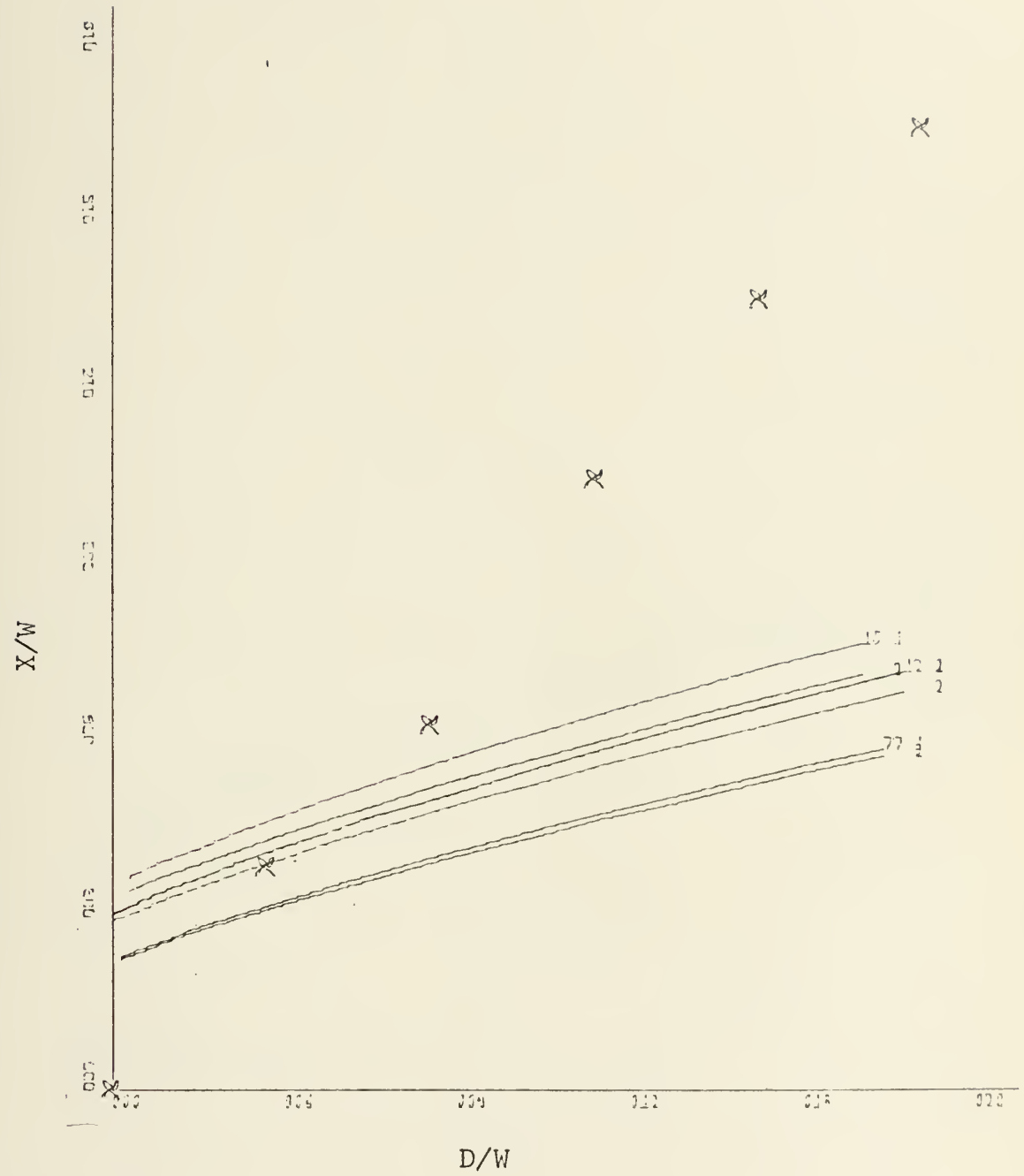

Figure 44. Attachment Distance vs. Offset Distance for a Concave Wall at 20 Degrees Incidence Using Methods One(1) and Two(2) and Comparing With Experimental Data, Jet Width of 1.31 inches, Re = 1.475×10^5, σ = 7.7, 12, 15.

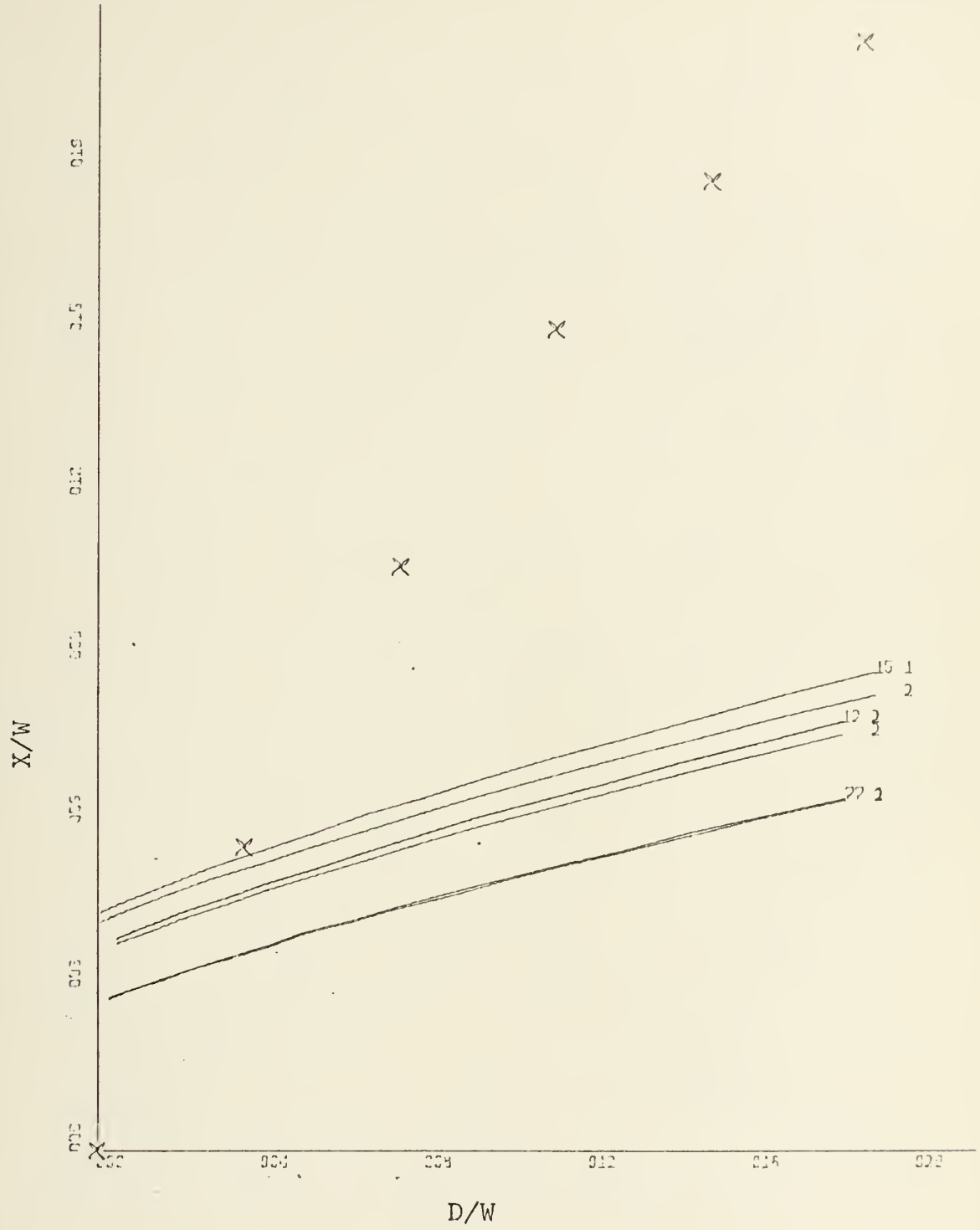

Figure 45. Attachment Distance vs. Offset Distance for a Concave Wall at 25 Degrees Incidence, Using Methods One(1) and Two(2) and Comparing With Experimental Data, Jet Width 1.31 Inches, Re = 1.475×10^5, σ = 7.7, 12, 15.

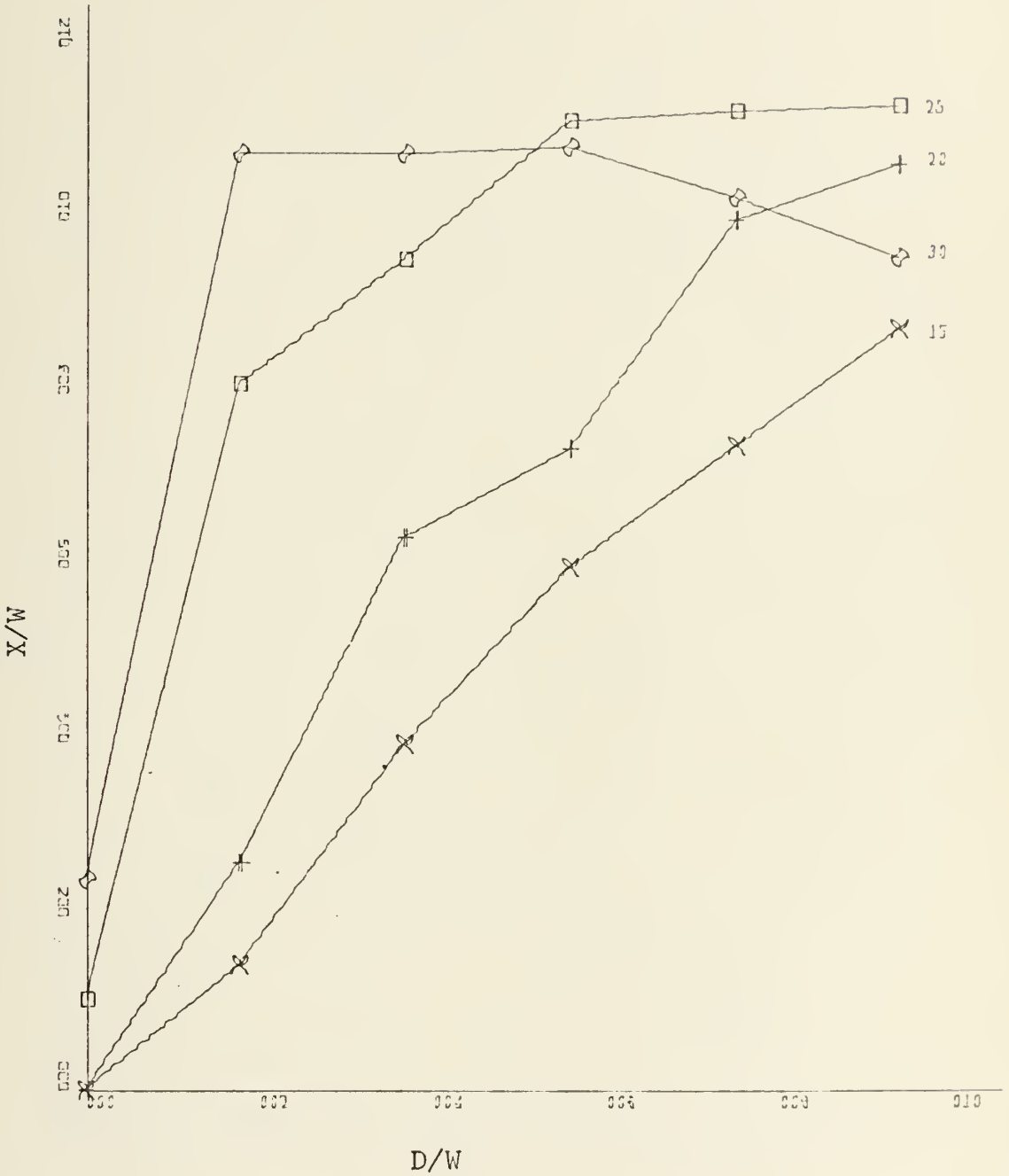

Figure 46. Attachment Distance vs. Offset Distance for Concave Wall, Re = 2.05 x 10^5, Constant Deflection Angles, and Jet Width of 2.62 Inches, α = 15, 20, 25, 30 degrees.

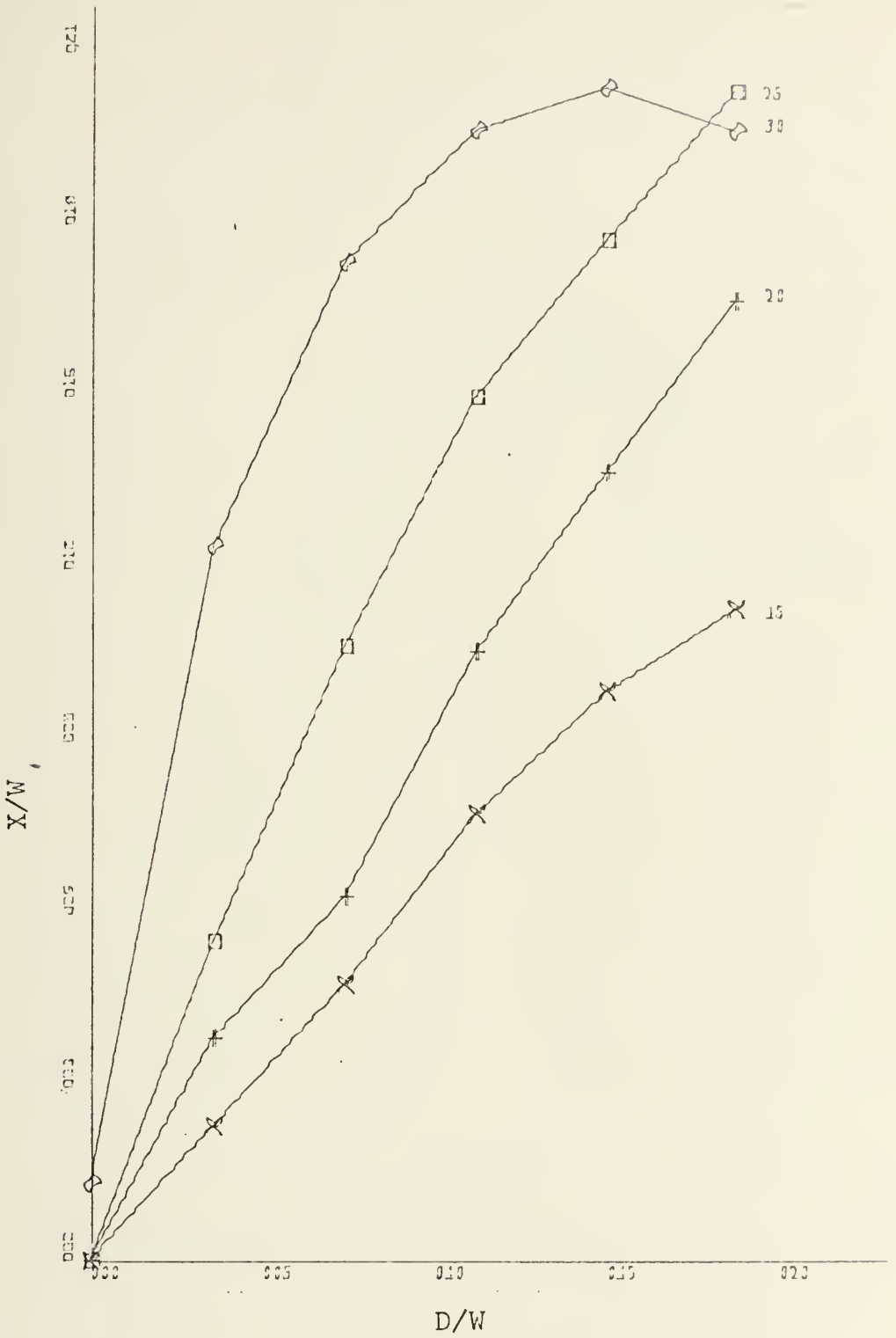

Figure 47. Attachment Distance vs. Offset Distance for Concave Wall, Re = 1.475×10^5, Constant Deflection Angles, and Jet Width of 1.31 inches, α = 15, 20, 25, 30 degrees.

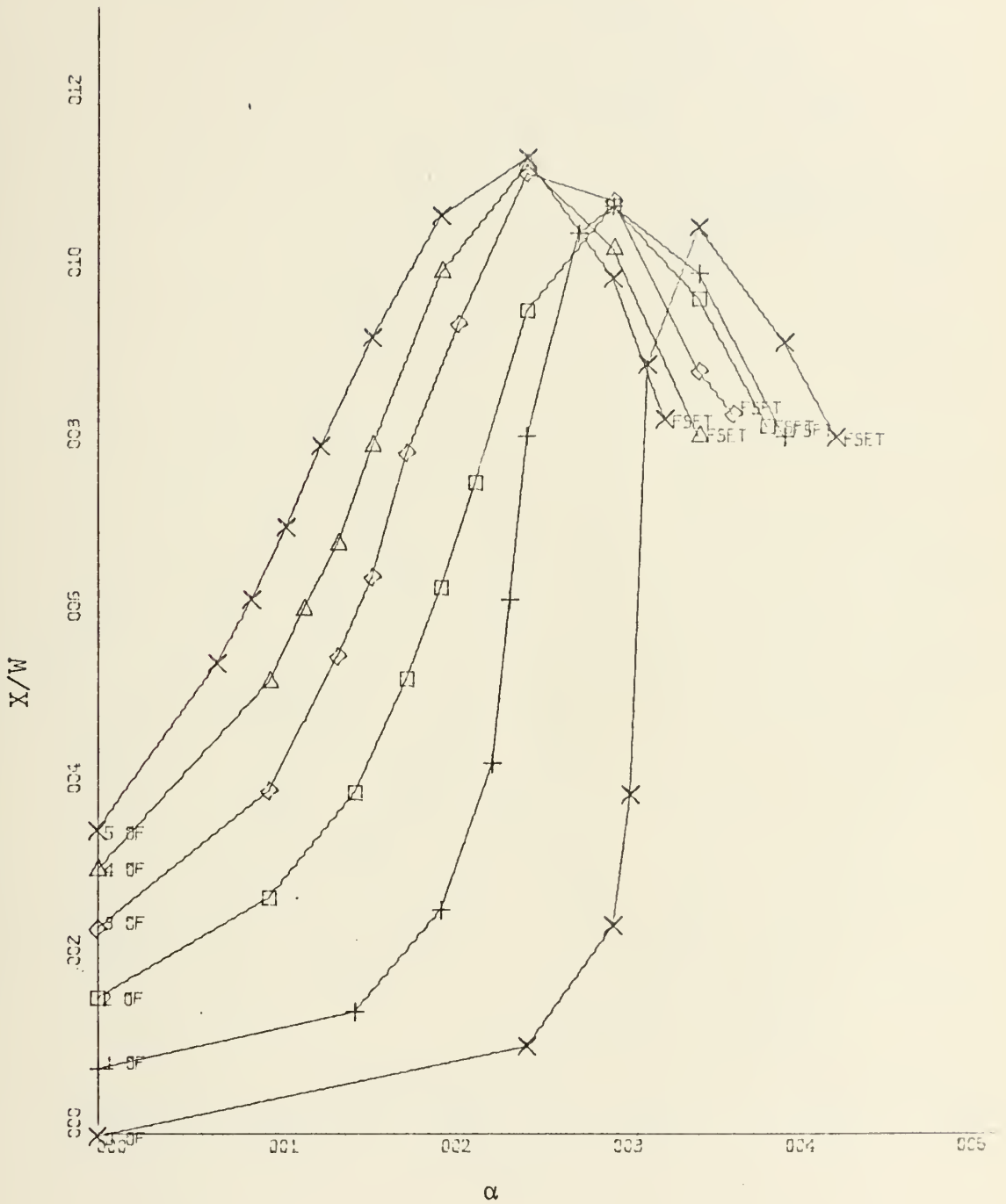

Figure 48. Attachment Distance vs. Deflection Angle for Various Offset Distances, Jet Width of 2.62 inches, Concave Wall, Re = 2.05 x 10^5, D/W of 00, 01, 02, 03, 04, 05.

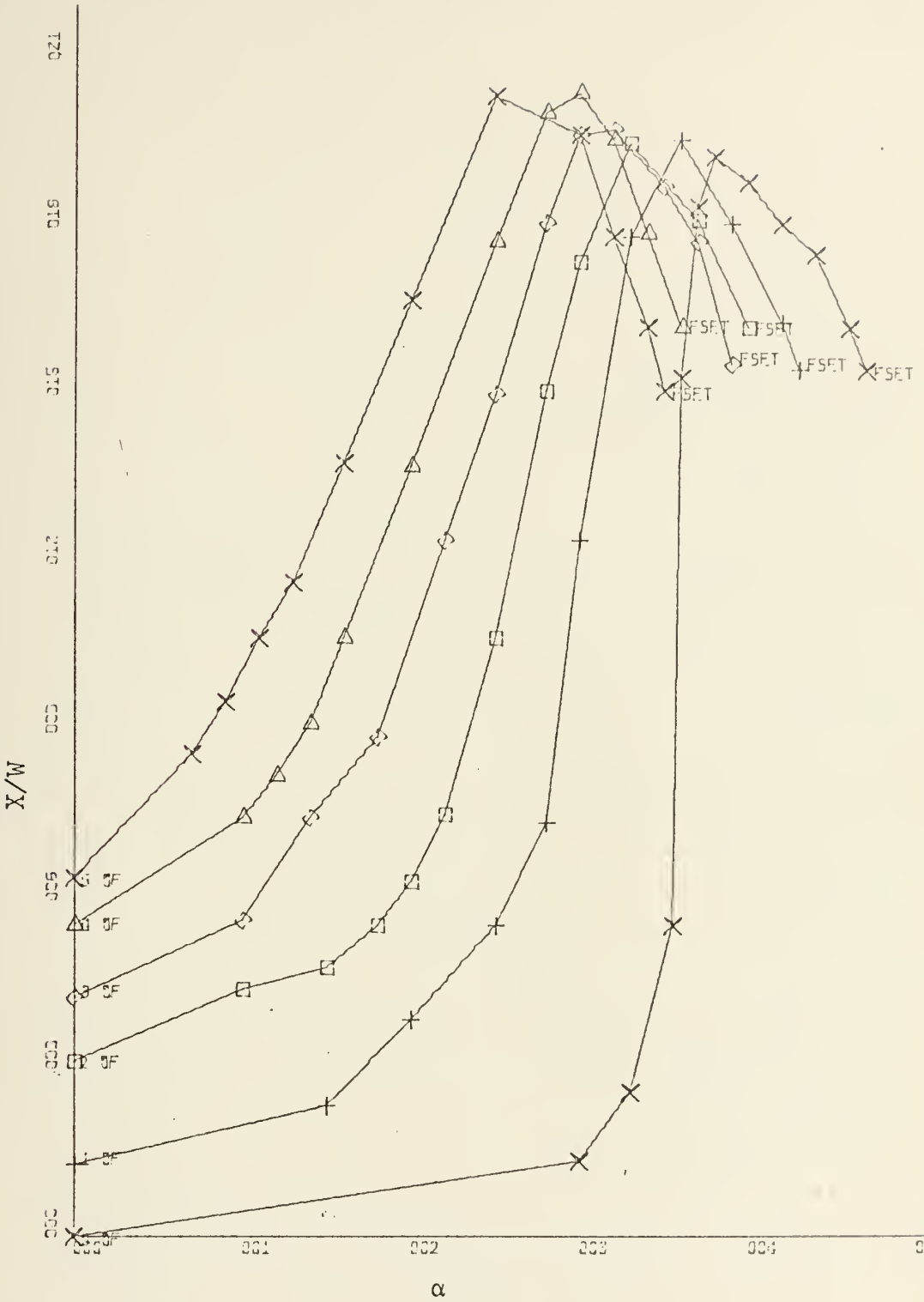

Figure 49. Attachment Distance vs. Deflection Angle for Jet Width of 1.31 Inches, Concave Wall, Re = 1.475×10^5, D/W of 00, 01, 02, 03, 04, 05.

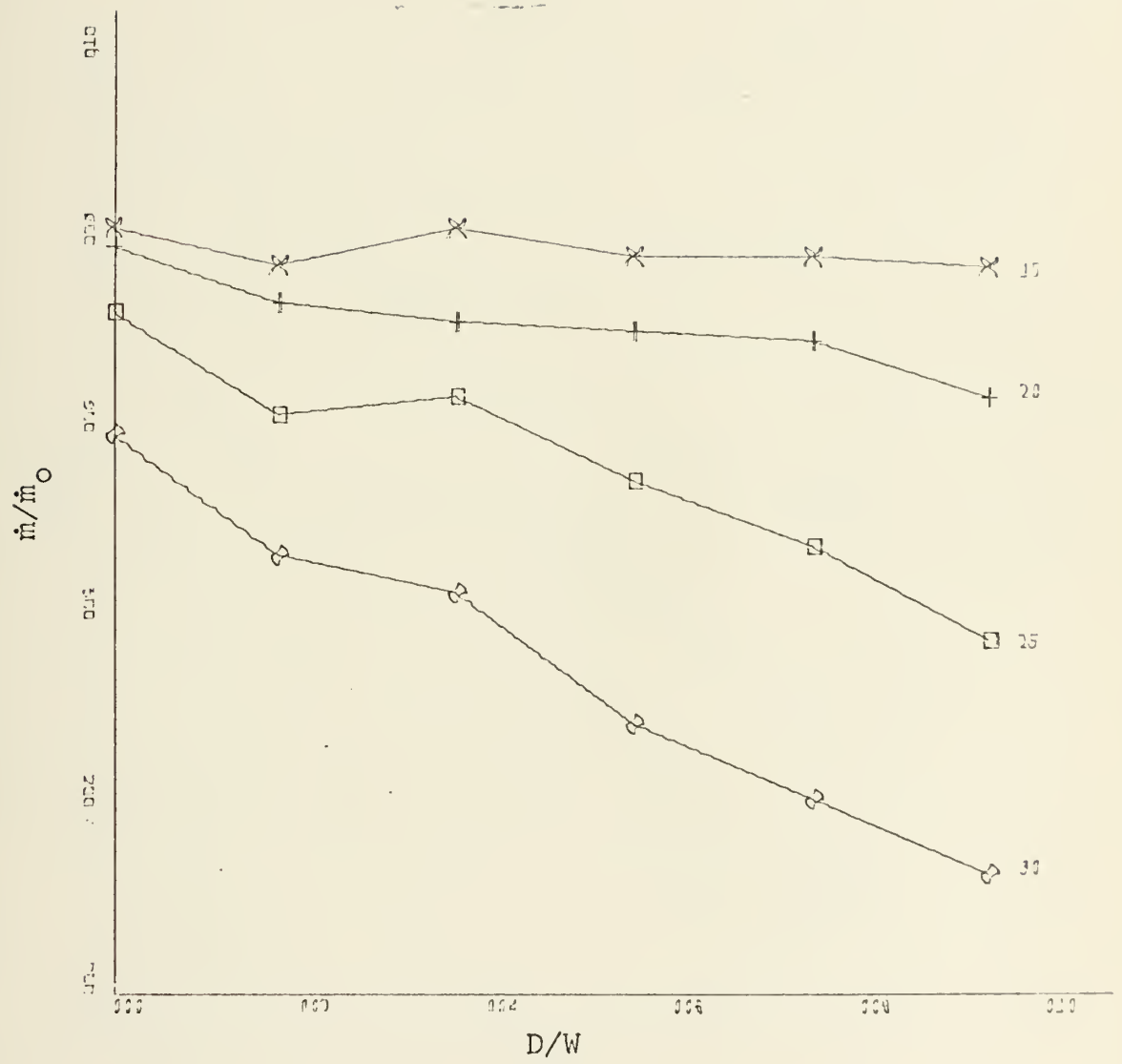

Figure 50. Flow Rate vs. Offset Distance for Concave Wall at Constant Deflection Angles, Jet Width of 2.62 Inches, Re = 2.05 x 10^5, α = 15, 20, 25, 30.

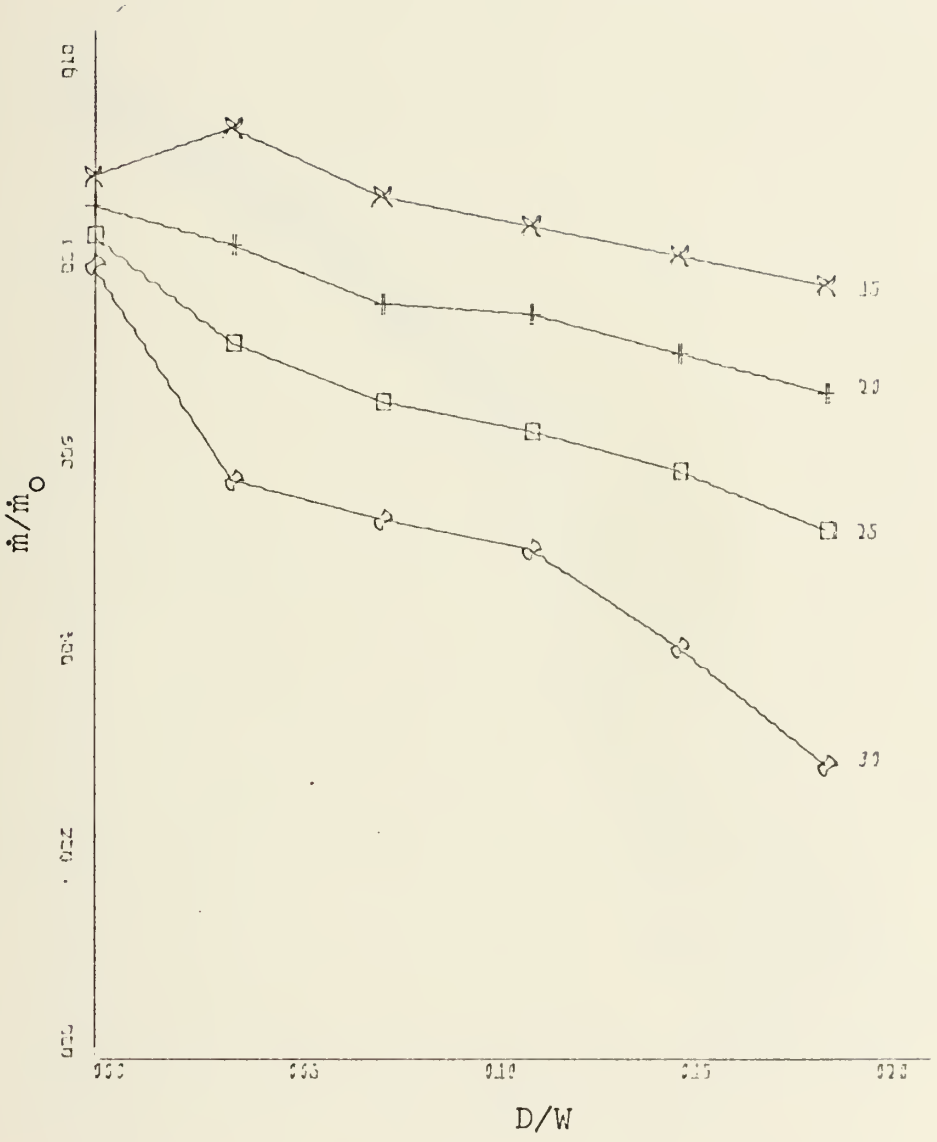

Figure 51. Flow Rate vs. Offset Distance for Concave Wall at Constant Deflection Angles
Jet Width of 1.31 Inches,
Re = 1.475×10^5, α = 15, 20, 25, 30.

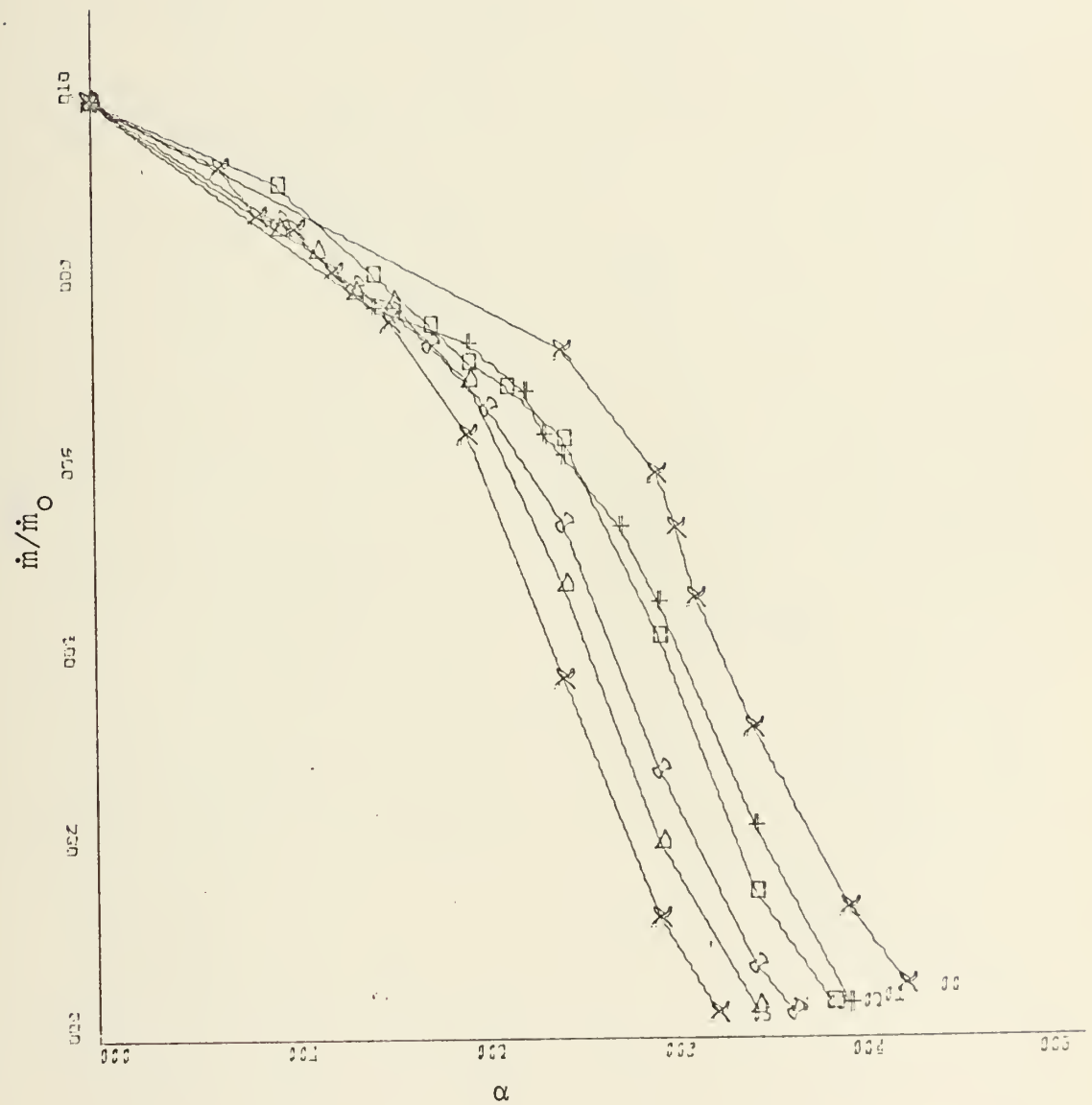

Figure 52. Flow Rate vs. Deflection Angle at Various Offset Distances for Concave Wall, Re = 2.05 x 10^5, Jet Width of 2.62 Inches, D/W of 00, 01, 02, 03, 04, 05.

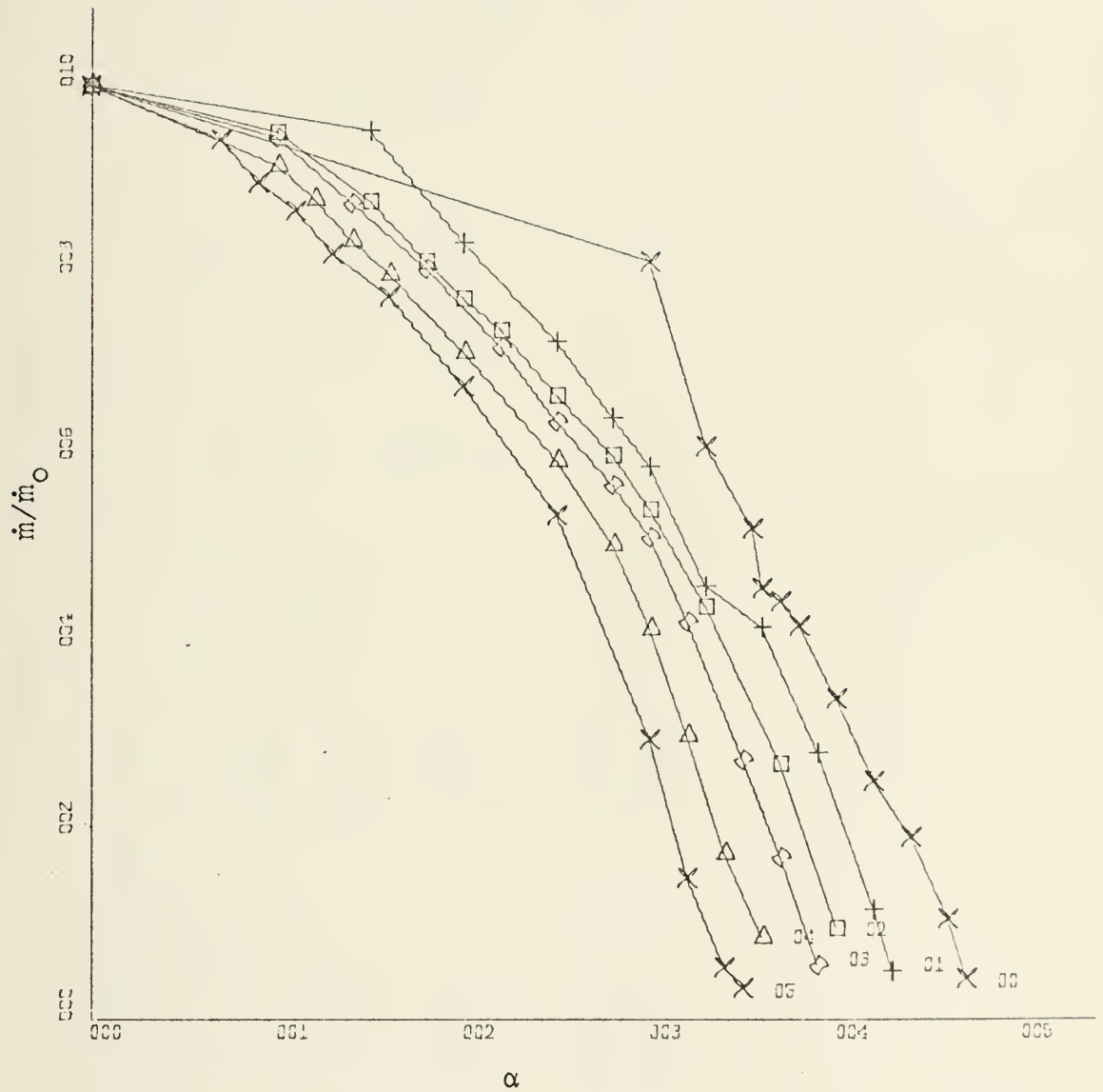

Figure 53. Flow Rate vs. Deflection Angle at Various Offset Distances for Concave Wall Re = 1.475×10^5, Jet Width of 1.31 Inches, D/W of 00, 01, 02, 03, 04, 05.

OUTLINE OF DATA PRESENTATION IV.

A. Comparison of Planar, Convex, and Concave Walls.

1.	a.	X/W vs. D/W	jet width = 2.62 in.	$N_{Re} = 2.05 \times 10^5$	α = 00,15,20,25 deg.	Fig. 54-57
	b.	X/W vs. D/W	jet width = 1.31 in.	$N_{Re} = 1.475 \times 10^5$	α = 00,15,20,25 deg.	Fig. 58-61
2.	a.	X/W vs. α	jet width = 2.62 in.	$N_{Re} = 2.05 \times 10^5$	D/W = 0.0,.18,.36,.56, .74,.94	Fig. 62=67
	b.	X/W vs. α	jet width = 1.31 in.	$N_{Re} = 1.475 \times 10^5$	D/W = 0.0,.36,.74, 1.12,1.48,1.88	Fig. 68-73
3.	a.	$\dot{m}/\dot{m}_o$ vs. D/W	jet width = 2.62 in.	$N_{Re} = 2.05 \times 10^5$	α = 00,15,20,25 deg.	Fig. 74-77
	b.	$\dot{m}/\dot{m}_o$ vs. D/W	jet width = 1.31 in.	$N_{Re} = 1.475 \times 10^5$	α = 00,15,20,25 deg.	Fig. 78-81

Figure 54. Attachment Distance vs. Offset Distance at 0 Degrees Deflection for Planar, Concave, and Convex Walls. Jet Width 2.62 Inches. Re = 2.05×10^5.

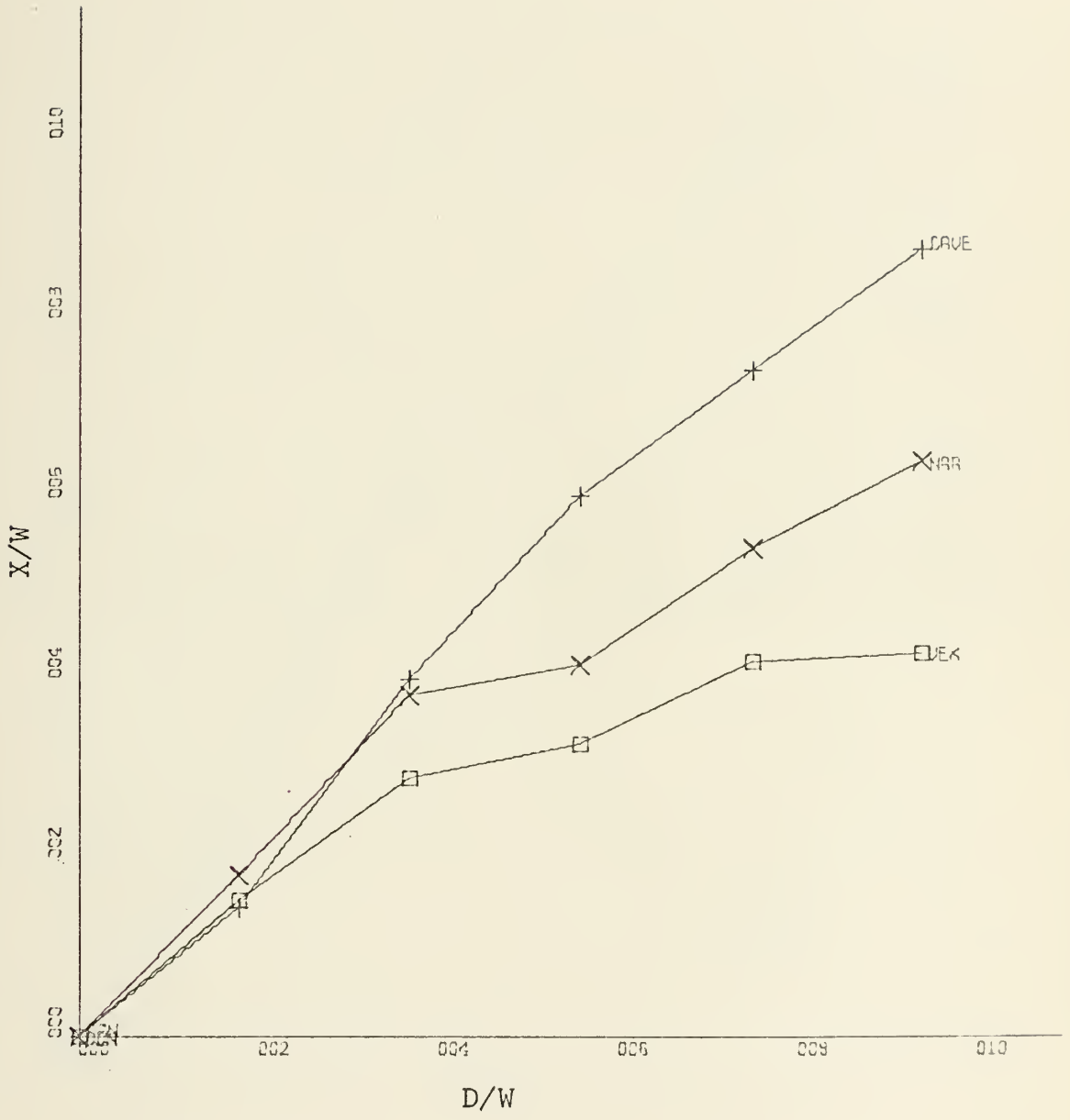

Figure 55. Attachment Distance vs. Offset Distance at 15 Degrees Wall Deflection for Planar, Concave, and Convex Walls, Jet Width 2.62 Inches, Re = 2.05×10^5.

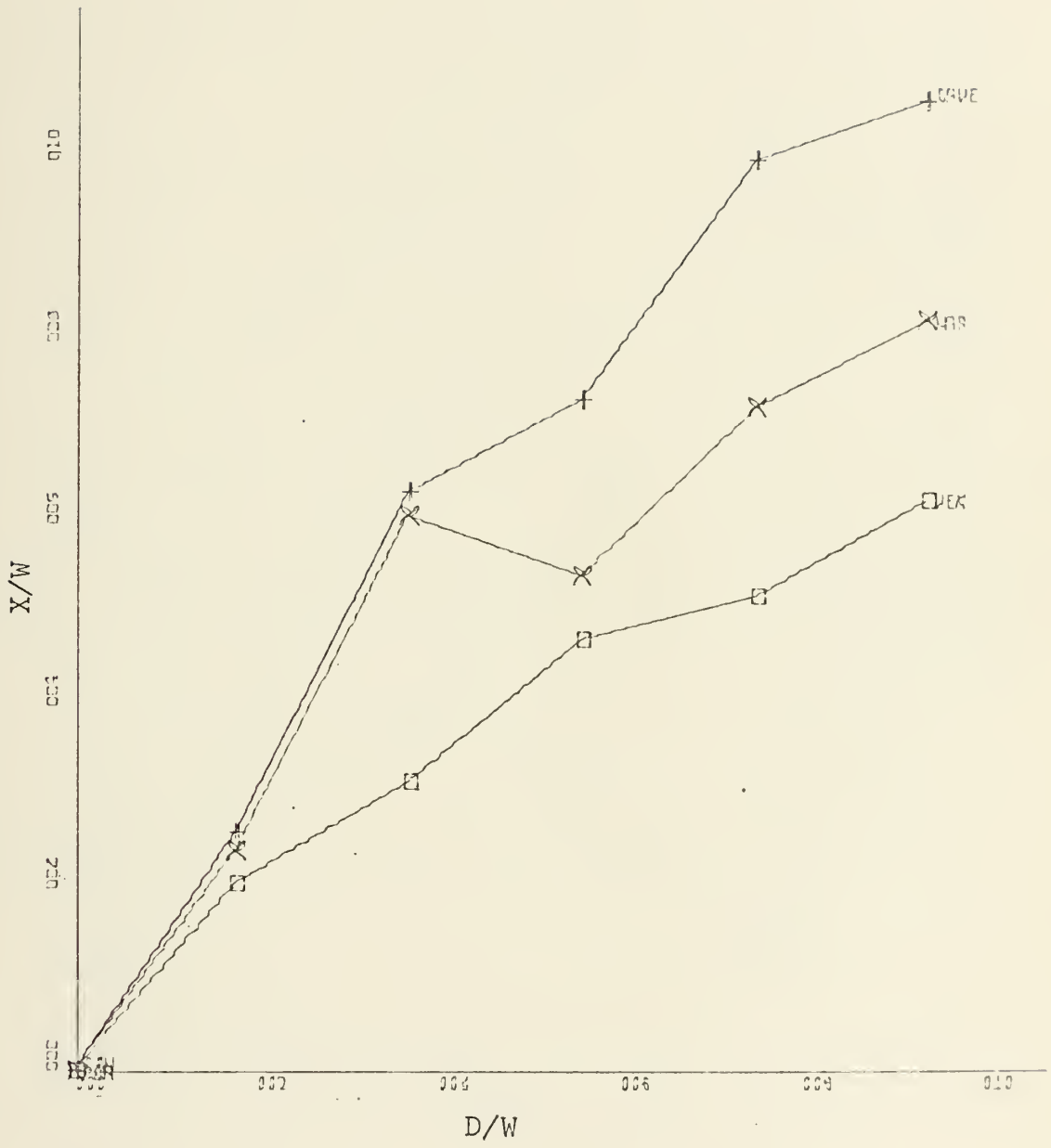

Figure 56. Attachment Distance vs. Offset Distance at 20 Degrees Wall Deflection for Planar, Concave, and Convex Walls, Jet Width of 2.62 Inches, Re = 2.05×10^5.

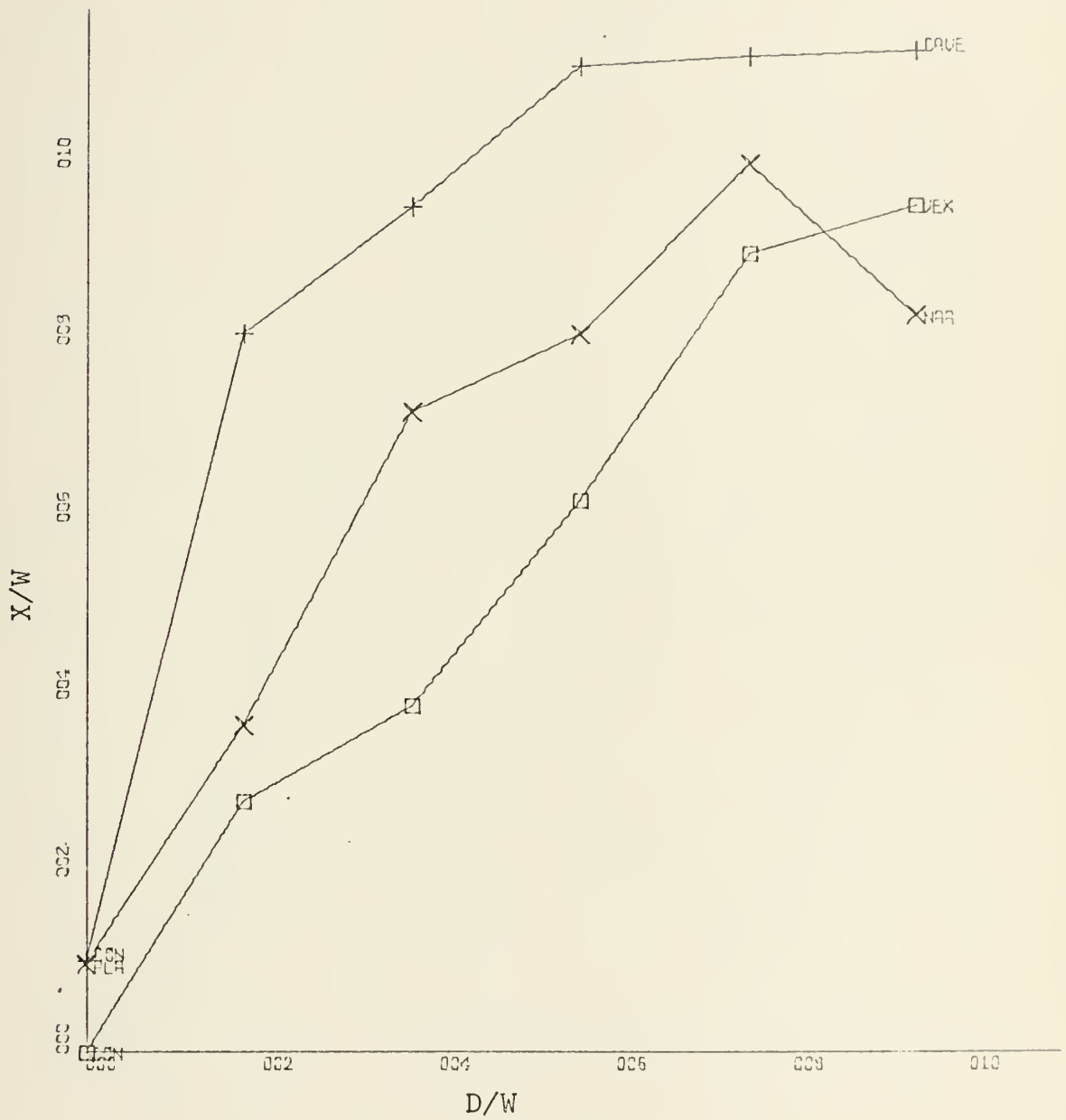

Figure 57. Attachment Distance vs. Offset at 25 Degrees Wall Deflection for Planar, Concave, and Convex Wall, Jet Width of 2.62 Inches, Re = 2.05×10^5.

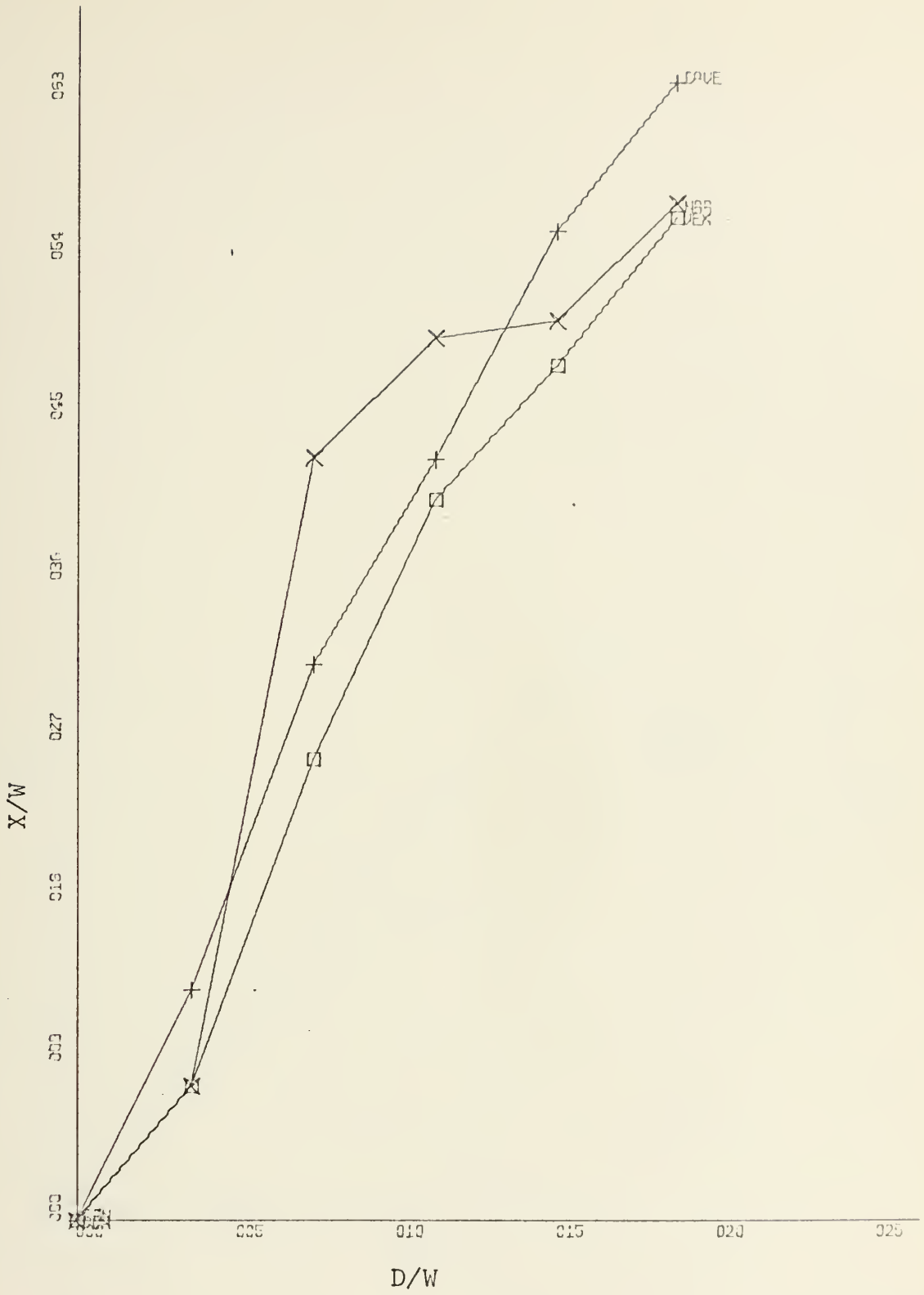

Figure 58. Attachment Distance vs. Offset Distance at 0 Degrees Wall Deflection for Planar, Concave, and Convex Walls, Jet Width of 1.31 Inches, Re = 1.475×10^5.

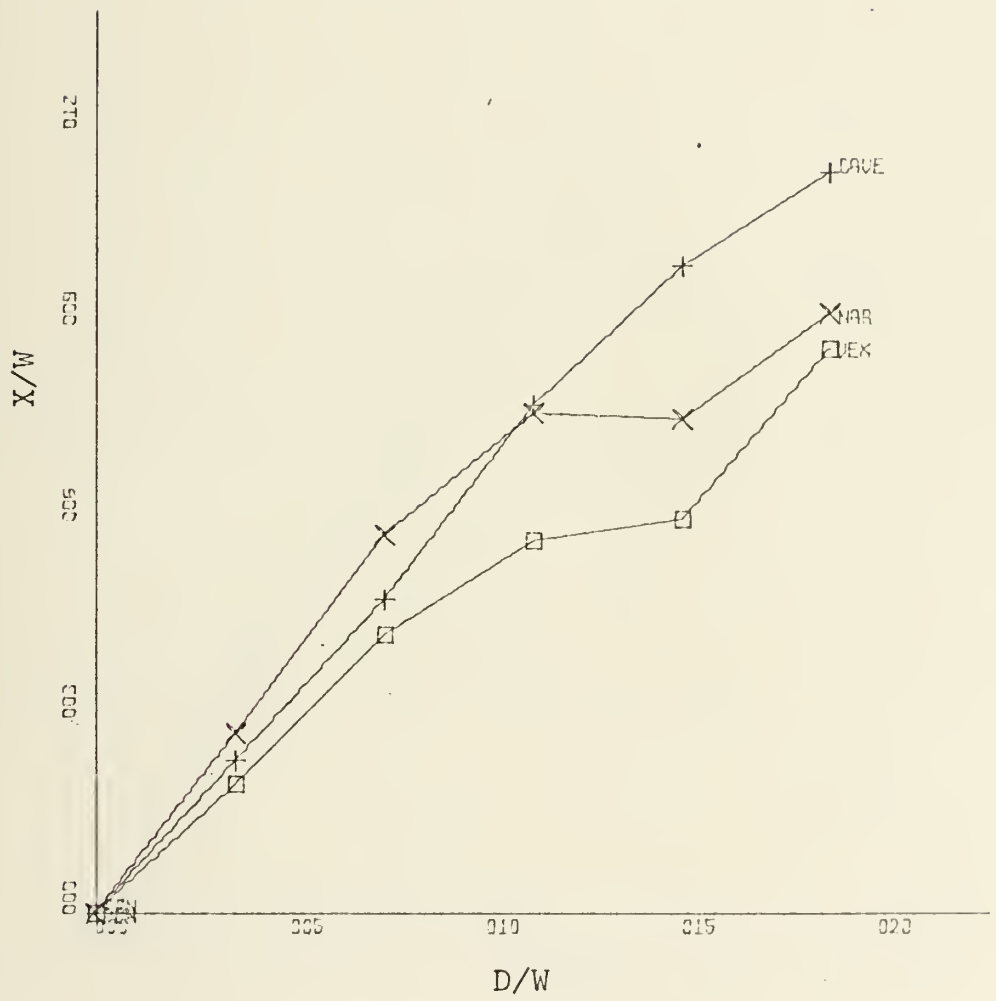

Figure 59. Attachment Distance vs. Offset Distance at 15 Degrees Wall Deflection for Planar, Concave, and Convex Walls, Jet Width 1.31 Inches, Re = 1.475×10^5.

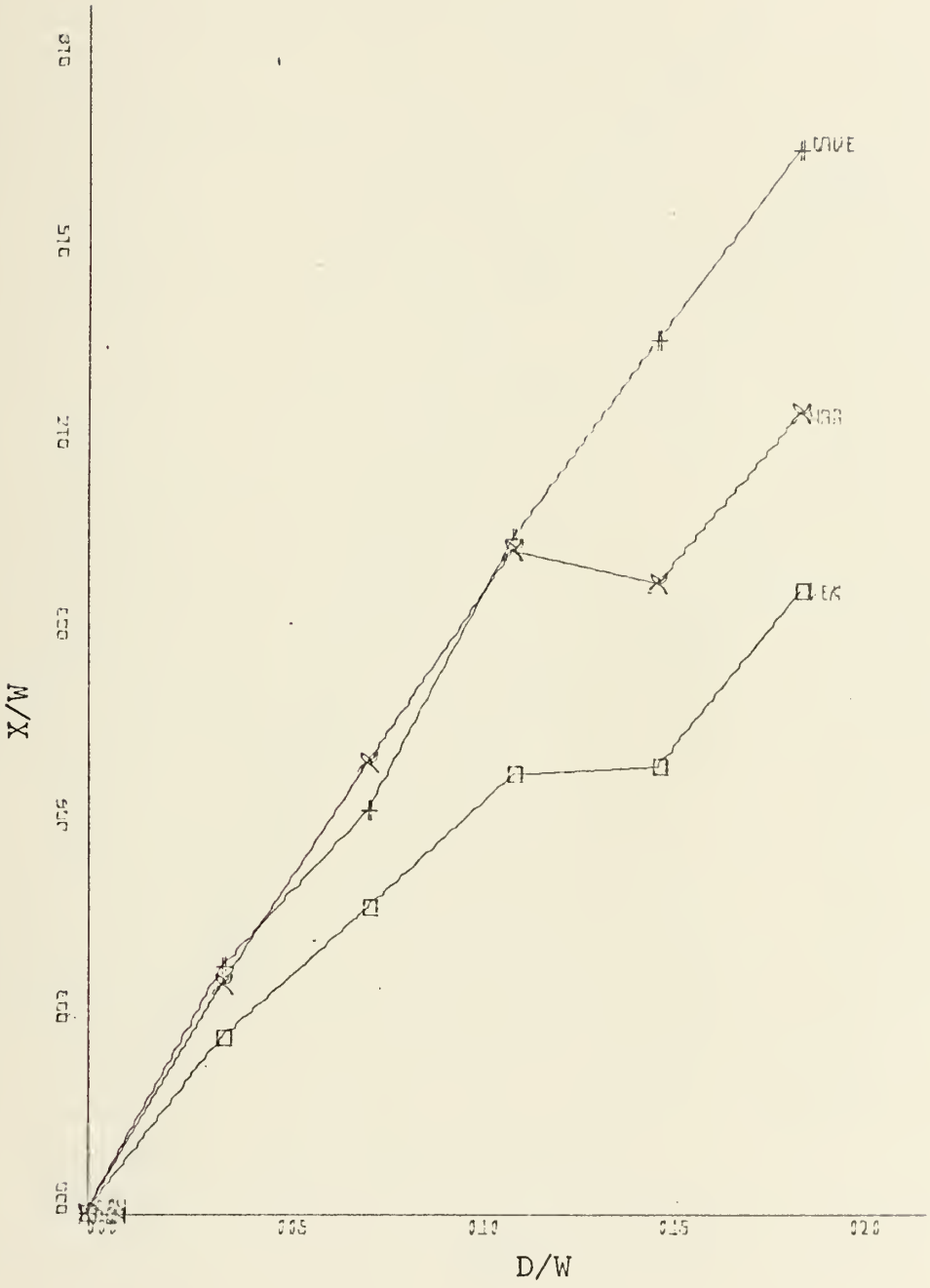

Figure 60. Attachment Distance vs. Offset Distance at 20 Degrees Wall Deflection for Planar, Concave, and Convex Walls, Jet Width of 1.31 Inches, Re = 1.475×10^5.

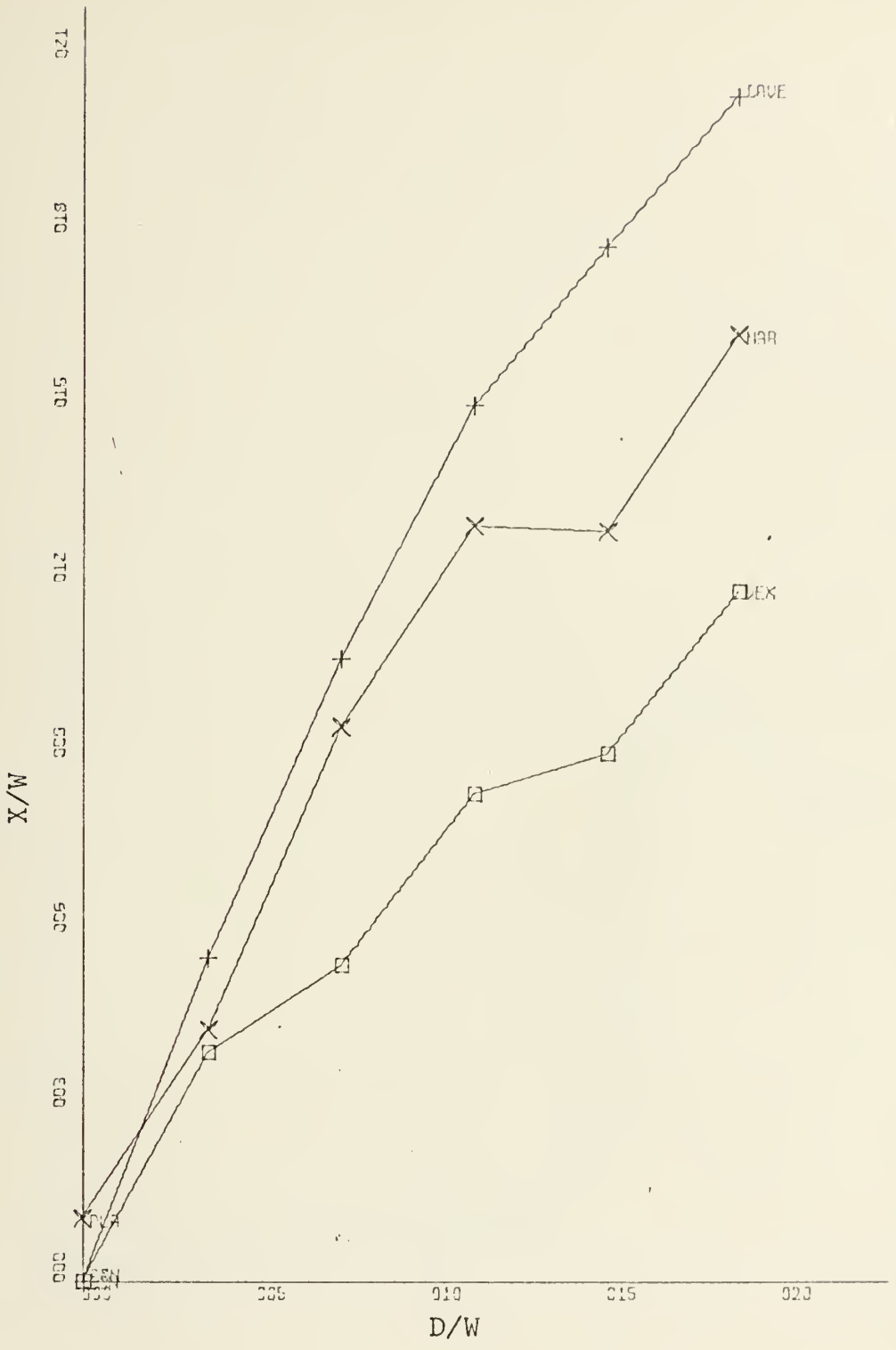

Figure 61. Attachment Distance vs. Offset Distance at 25 Degrees Wall Deflection for Planar, Concave, and Convex Walls, Jet Width of 1.31 Inches, Re = 1.475×10^5.

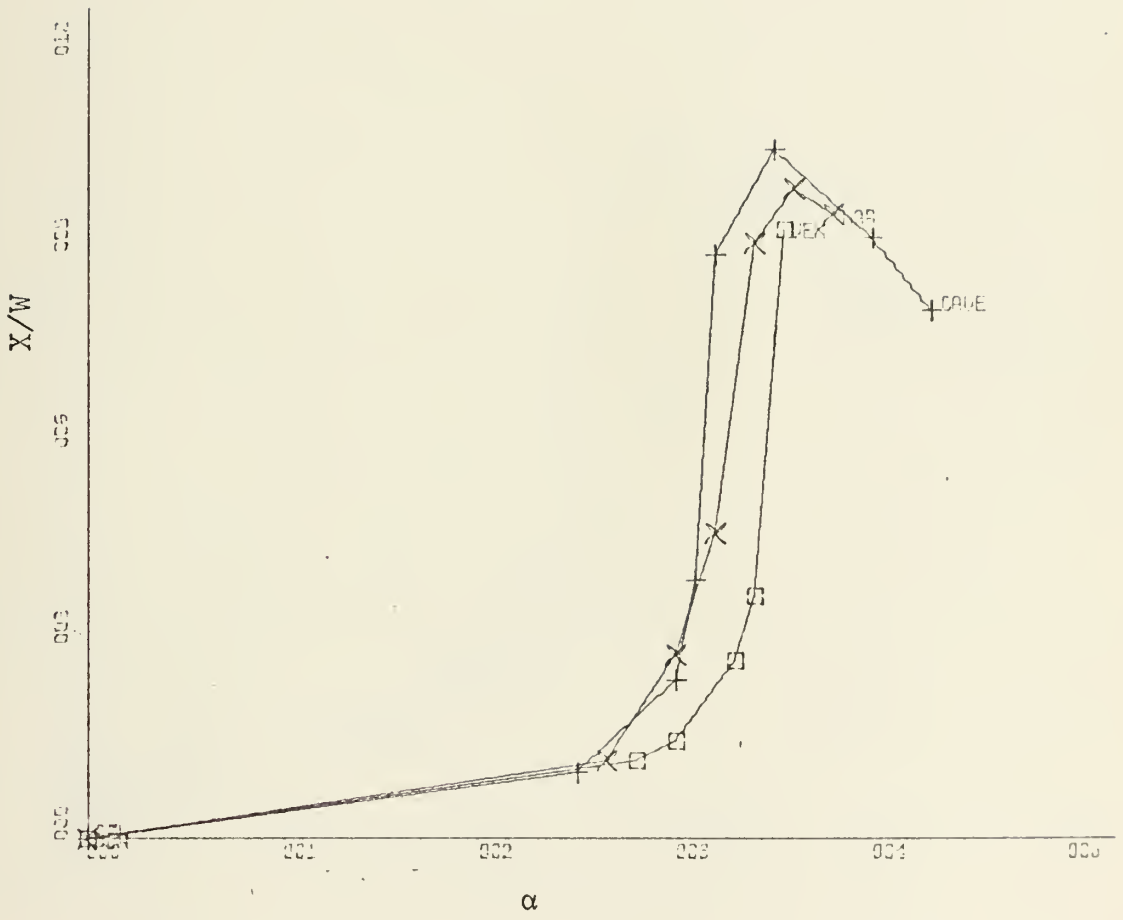

Figure 62. Attachment Distance vs. Deflection Angle for Jet Width of 2.62 Inches, Planar, Concave, and Convex Walls, Offset Distance (D/W) of 0.0, Re = 2.05 x 10^5.

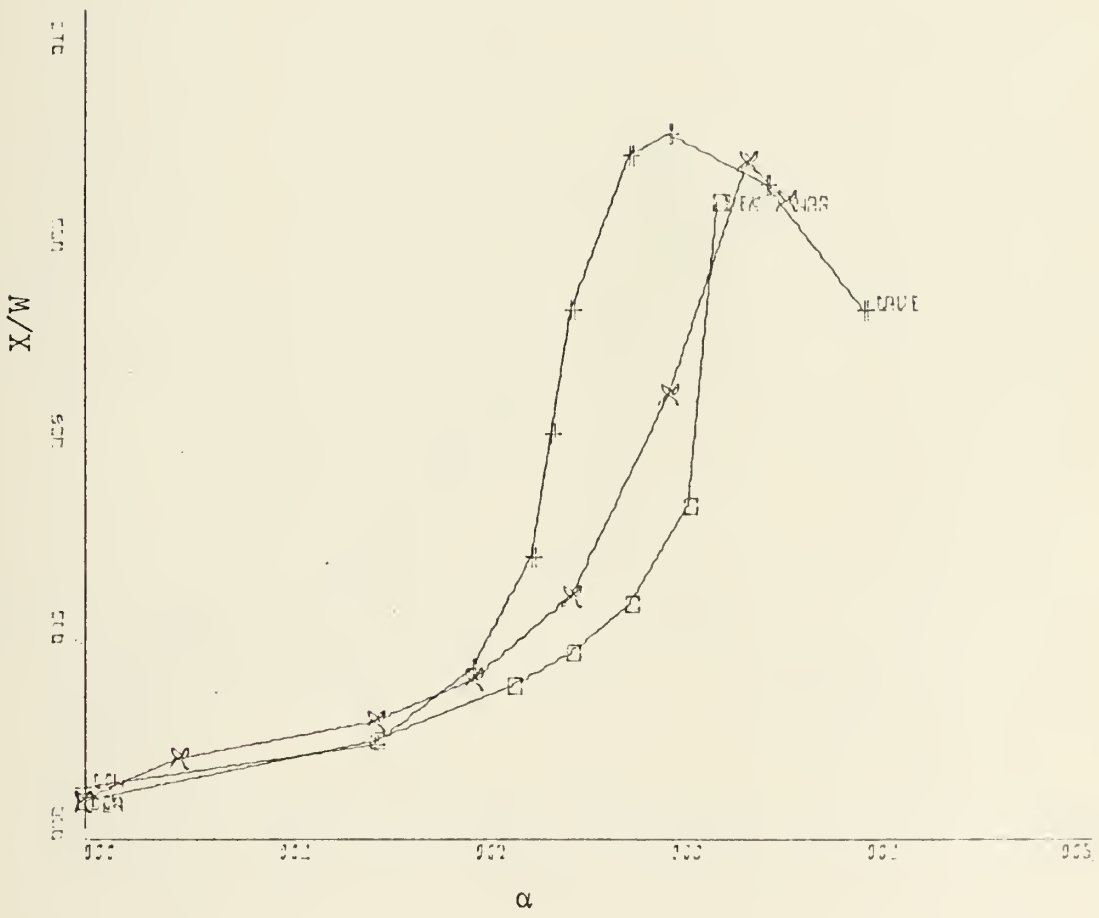

Figure 63. Attachment Distance vs. Deflection Angle for a Jet Width of 2.62 Inches for Planar, Concave, and Convex Walls, Offset Distance (D/W) of .18, Re = 2.05 x 10^5.

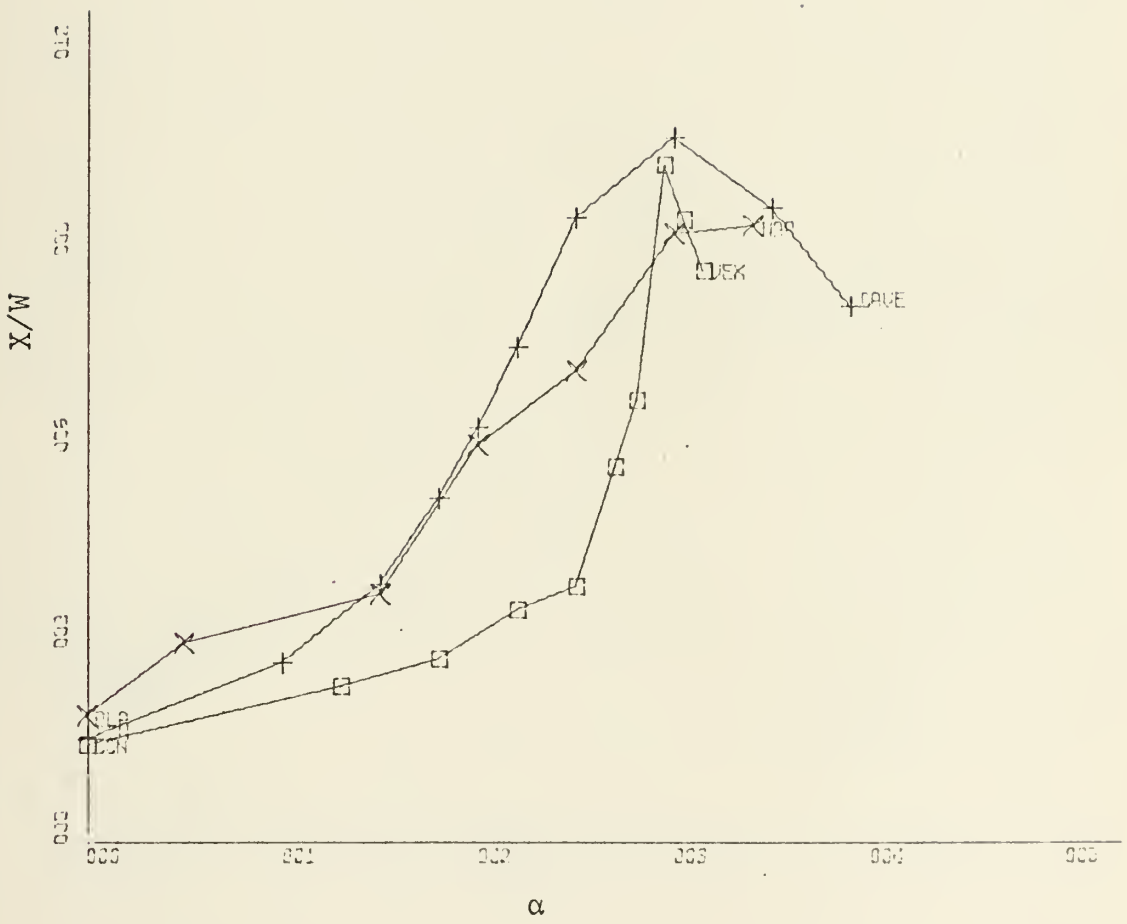

Figure 64. Attachment Distance vs. Deflection Angle for Jet Width of 2.62 Inches, Planar, Concave, and Convex Walls, Offset Distance (D/W) of .36, Re = 2.05×10^5.

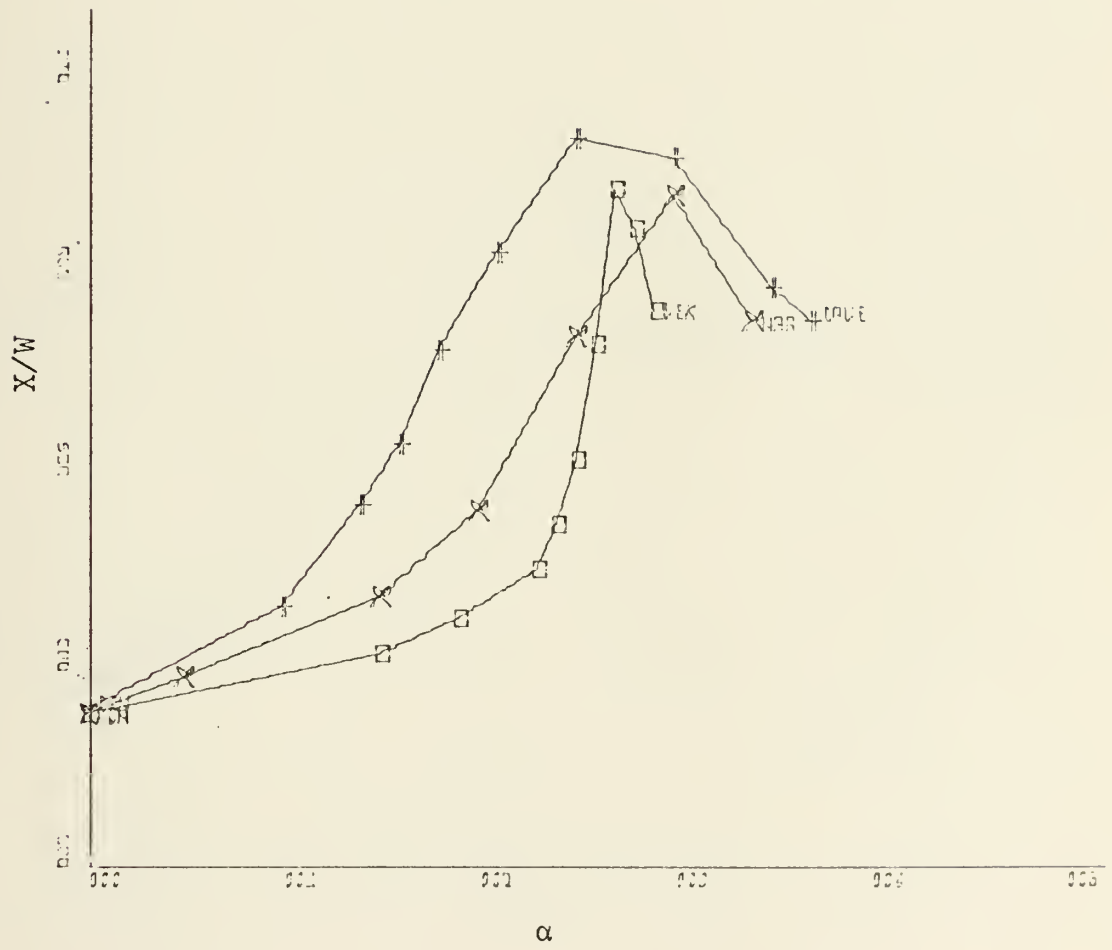

Figure 65. Attachment Distance vs. Deflection Angle for Jet Width 2.62 Inches, Planar, Concave, and Convex Walls, Offset Distance (D/W) of .56, Re = 2.05 x 10^5.

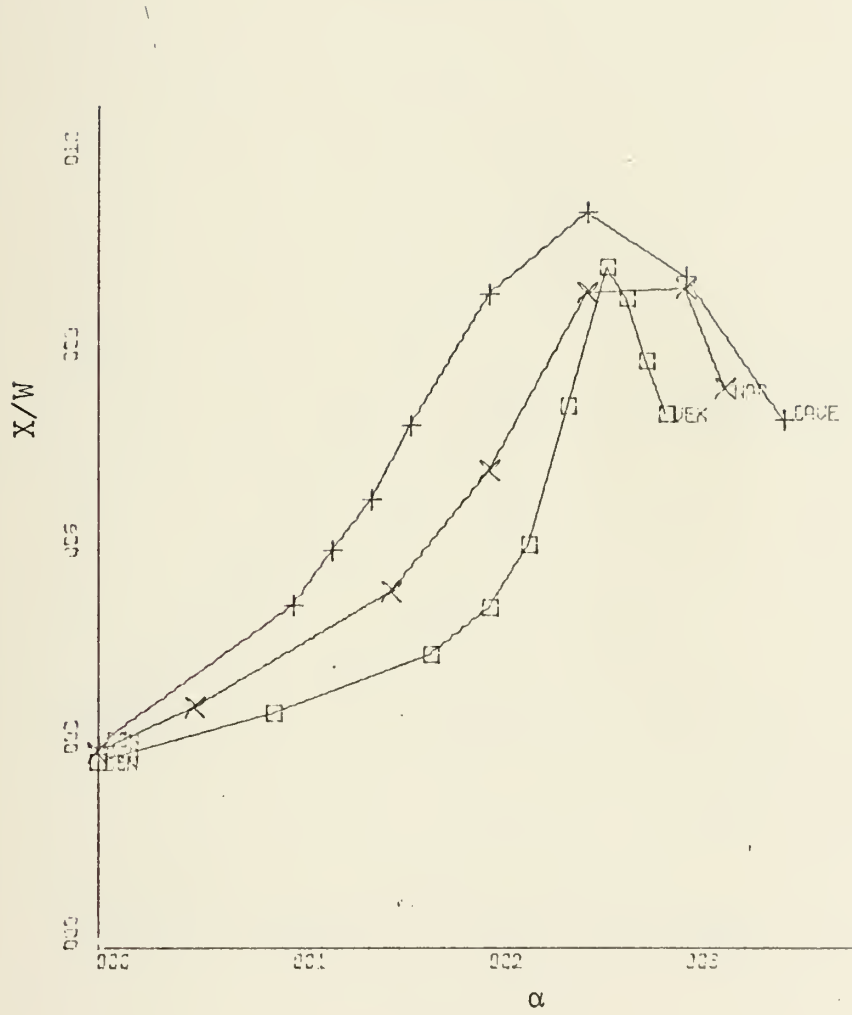

Figure 66. Attachment Distance vs. Deflection Angle for Jet Width of 2.62 Inches, Planar, Concave and Convex Walls, Offset Distance (D/W) of 0.74, Re = 2.05 x 10^5.

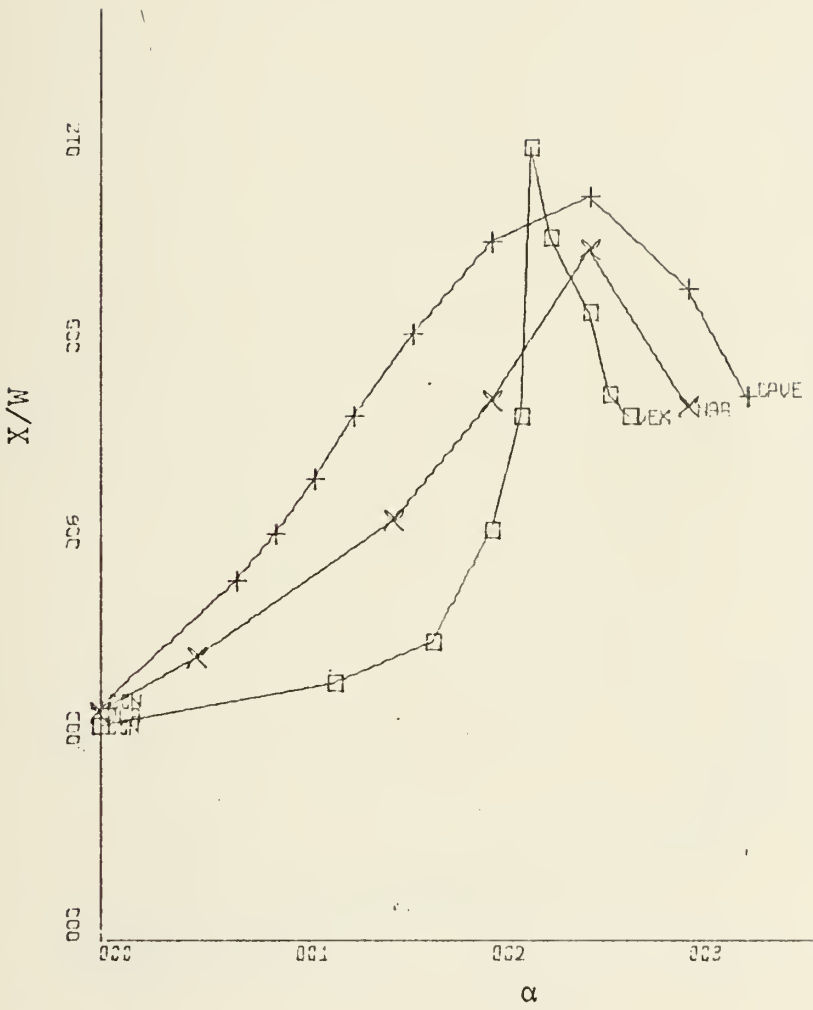

Figure 67. Attachment Distance vs. Deflection Angle for Jet Width of 2.62 Inches, Planar, Concave, and Convex Walls, Offset Distance (D/W) of 0.94, Re = 2.05 x 10^5.

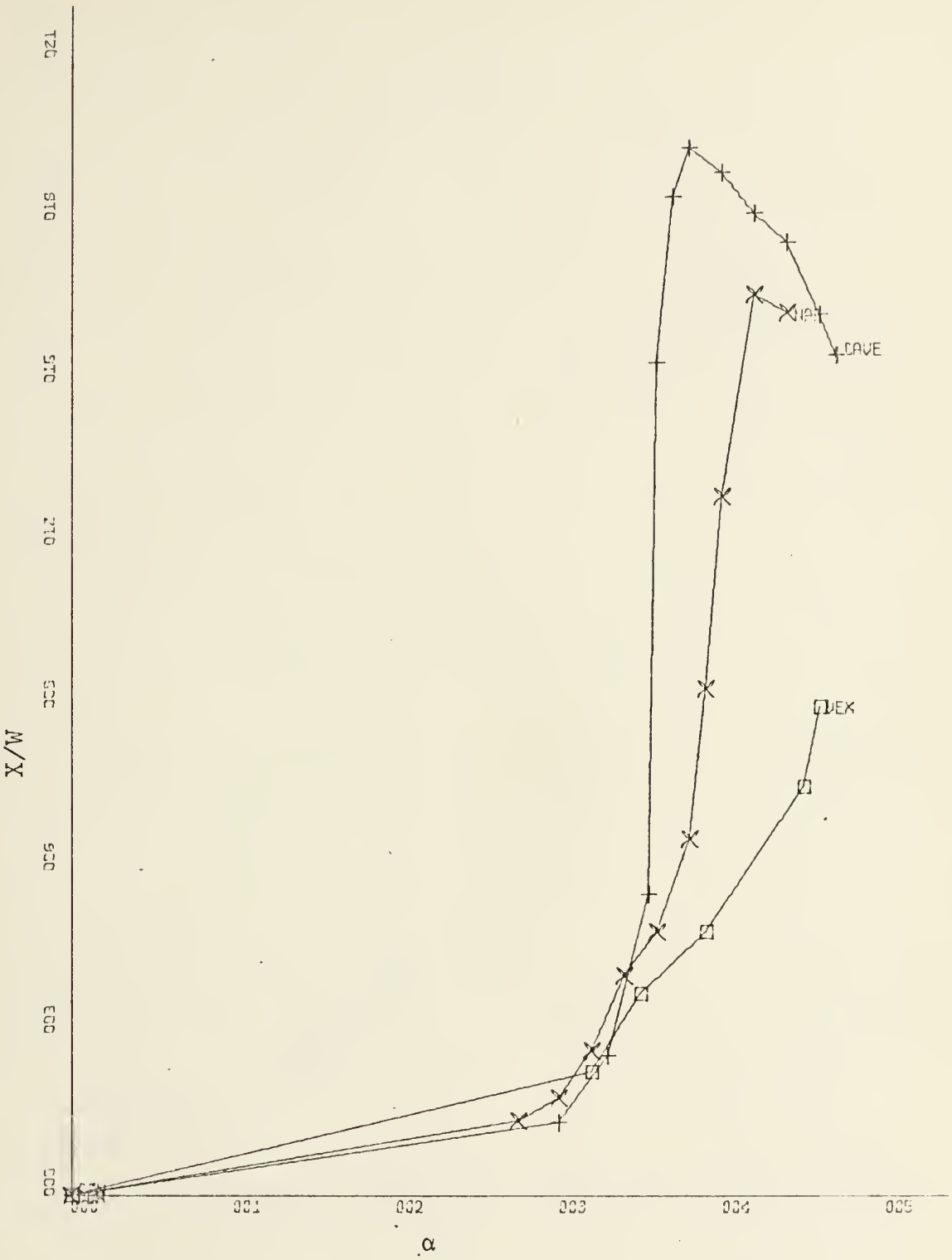

Figure 68. Attachment Distance vs. Deflection Angle for Jet Width of 1.31 Inches for Planar, Concave, and Convex Walls at Offset Distance (D/W) of 0.0, Re = 1.475×10^5.

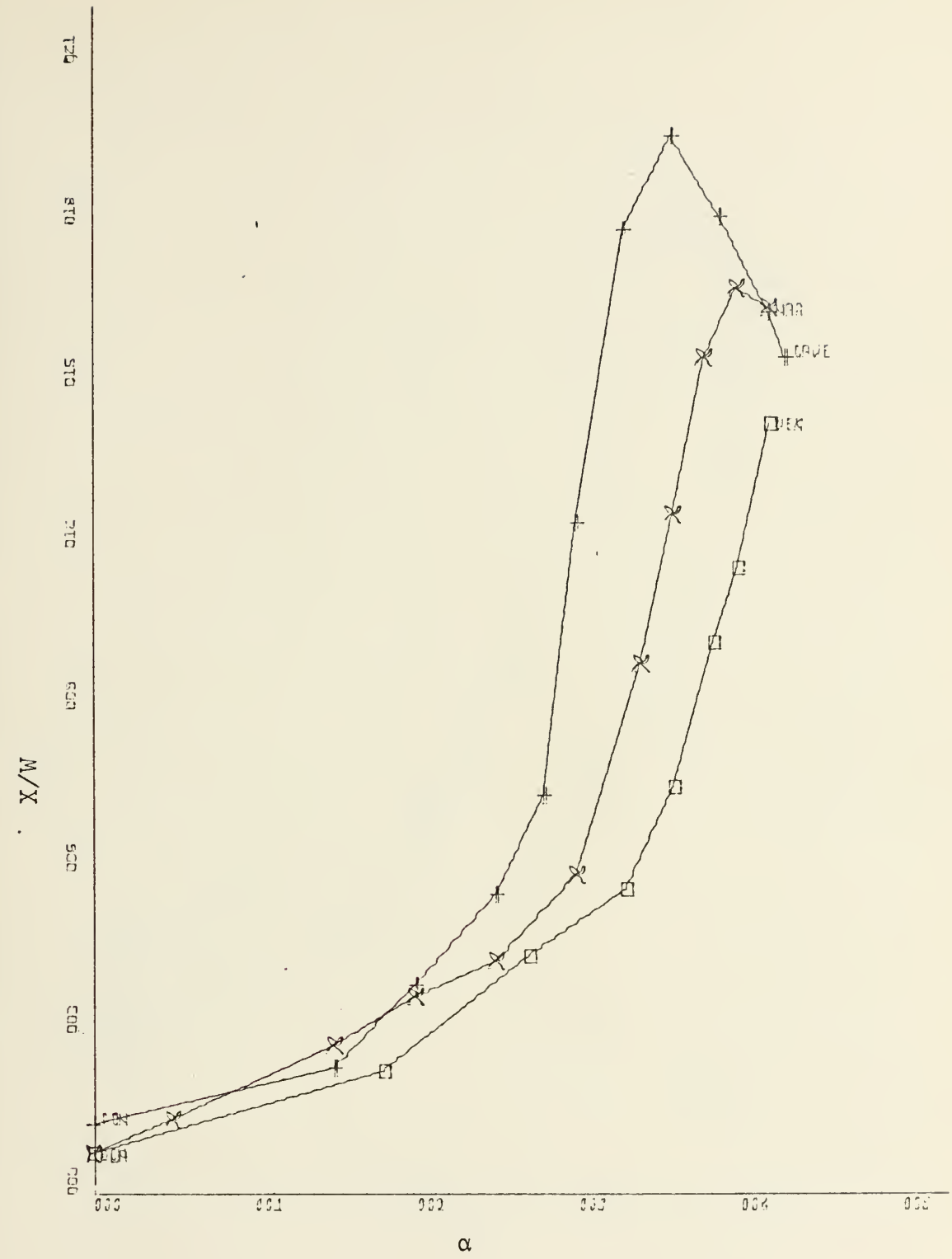

Figure 69. Attachment Distance vs. Deflection Angle for Jet Width of 1.31 Inches, for Planar, Concave, and Convex Walls at Offset Distance (D/W) of 0.36, Re = 1.475×10^5.

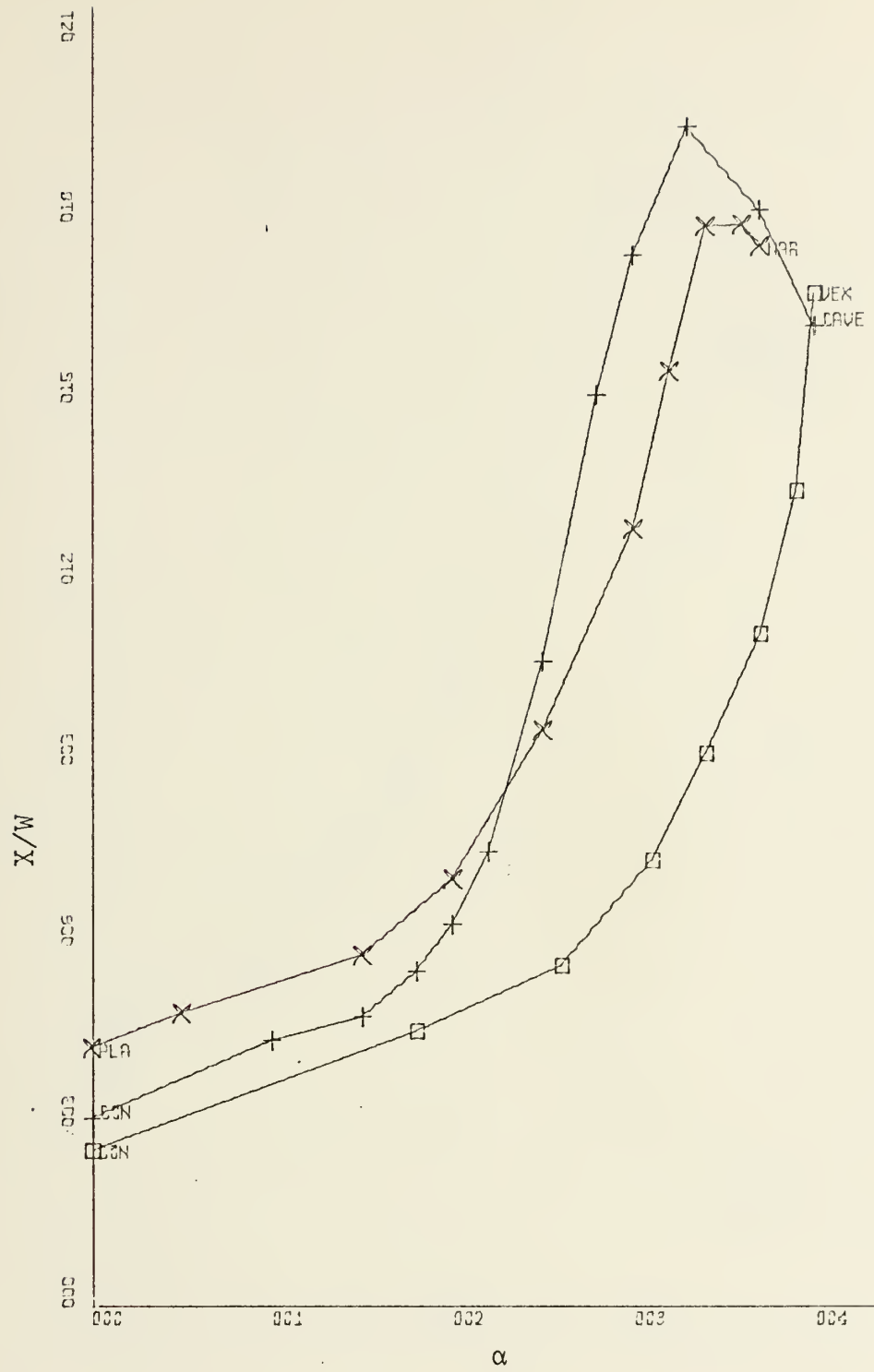

Figure 70. Attachment Distance vs. Deflection Angle for Jet Width of 1.31 Inches, Planar, Concave, and Convex Walls, Offset Distance (D/W) of 0.74, Re = 1.475×10^5.

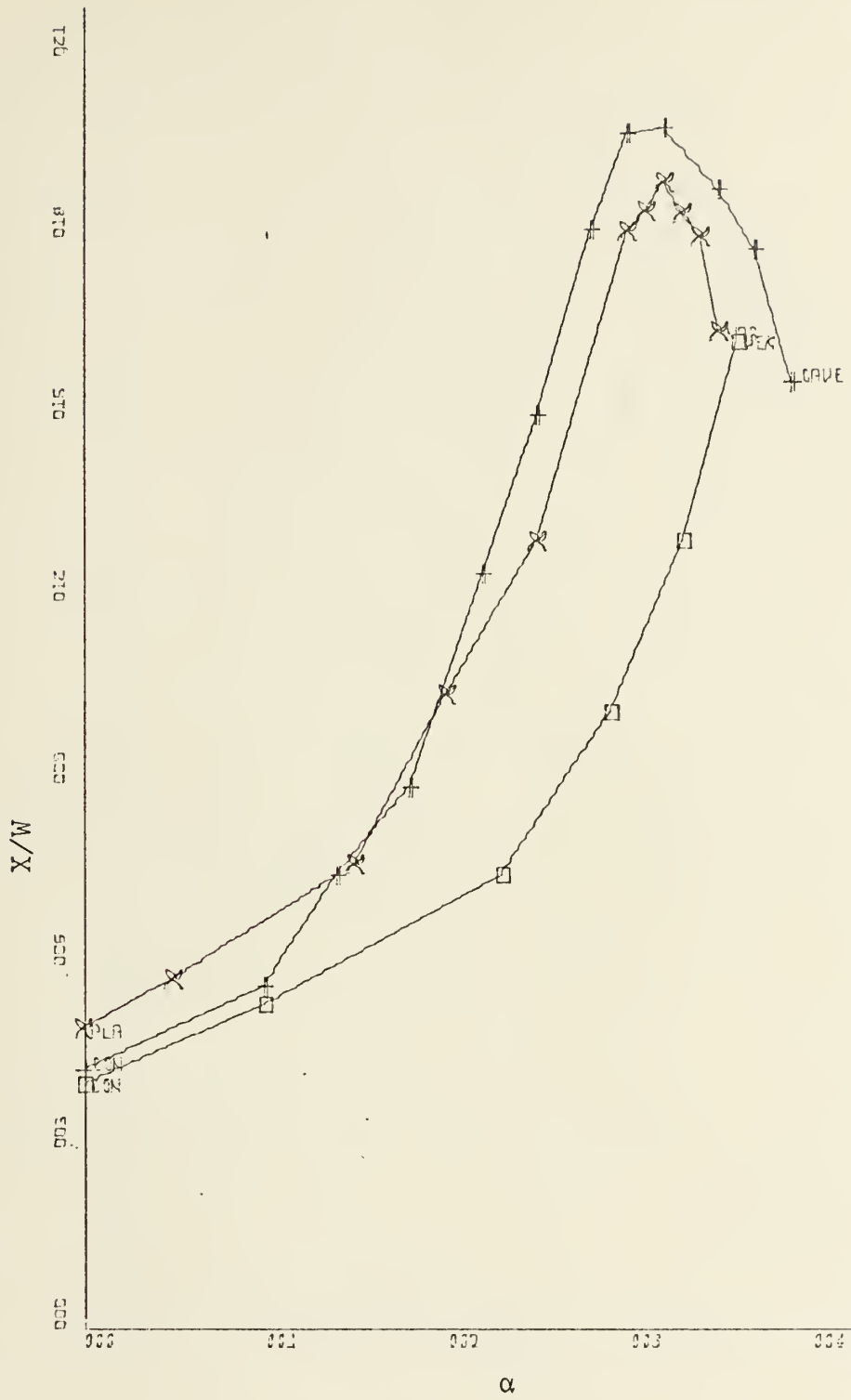

Figure 71. Attachment Distance vs. Deflection Angle for Jet Width of 1.31 Inches, Planar, Concave, and Convex Walls, Offset Distance (D/W) of 1.12, Re = 1.475×10^5.

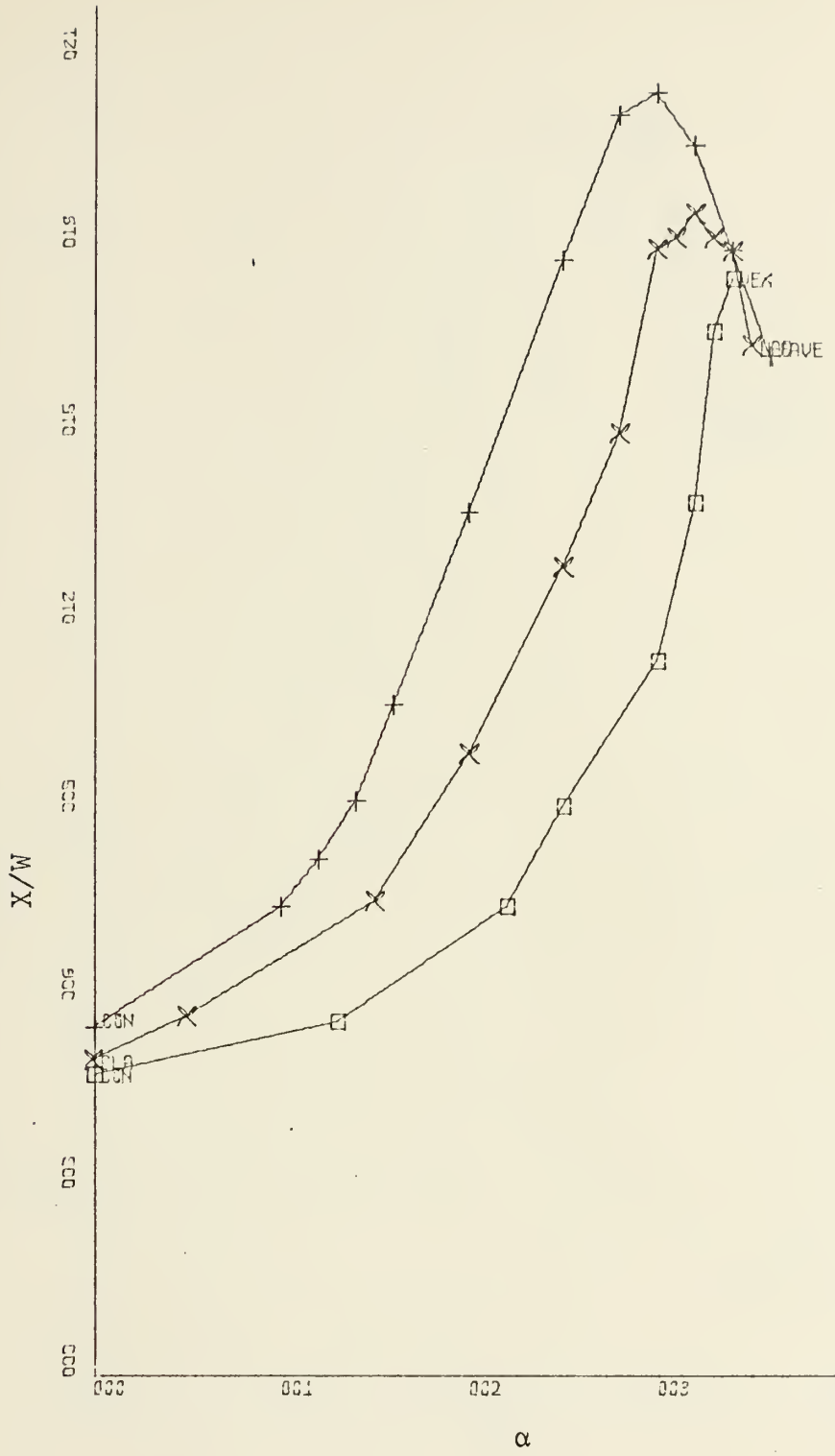

Figure 72. Attachment Distance vs. Deflection Angle for Jet Width of 1.31 Inches, Planar, Concave, and Convex Walls, Offset Distance (D/W) of 1.48, Re = 1.475×10^5.

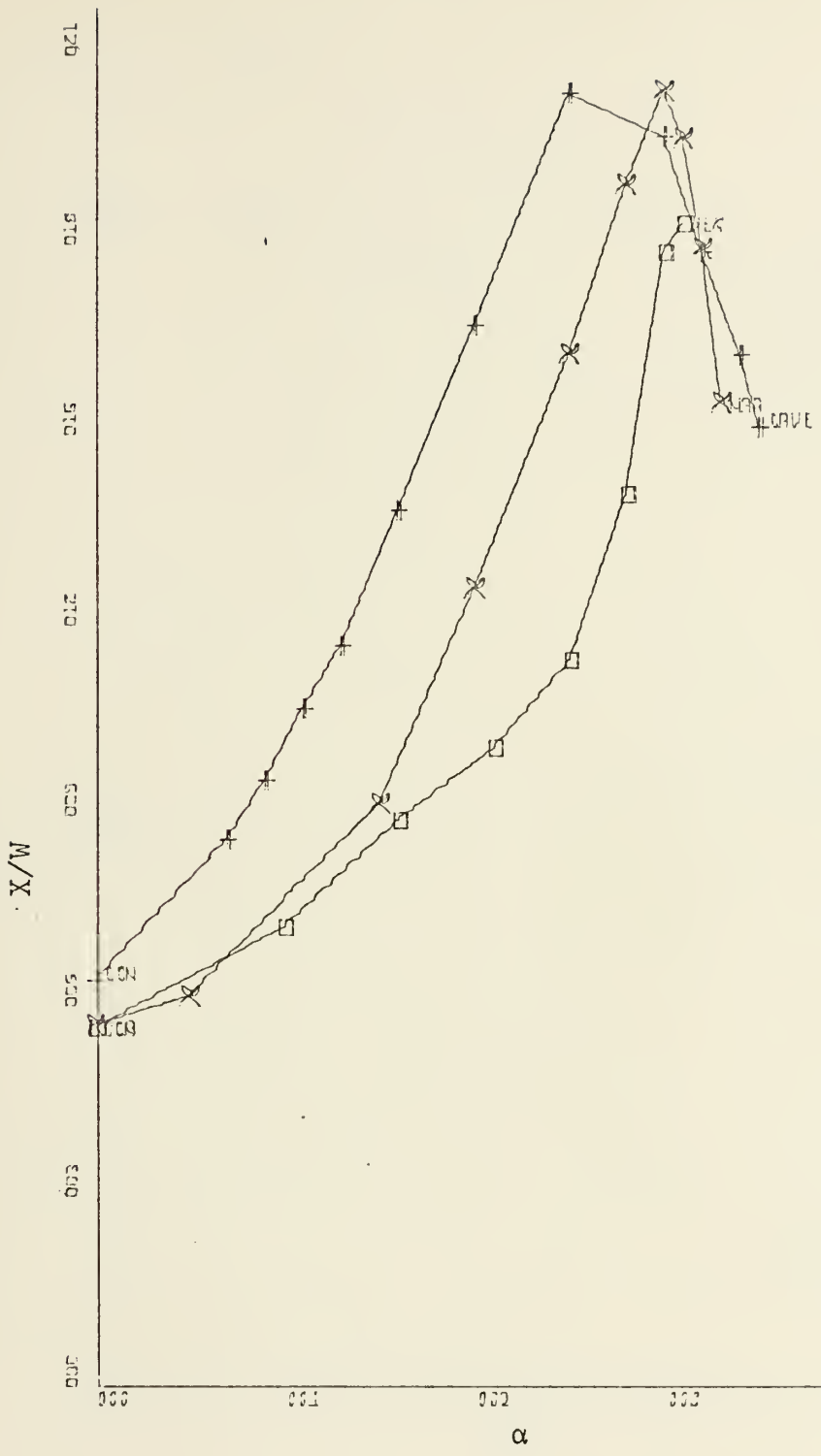

Figure 73. Attachment Distance vs. Deflection Angle for Jet Width of 1.31 Inches, Planar, Concave, and Convex Walls, Offset Distance (D/W) of 1.88, Re = 1.475×10^5.

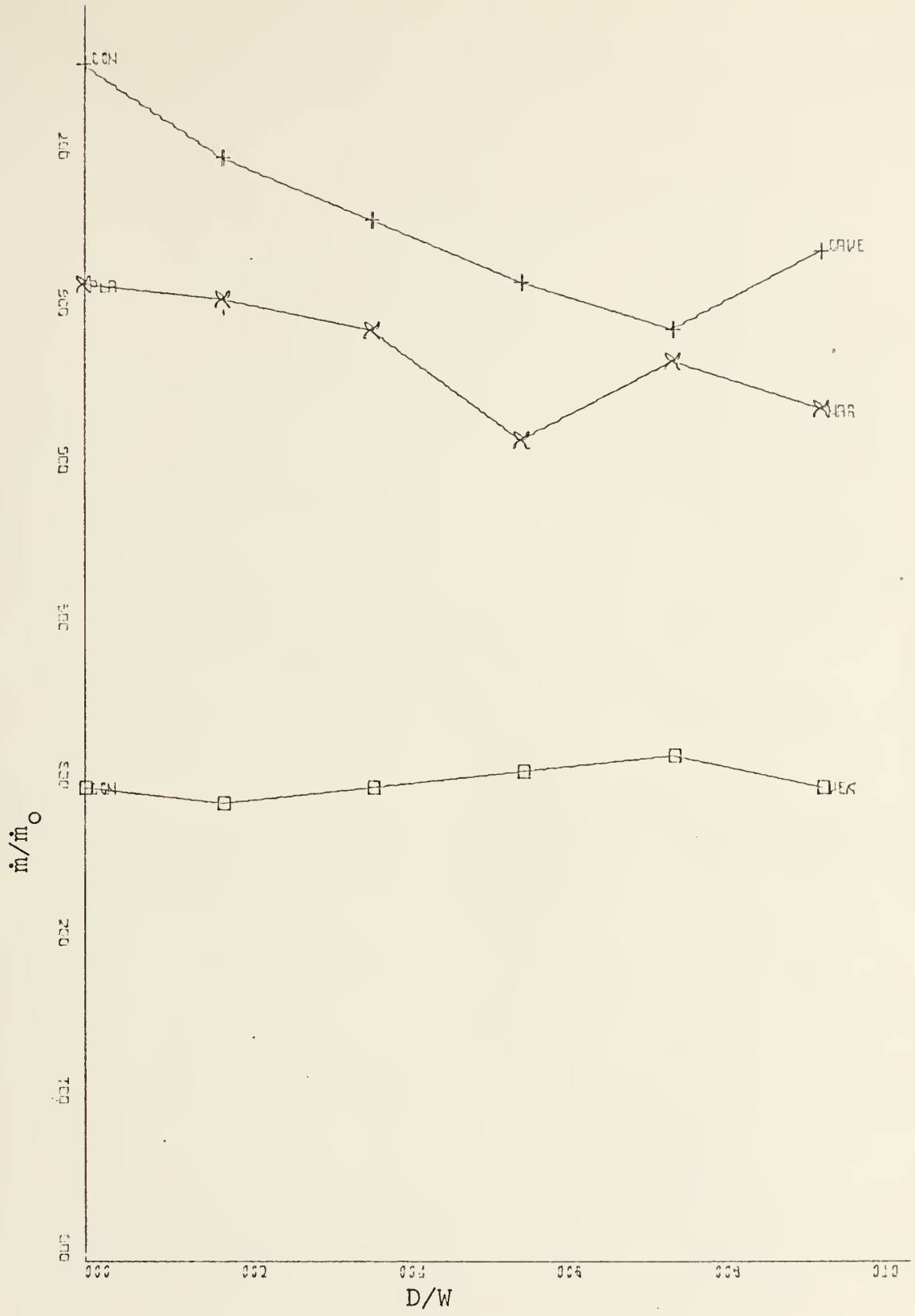

Figure 74. Flow Rate vs. Offset Distance for Planar, Concave, and Convex Walls, at 0 Degrees Deflection Angle, Jet Width of 2.62 Inches, Re = 2.05×10^5.

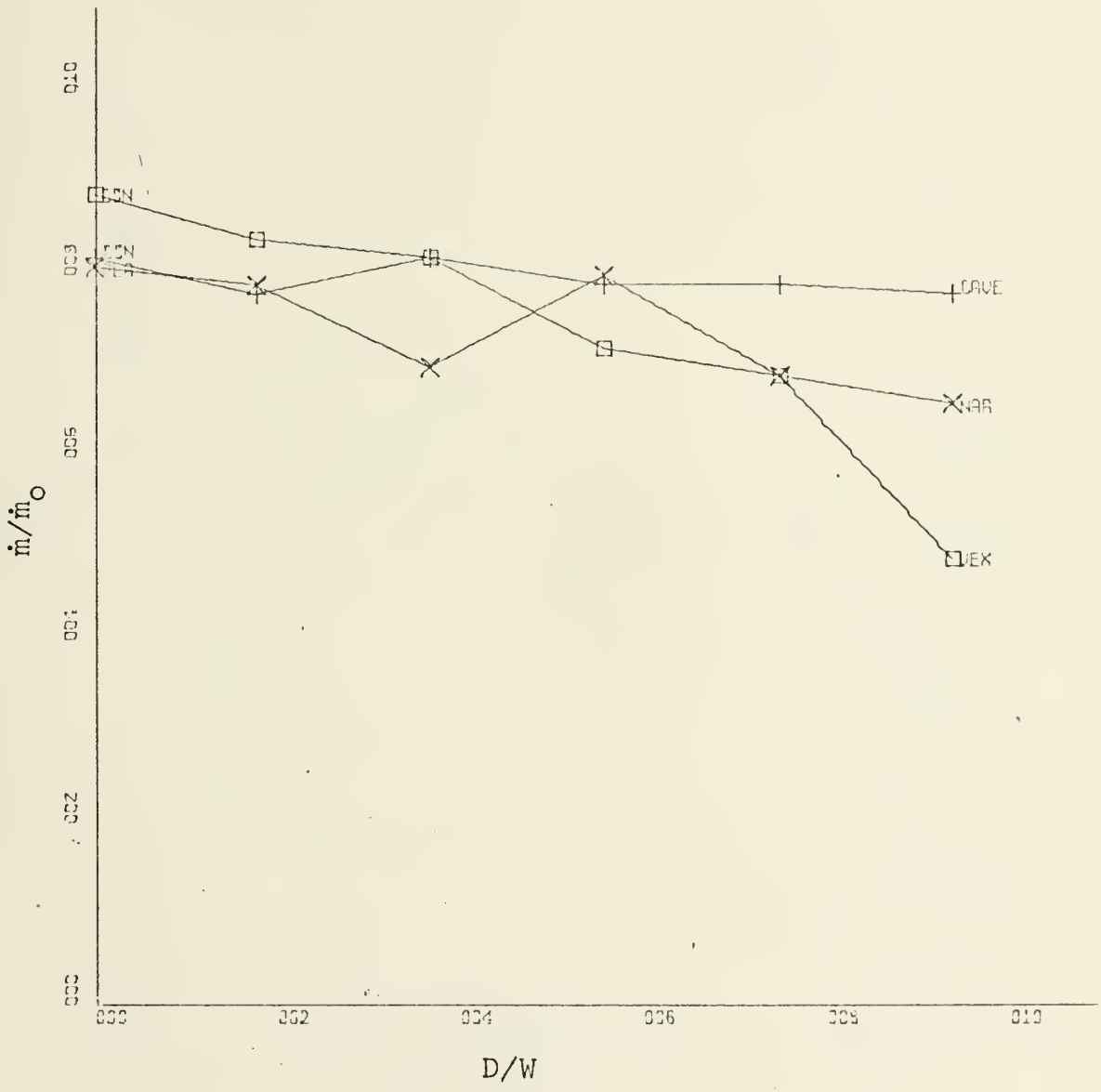

Figure 75. Flow Rate vs. Offset Distance for Planar, Concave, and Convex Walls, at 15 Degrees Deflection Angle, Jet Width of 2.62 Inches, Re = 2.05 x 10^5.

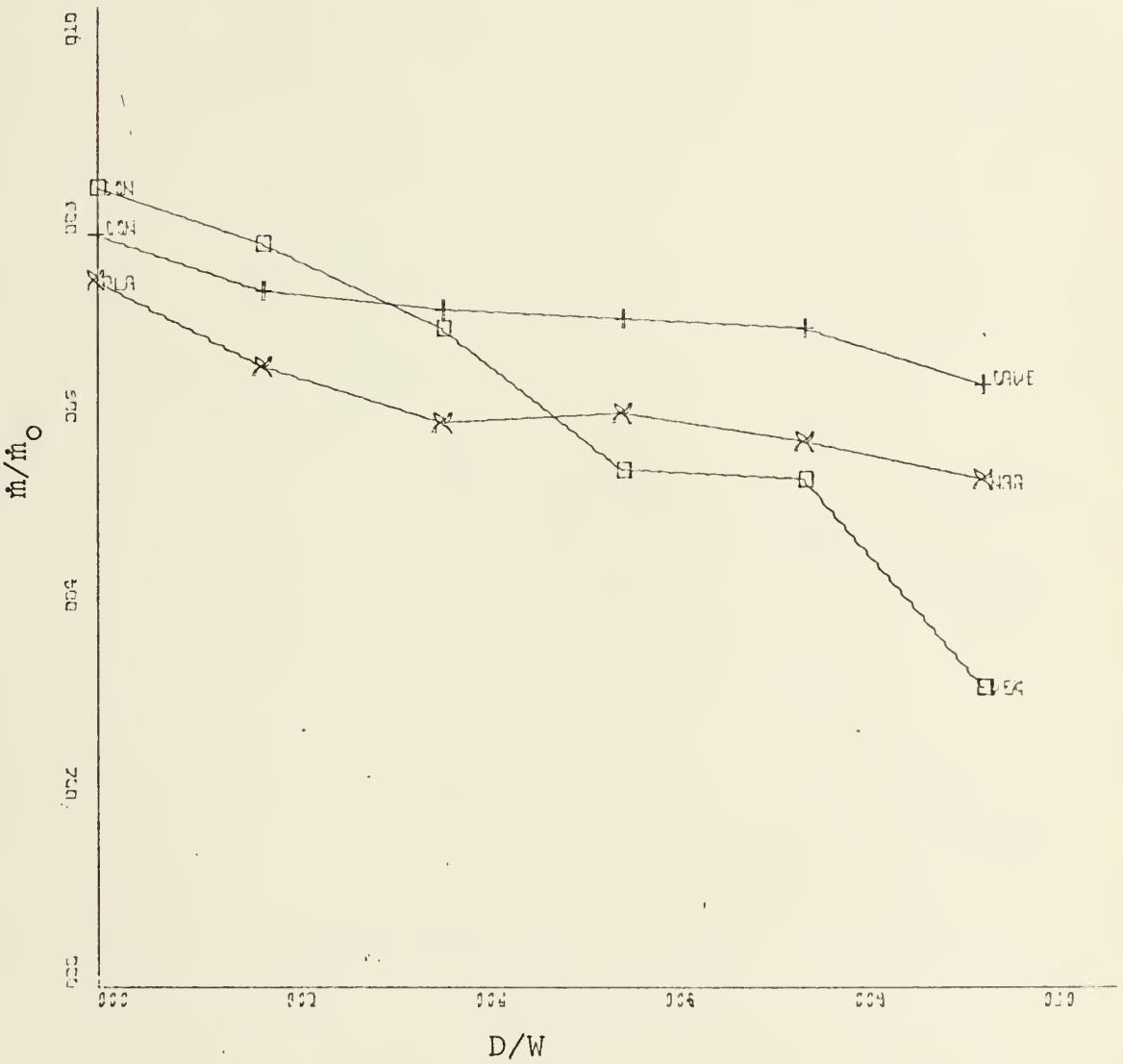

Figure 76. Flow Rate vs. Offset Distance for Planar, Concave, and Convex Walls, at 20 Degrees Deflection Angle, Jet Width of 2.62 Inches, Re = 2.05×10^5.

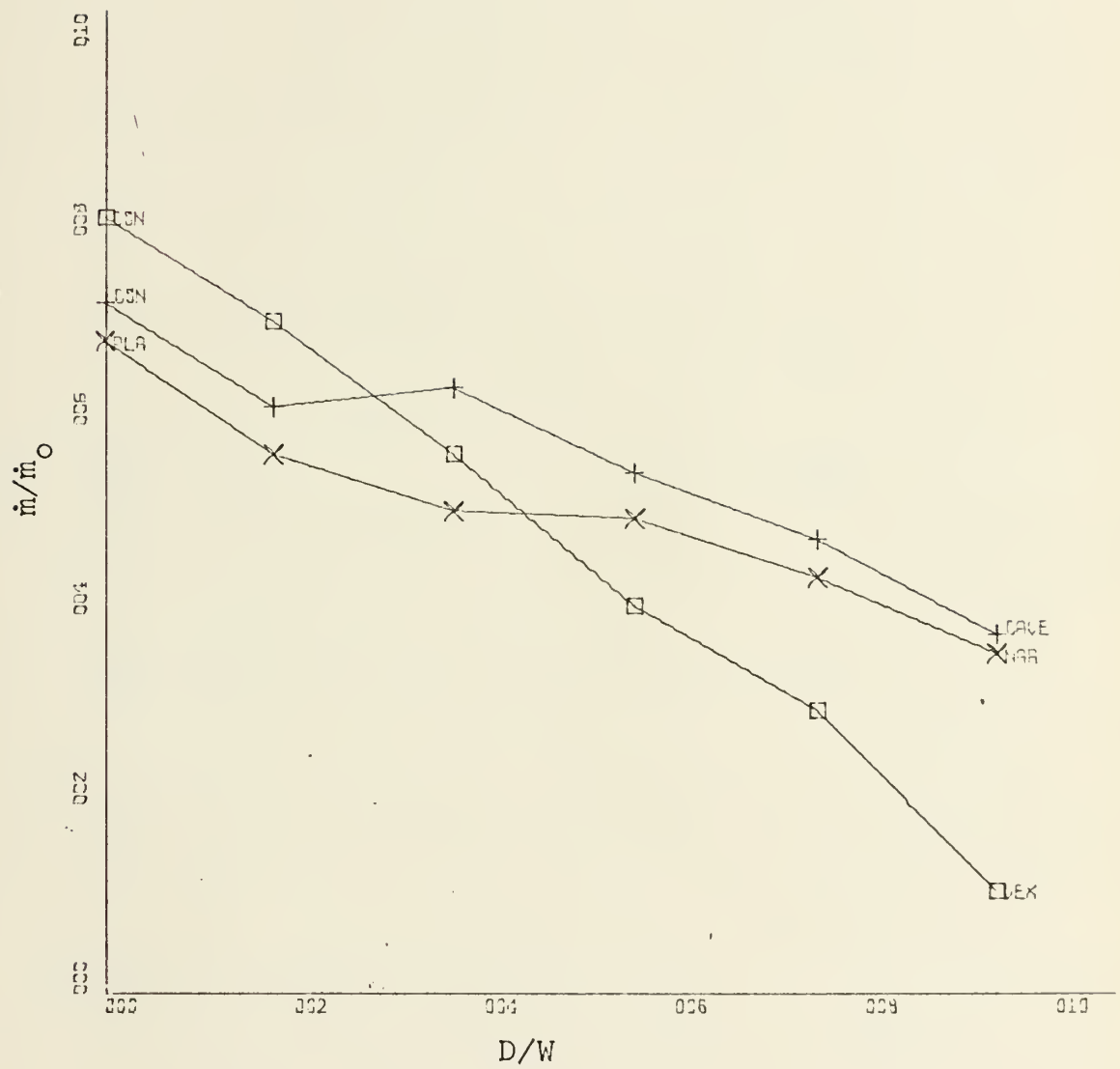

Figure 77. Flow Rate vs. Offset Distance for Planar, Concave, and Convex Walls, at 25 Degrees Deflection Angle, Jet Width of 2.62 Inches, Re = 2.05 x 10^5.

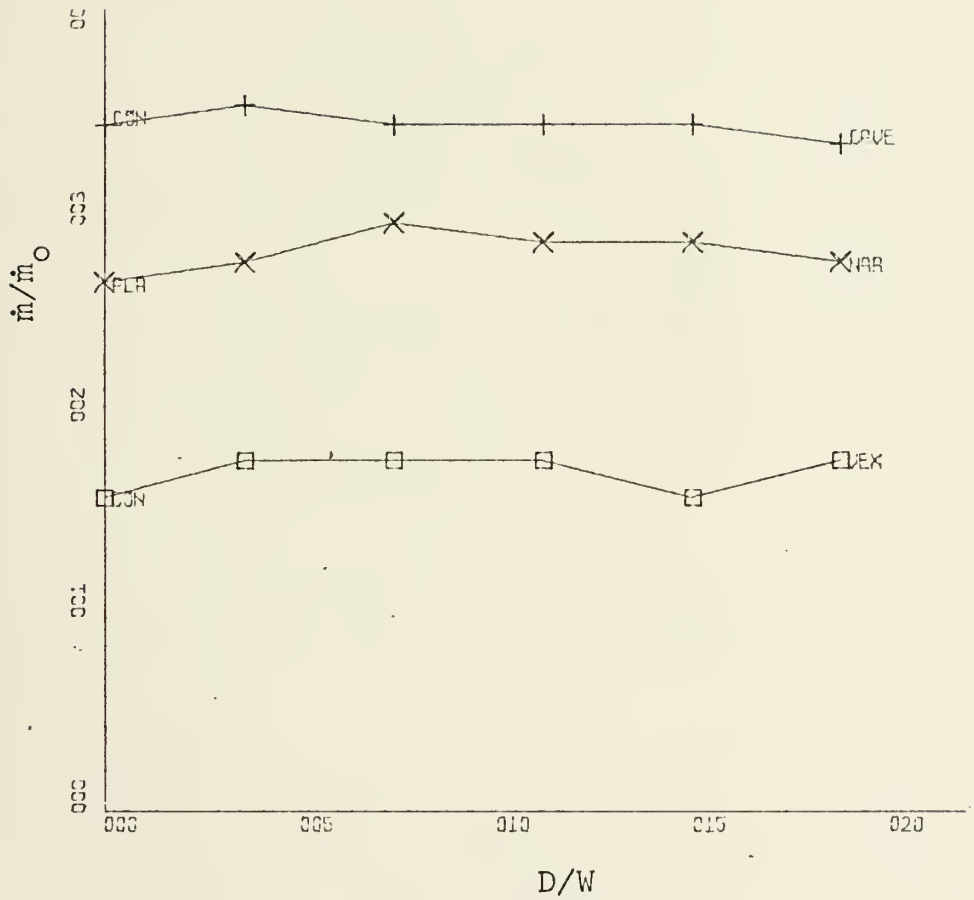

Figure 78. Flow Rate vs. Offset Distance for Planar, Concave, and Convex Walls, at 0 Degrees Deflection Angle, Jet Width of 1.31 Inches, Re = 1.475×10^5.

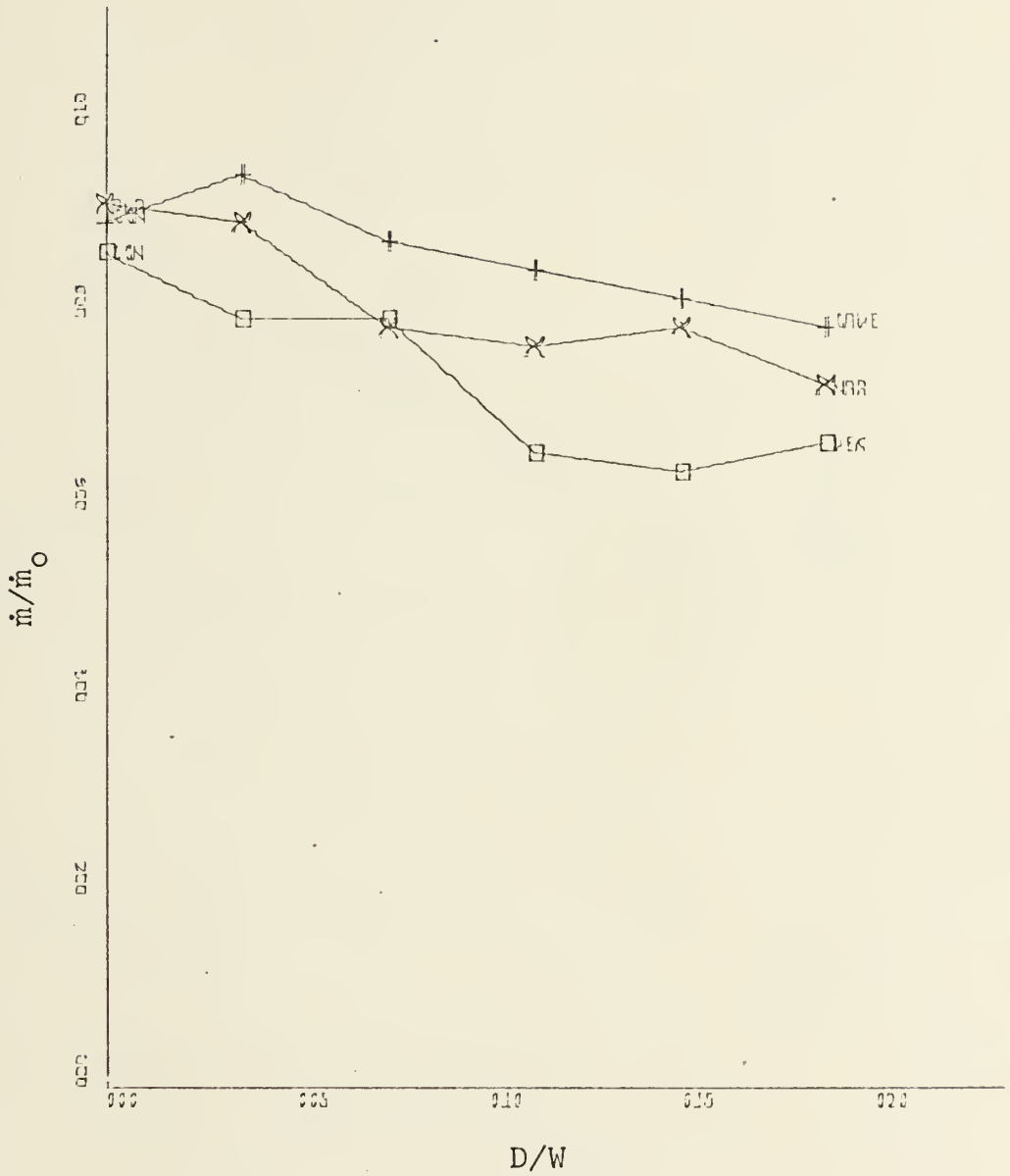

Figure 79. Flow Rate vs. Offset Distance for Planar, Concave, and Convex Walls at 15 Degrees Deflection Angle, Jet Width 1.31 Inches, Re = 1.475×10^5.

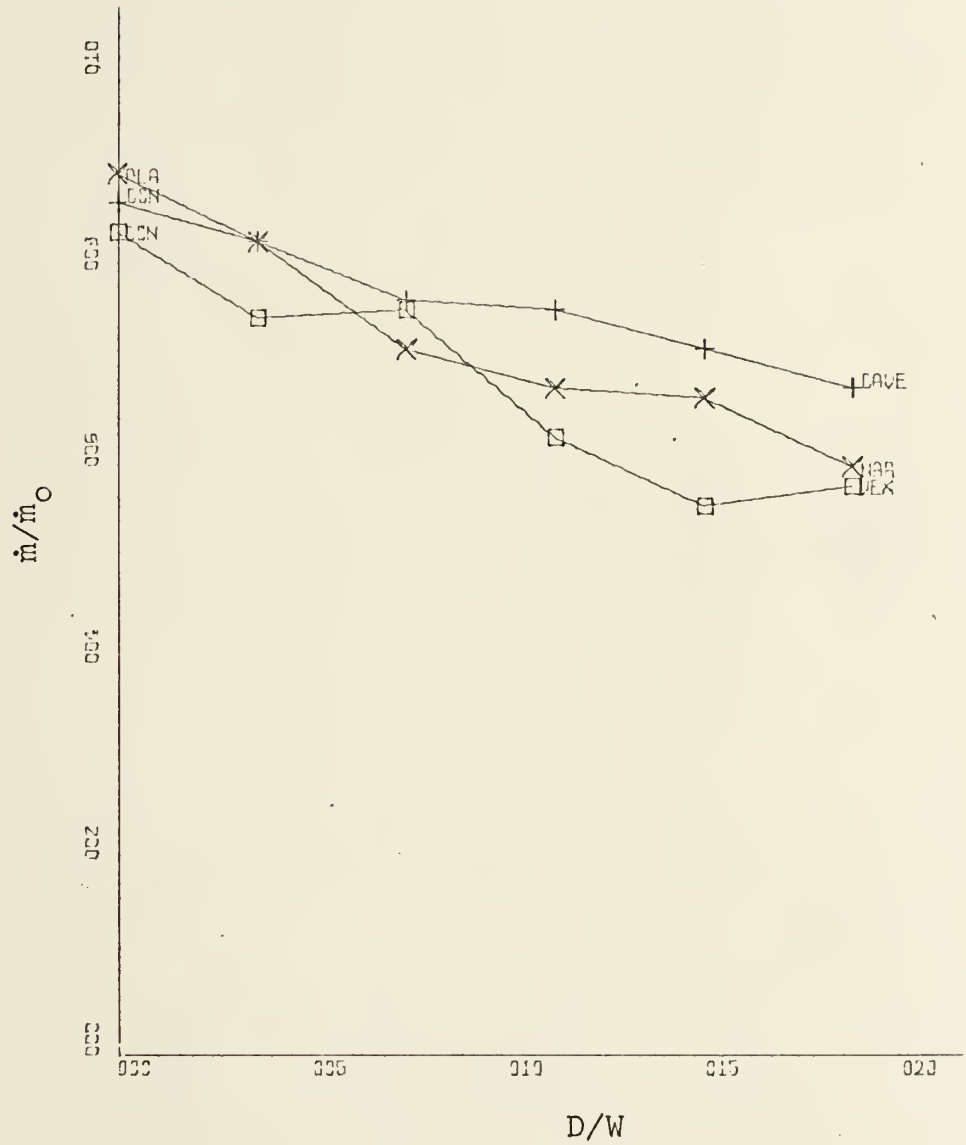

Figure 80. Flow Rate vs. Offset Distance for Planar, Concave, and Convex Walls at 20 Degrees Deflection Angle, Jet Width of 1.31 Inches, Re = 1.475×10^5.

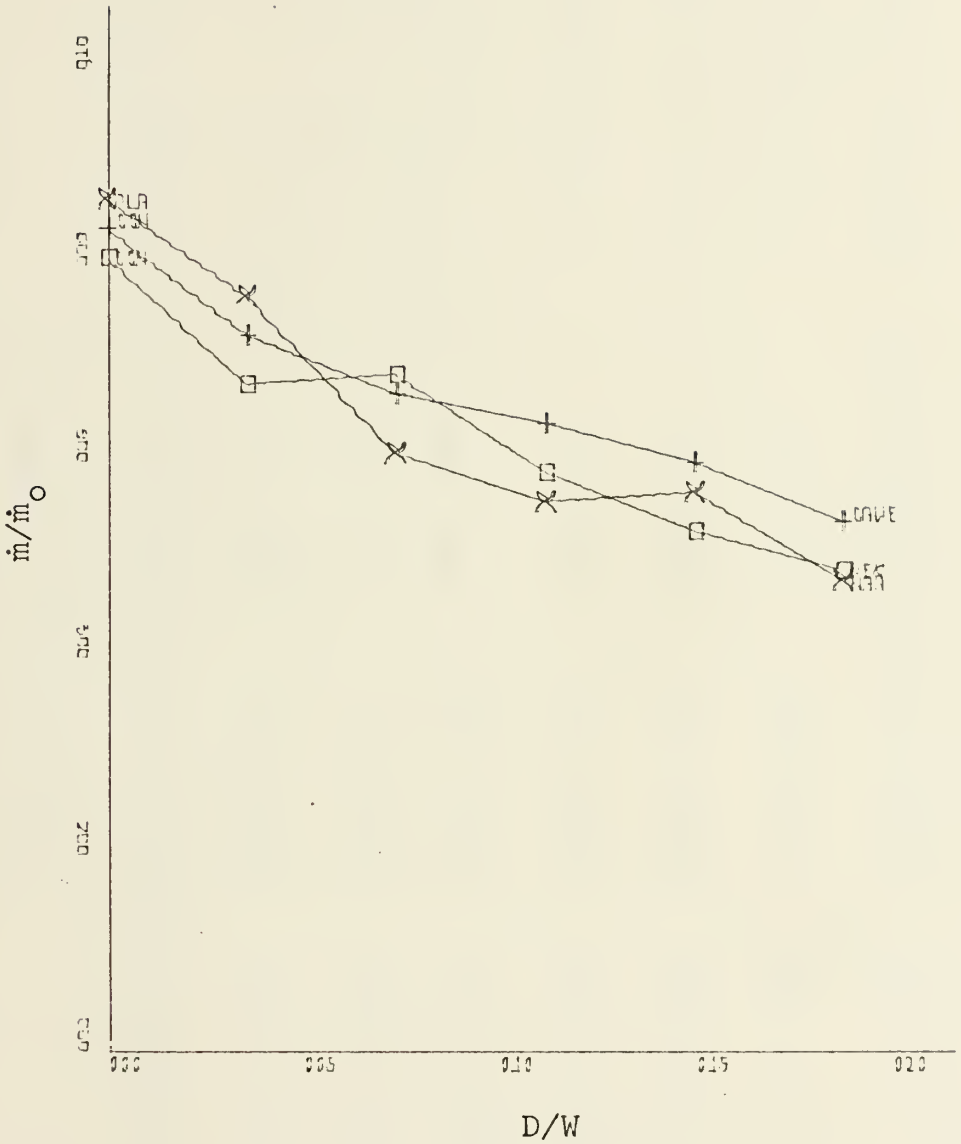

Figure 81. Flow Rate vs. Offset Distance for Planar, Concave, and Convex Walls at 25 Degrees Deflection Angle, Jet Width of 1.31 Inches, Re = 1.475×10^5.

OUTLINE OF DATA PRESENTATION V.

A. Surface Pressure Coefficient for Jet Width of 2.62 in., $N_{Re} = 2.05 \times 10^5$.

1.	a.	C_{p_s} vs. X_s/W	planar wall	D/W = 00=0.0, 03=.56, 05=.94	α = 15 deg.	Fig. 82
	b.	C_{p_s} vs. X_s/W	convex wall	D/W = 00=0.0, 02=.36, 03=.56	α = 28 deg.	Fig. 83
	c.	C_{p_s} vs. X_s/W	concave wall	D/W = 00=0.0, 02=.36, 04=.74	α = 25 deg.	Fig. 84
2.	a.	C_{p_s} vs. X_s/W	planar wall	D/W = 0.0	α = 26.5, 32, 38 deg.	Fig. 85
	b.	C_{p_s} vs. X_s/W	convex wall	D/W = 0.0	α = 15 , 32.5 deg.	Fig. 86
	c.	C_{p_s} vs. X_s/W	concave wall	D/W = 0.18	α = 25 , 40 deg.	Fig. 87
3.	a.	C_{p_s} vs. X_s/W	planar, convex, and concave walls	D/W = 0.0	α = 30 deg.	Fig. 88

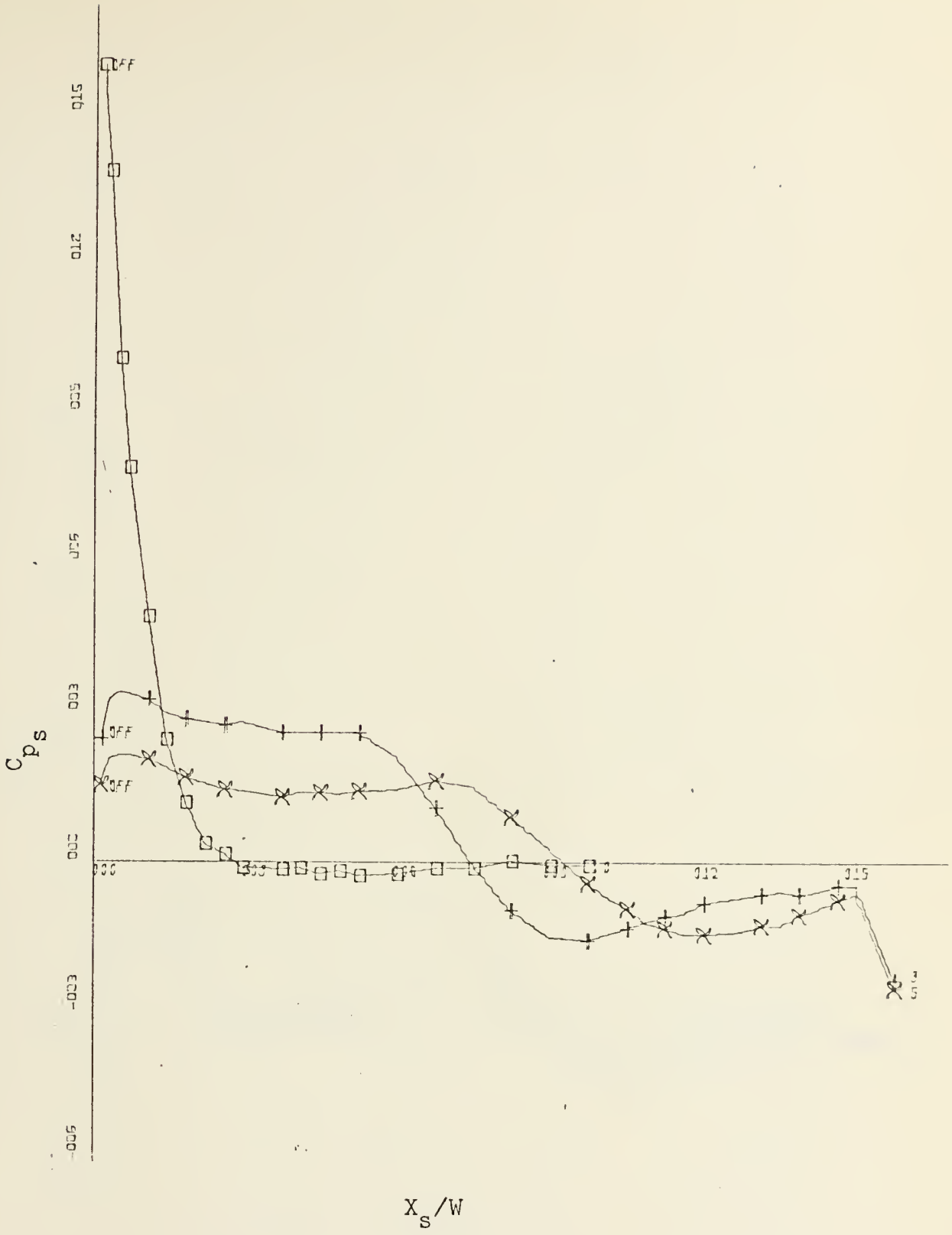

Figure 82. Surface Pressure Coefficient vs. Wall Position for Planar Wall at 15 Degrees Deflection Angle, for Various Offset Distances, Re = 2.05 x 10^5, Jet Width of 2.62 Inches.

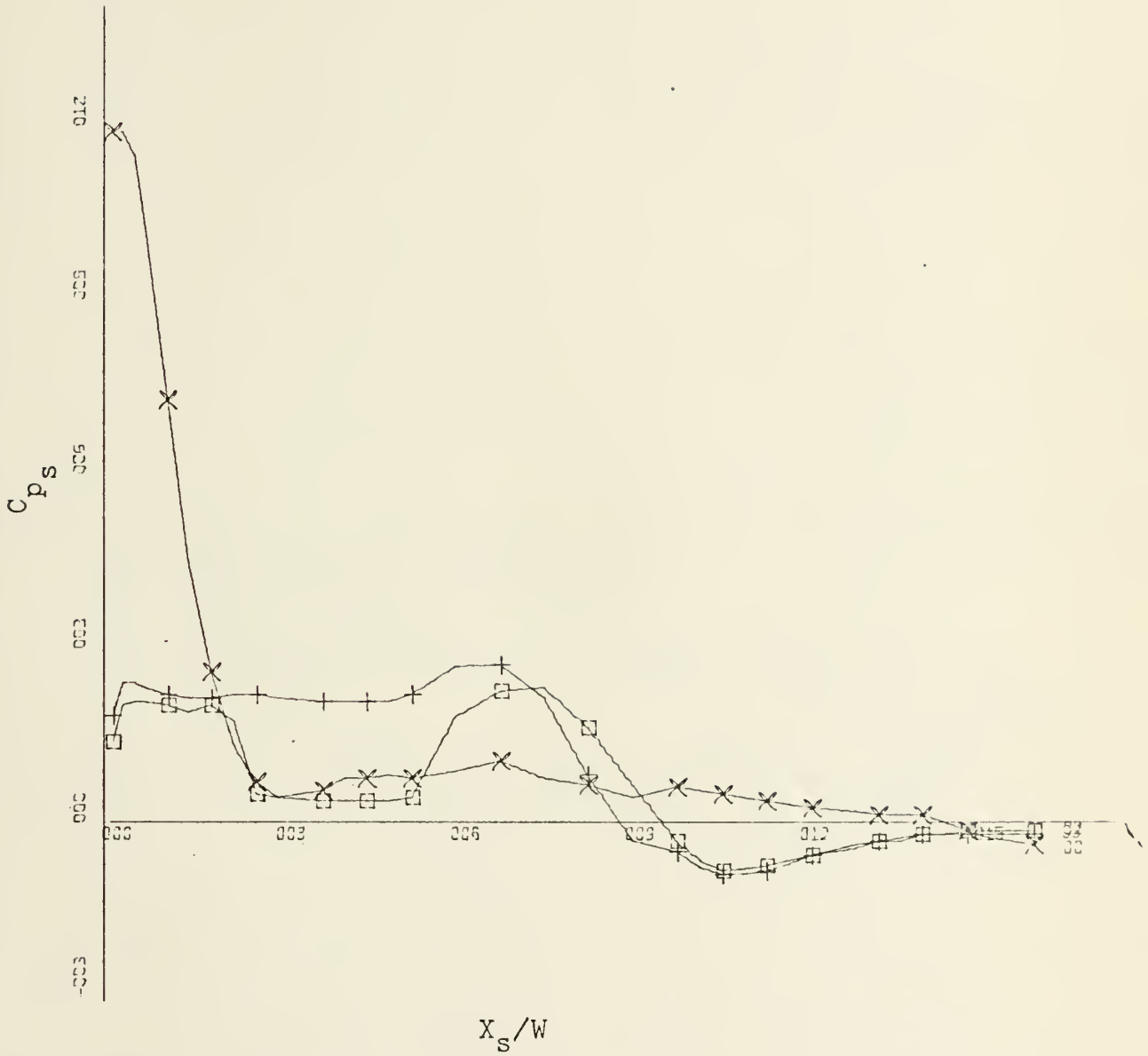

Figure 83. Surface Pressure Coefficient vs. Wall Position for Convex Wall at 28 Degrees Deflection Angle, for Various Offset Distances, Re = 2.05 x 10^5, Jet Width of 2.62 Inches.

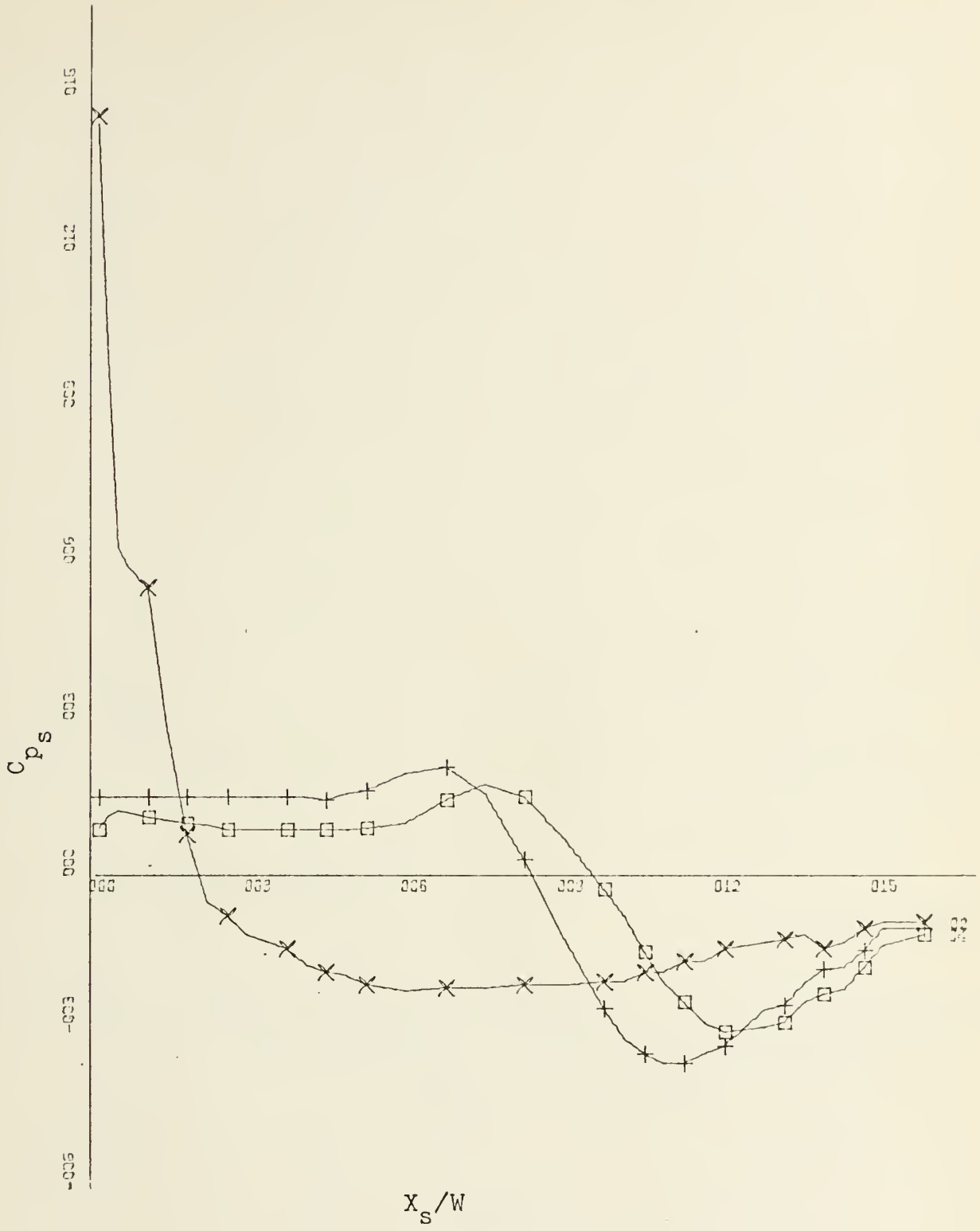

Figure 84. Surface Pressure Coefficient vs. Wall Position for Concave Wall at 25 Degrees Deflection Angle, for Various Offset Distances, Re = 2.05 x 10^5, Jet Width of 2.62 Inches.

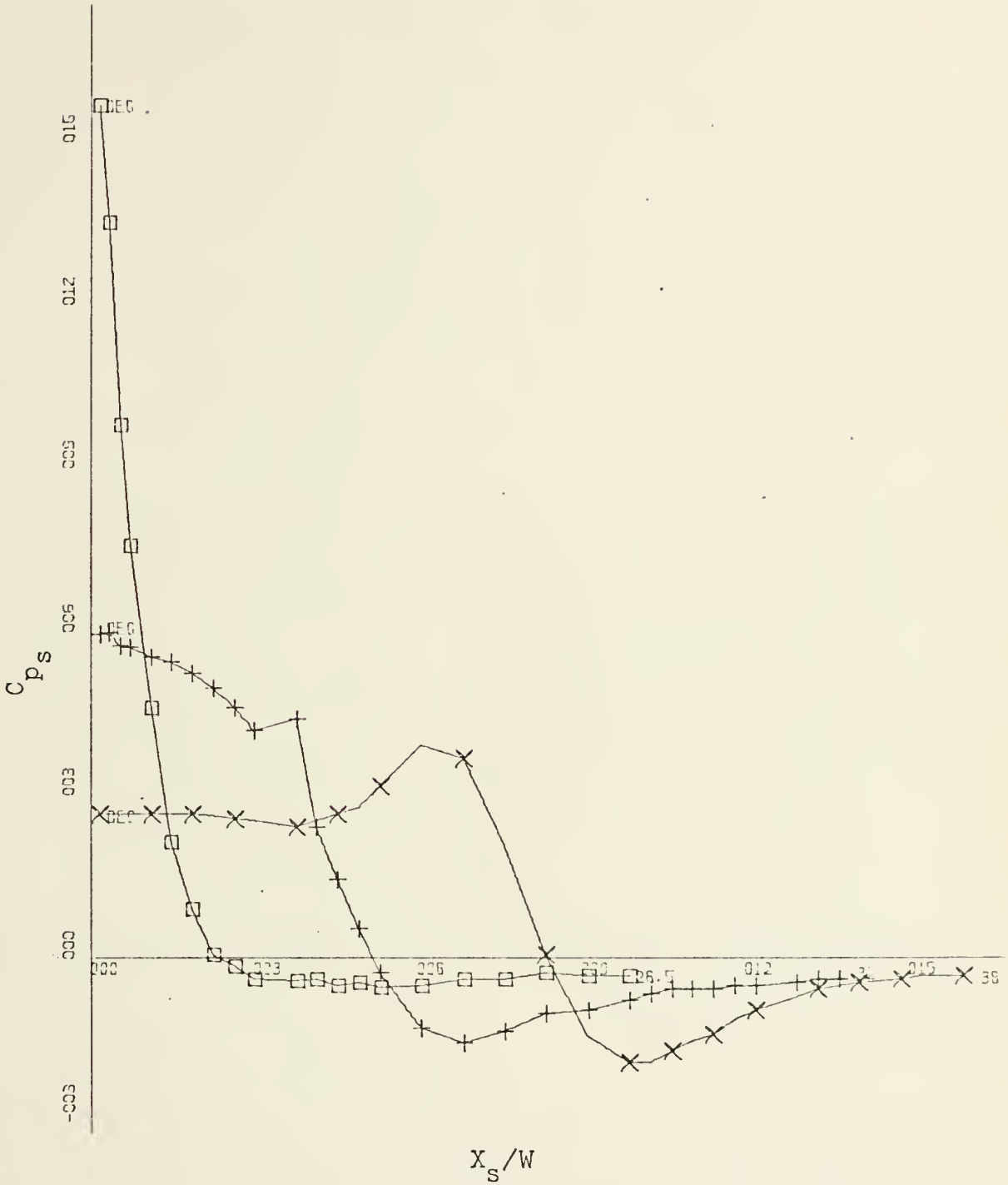

Figure 85. Surface Pressure Coefficient vs. Wall Position for Planar Wall at Various Deflection Angles and Offset Distance (D/W) of 0.0, Jet Width of 2.62 Inches, Re = 2.05 x 10^5, α = 26.5, 32, 38 Degrees.

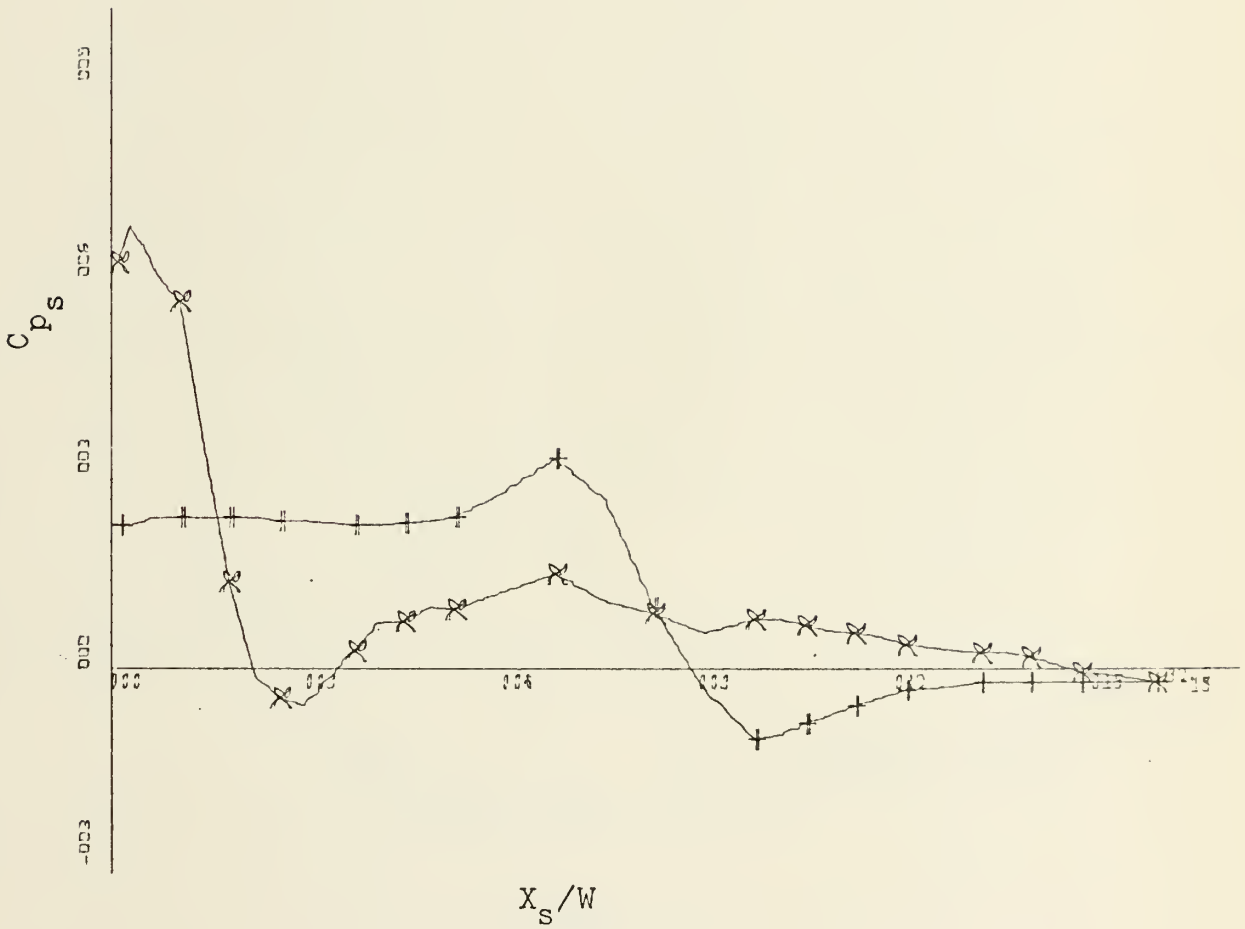

Figure 86. Surface Pressure Coefficient vs. Wall Position for Convex Wall at Various Deflection Angles and Offset Distance (D/W) of 0.0 , Jet Width of 2.62 Inches, Re = 2.05 x 10^5, α = 15, 32.5 degrees.

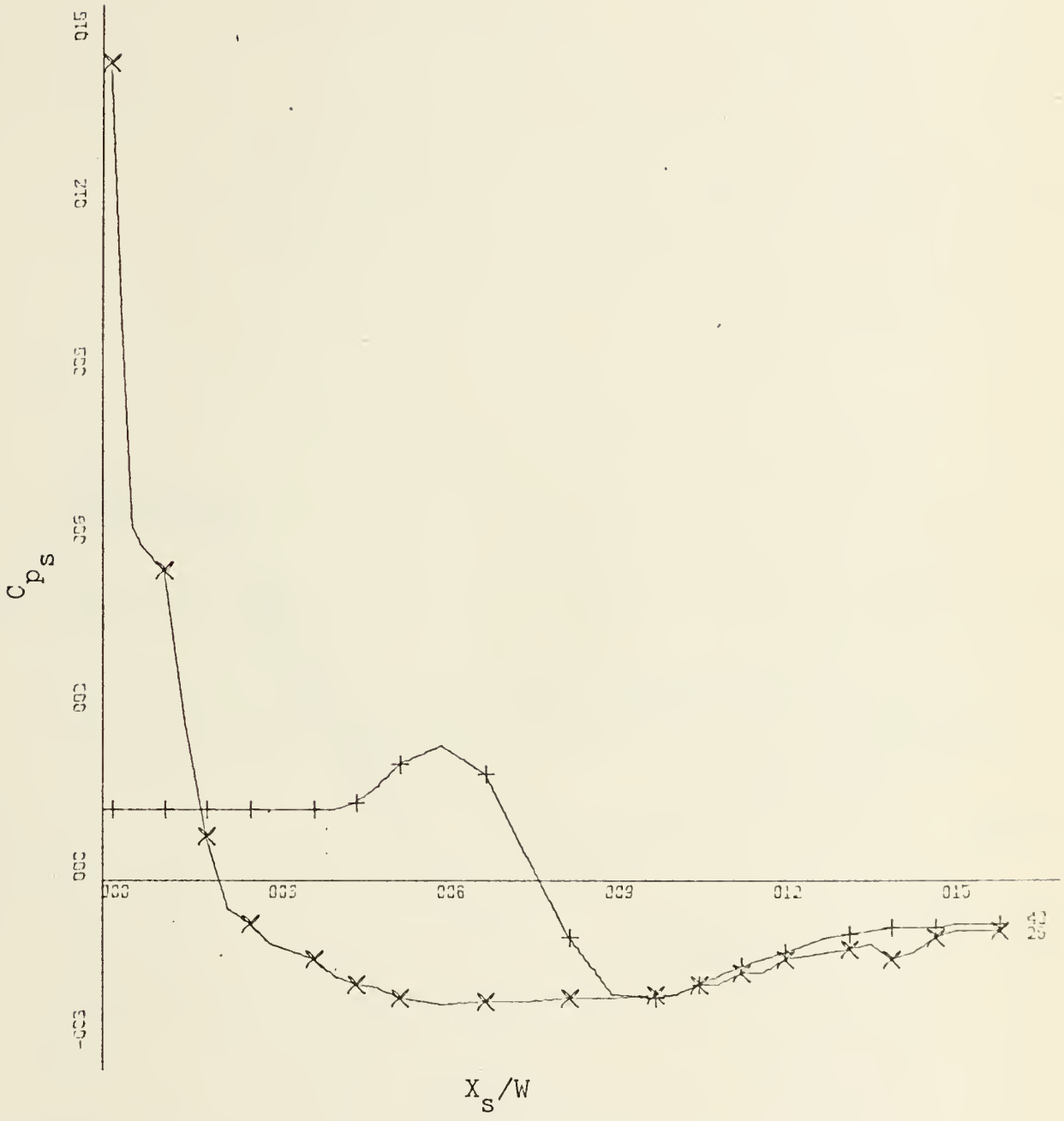

Figure 87. Surface Pressure Coefficient vs. Wall Position for Concave Wall at Various Deflection Angles and Offset Distance (D/W) of 0.18, Jet Width of 2.62 Inches, Re = 2.05×10^5, α = 25, 40 degrees.

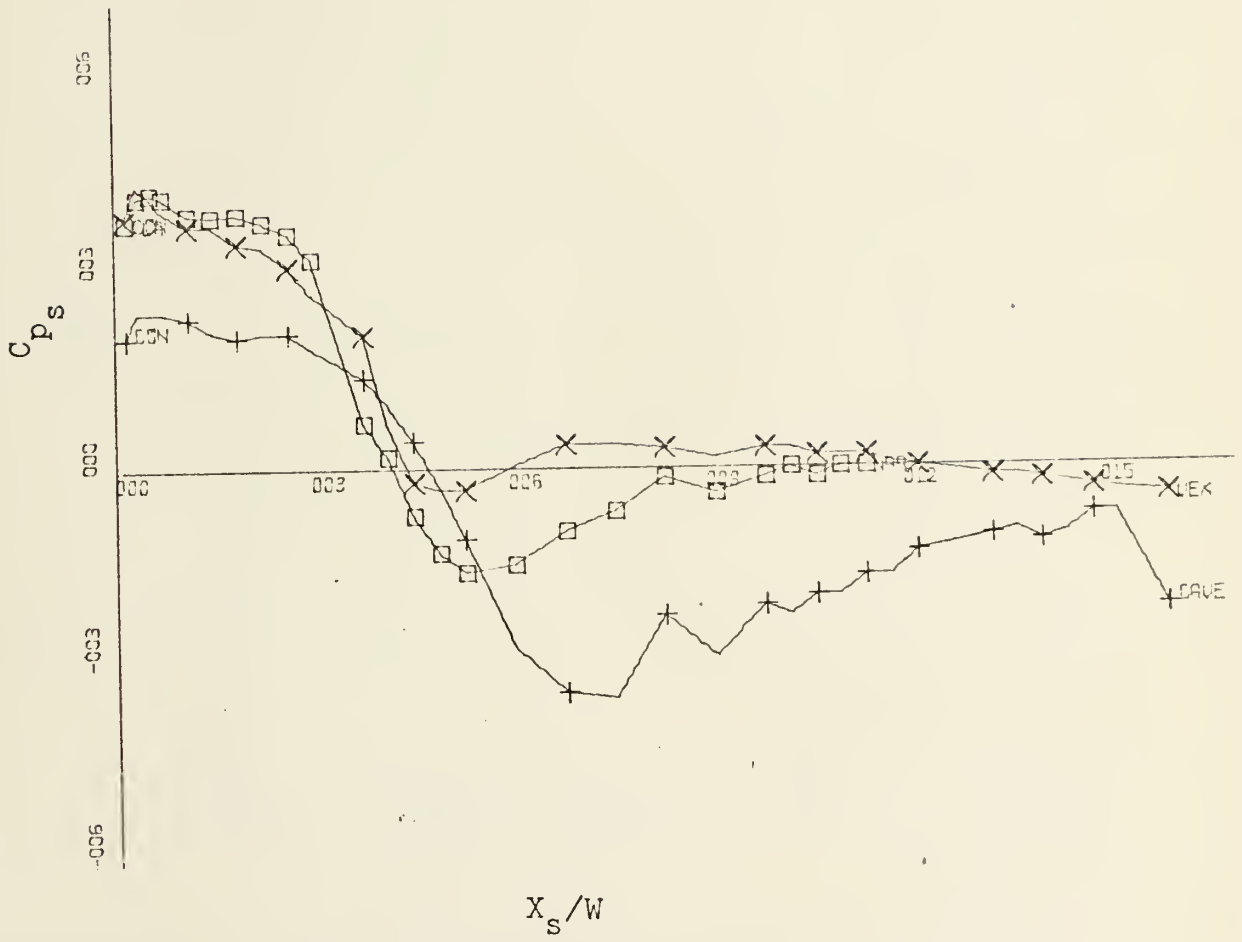

Figure 88. Surface Pressure Coefficient vs. Wall Position for Planar, Concave, and Convex Walls, for 30 Degrees Deflection Angle and Offset Distance (D/W) of 0.0, Jet Width of 2.62 Inches, Re = 2.05×10^5.

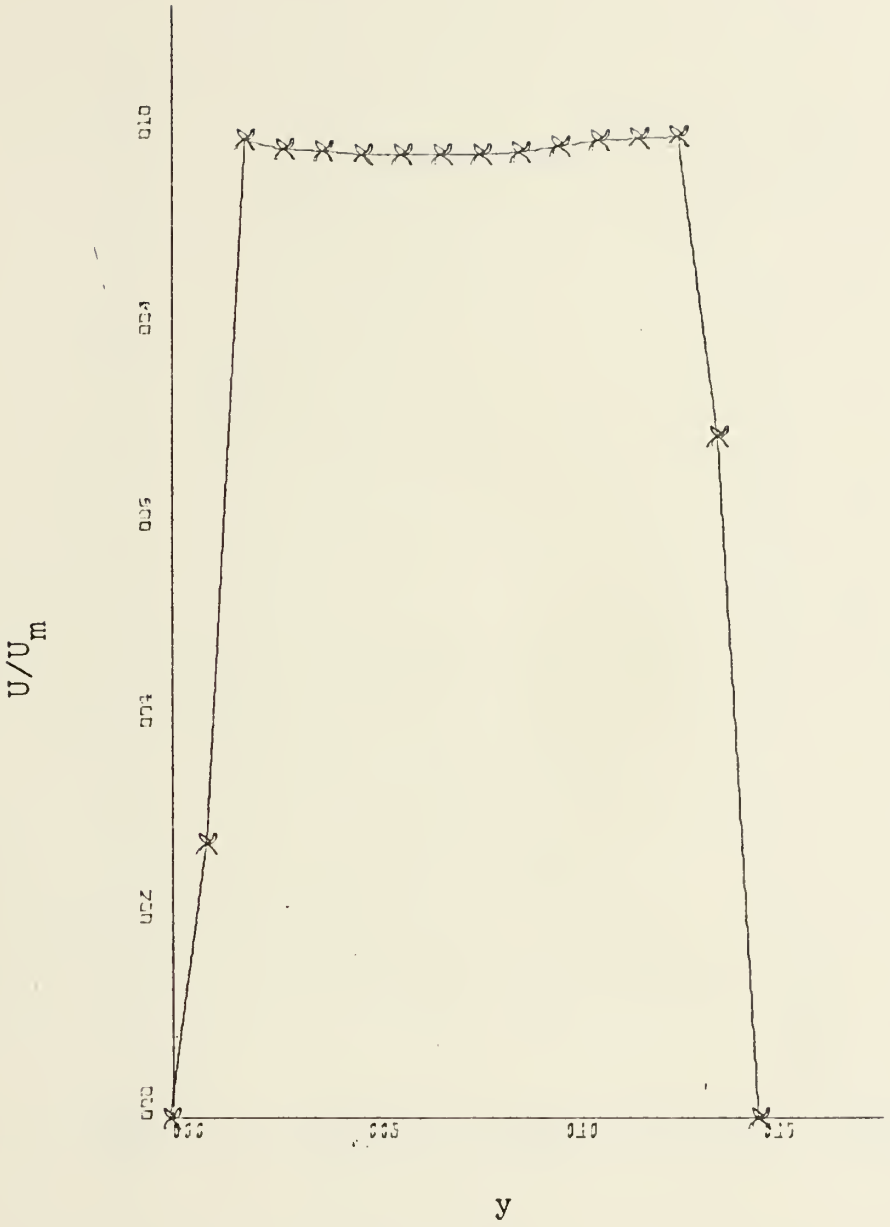

Figure 89. Velocity Profile at 0.5 Inches Downstream of Jet Exit for Jet Width of 1.31 Inches.

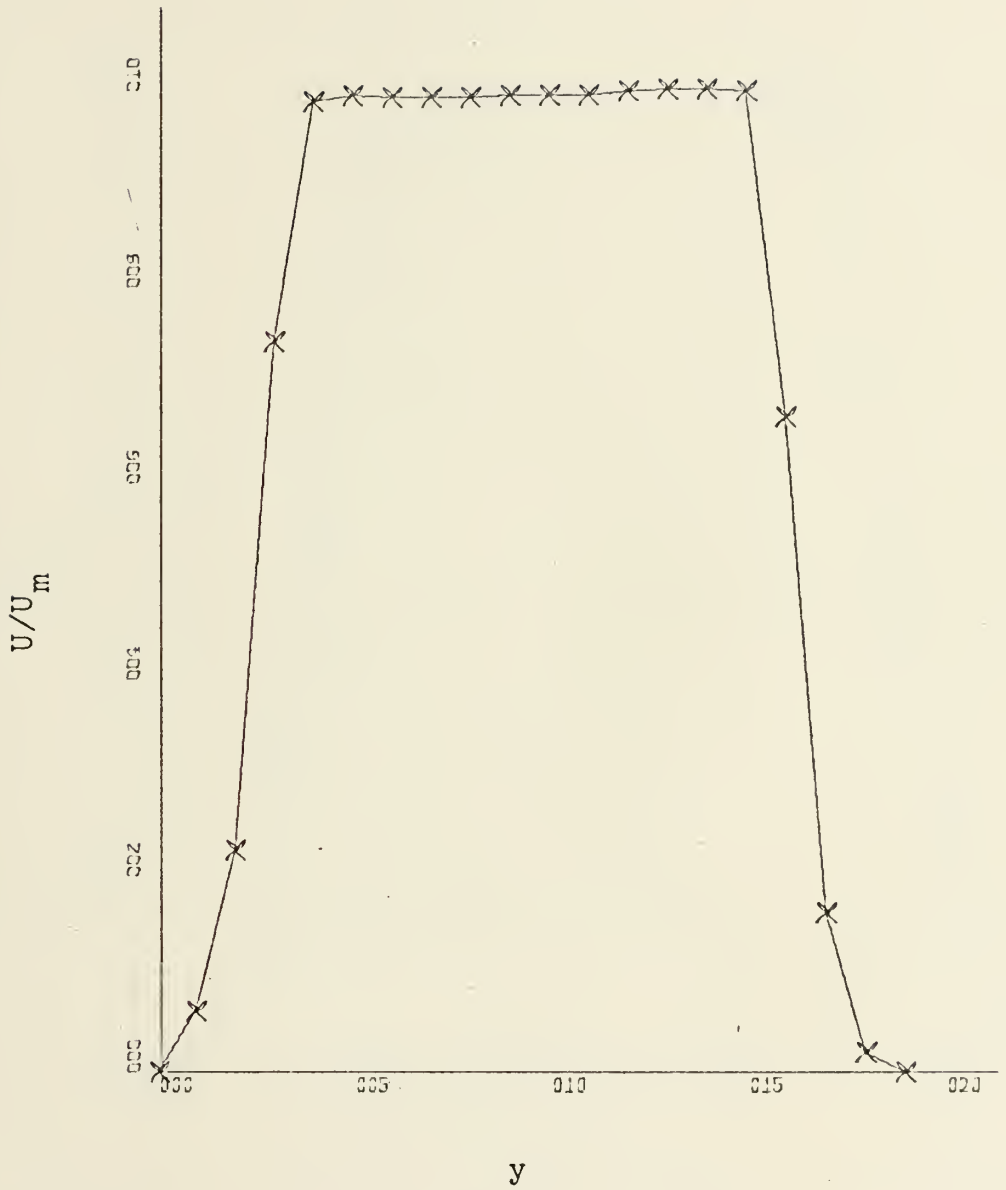

Figure 90. Velocity Profile at 1.31 Inches (1 Jet Width) Downstream of Jet Exit for Jet Width of 1.31 Inches.

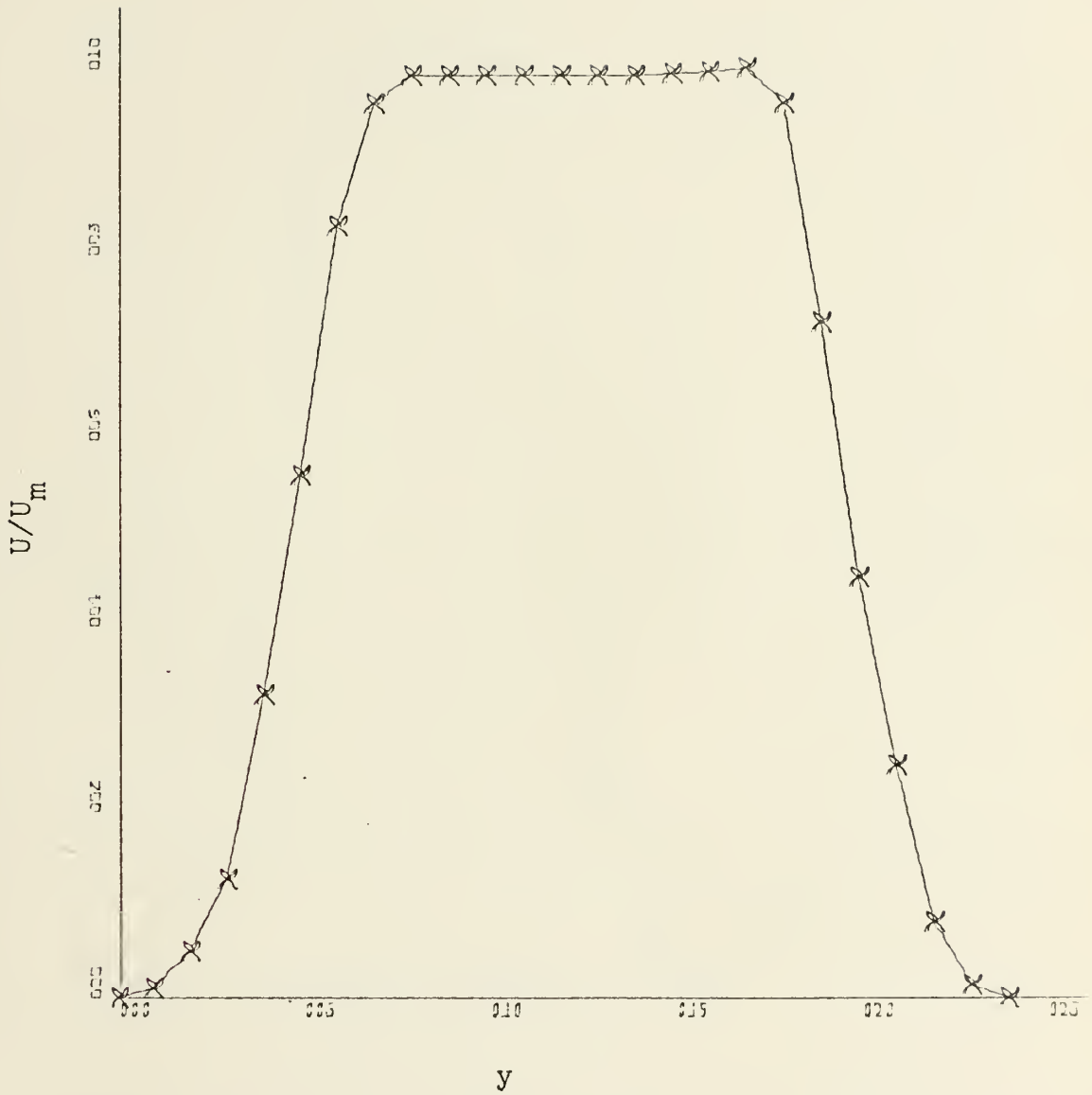

Figure 91. Velocity Profile at 2.62 Inches (2 Jet Widths) Downstream of Jet Exit for Jet Width of 1.31 Inches.

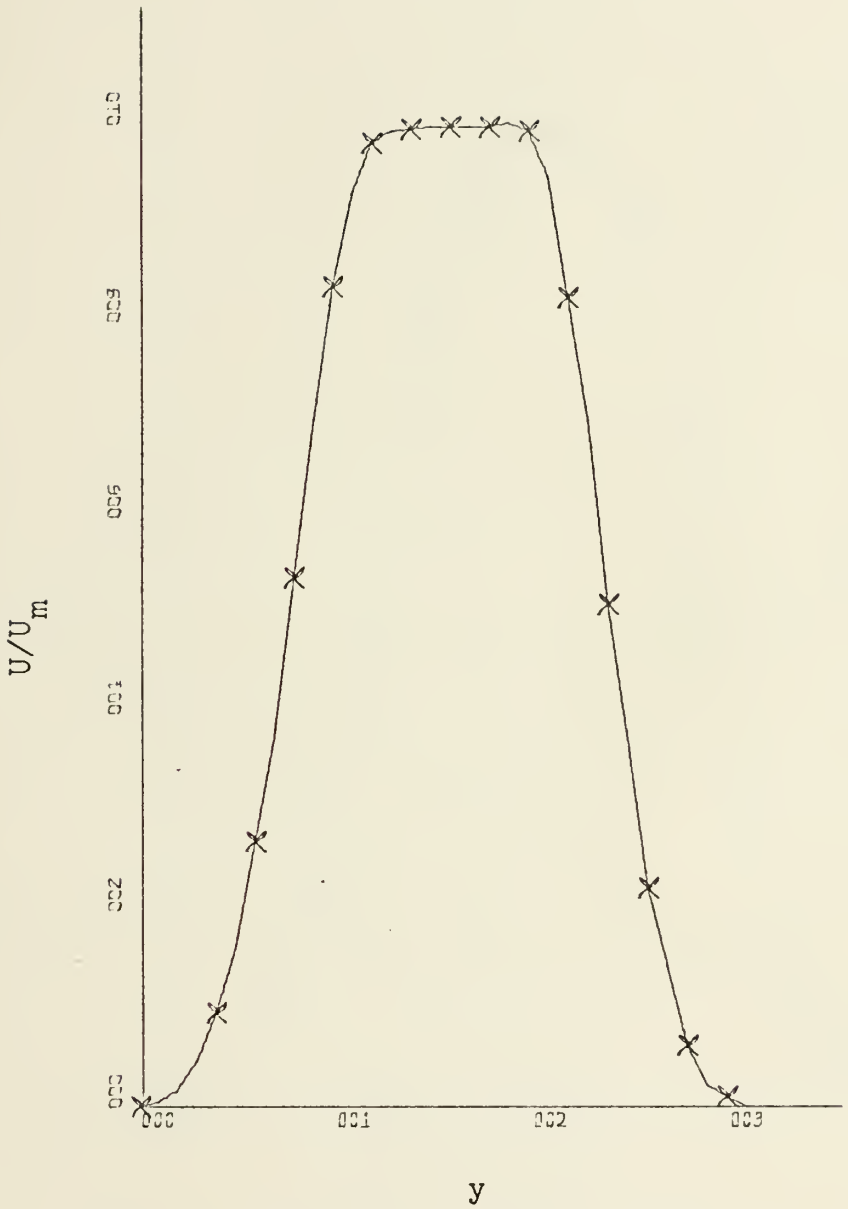

Figure 92. Velocity Profile at 5.24 Inches (4 Jet Widths) Downstream of Jet Exit for Jet Width of 1.31 Inches.

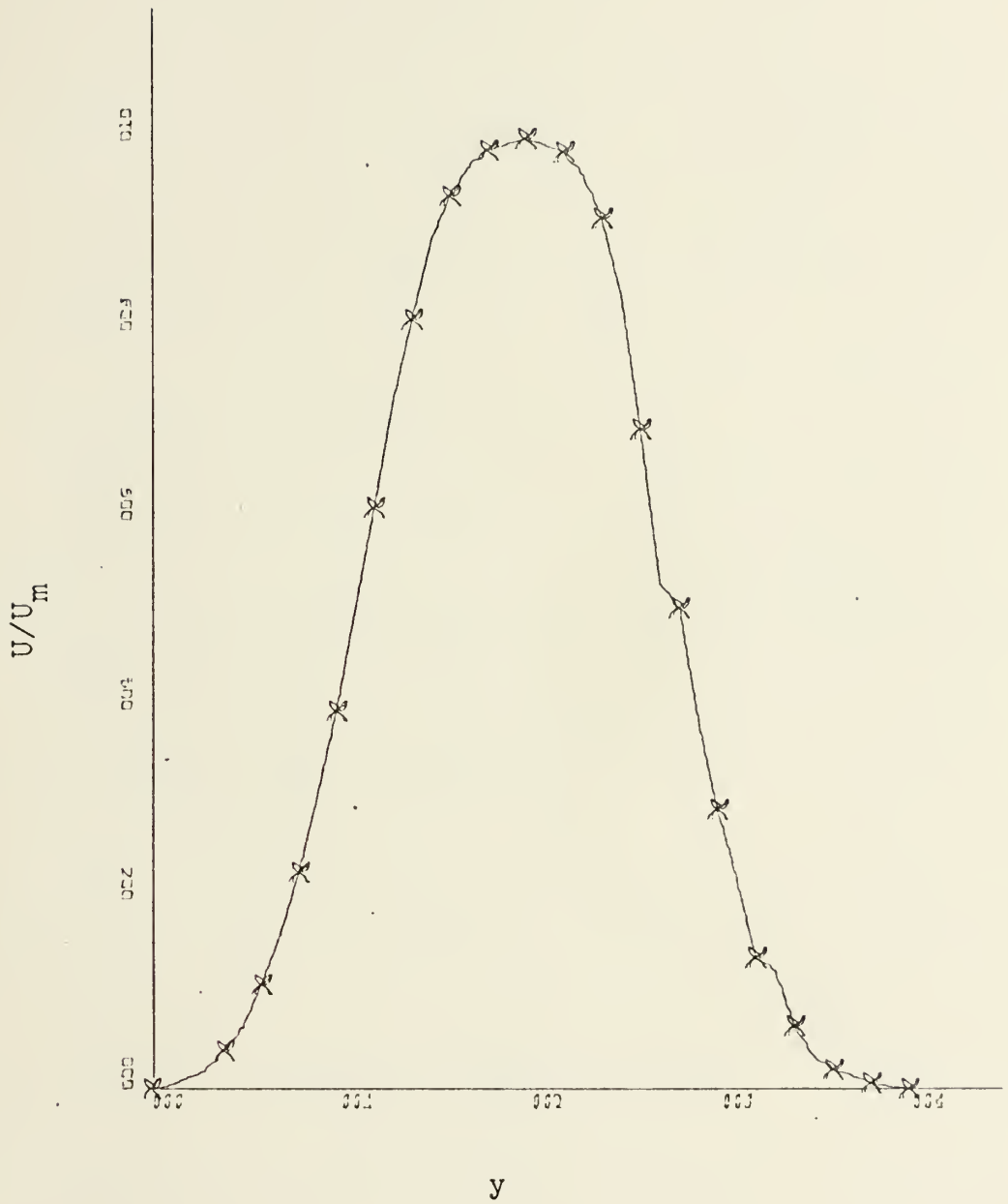

Figure 93. Velocity Profile at 7.86 Inches (6 Jet Widths) Downstream of Jet Exit for Jet Width of 1.31 Inches.

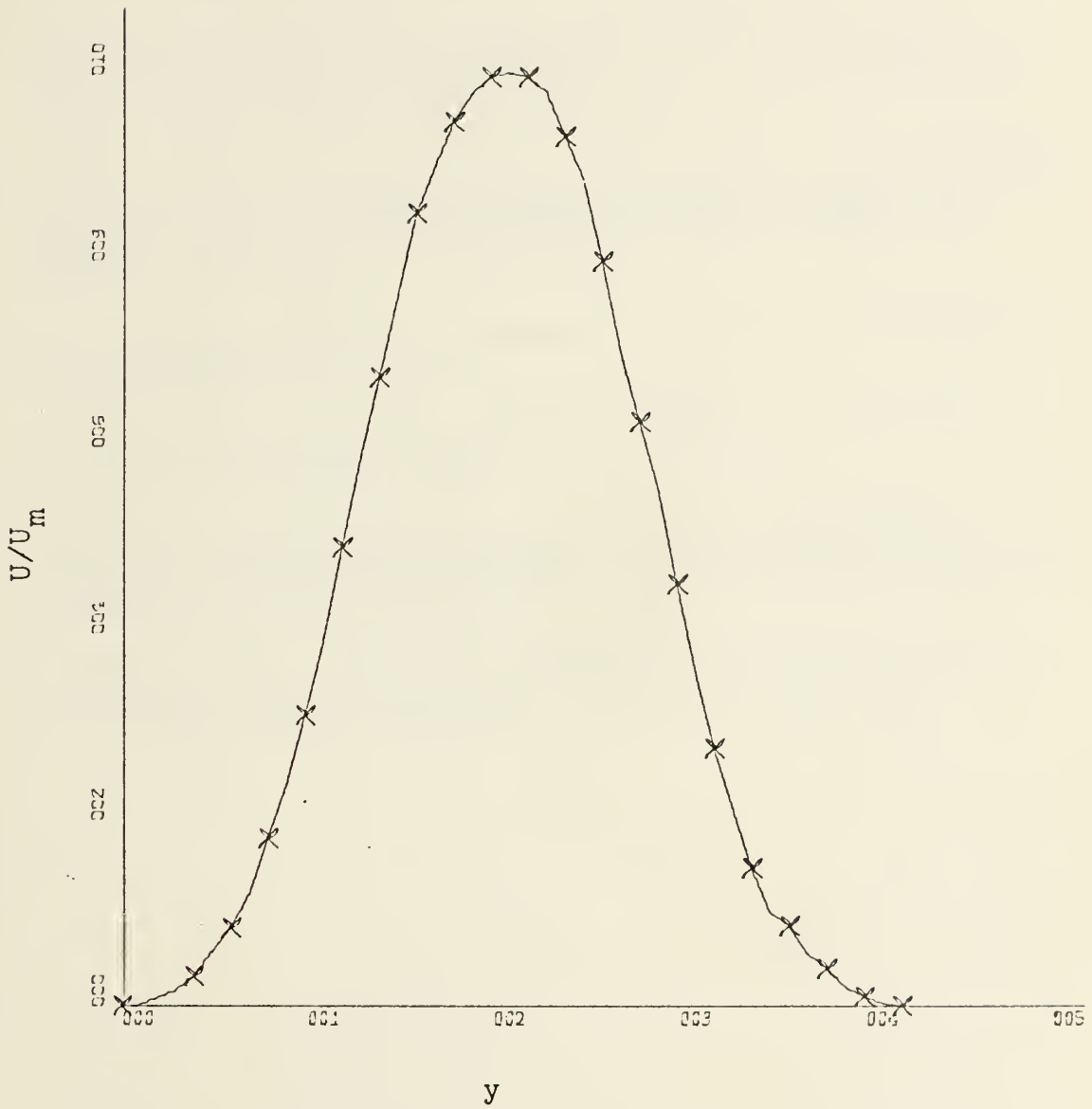

Figure 94. Velocity Profile at 9.58 Inches Downstream of Jet Exit for Jet Width of 1.31 Inches.

LIST OF REFERENCES

1. Newman, B.G., "Deflection of Plane Jets by Adjacent Boundaries - Coanda Effect," Boundary Layer and Flow Control, It's Principles and Applications, p. 232-264, Pergamon Press, 1961.

2. Borque, C., and Newman, B.G., "Reattachment of a Two-Dimensional, Incompressible Jet to an Adjacent Flat Plate, Aeronautical Quarterly, v. 11, p. 201-232, August 1960.

3. Harry Diamond Laboratories, Report 1087, Jet Attachment Distance as a Function of Adjacent Wall Offset and Angle, Levin, S.G., and Manion, F.M., p. 5-31, 31 December 1962.

4. The American Society of Mechanical Engineers, Advances in Fluidics, p.

5. Foster, K., and Parker, G.A., Fluidics, p. 131-145, Wiley Interscience, 1970.

6. Wille, R., and Fernholz, H., "Report on the First European Mechanics Colloquium on the Coanda Effect," Journal of Fluid Mechanics, v. 23, p. 801-819, 1965.

7. Sawyer, R.A., "Two-Dimensional Reattaching Jet Flows, Including the Effects of Curvature on Entrainment," Journal of Fluid Mechanics, v. 17, p. 481, 1963.

INITIAL DISTRIBUTION LIST

		No. Copies
1.	Defense Documentation Center Cameron Station Alexandria, Virginia 22314	2
2.	Library, Code 0212 Naval Postgraduate School Monterey, California 93940	2
3.	Asst. Professor G.J. Hokenson Code 57 Hw (thesis advisor) Department of Aeronautics Naval Postgraduate School Monterey, California 93940	1
4.	Prof. R. W. Bell Department of Aeronautics Naval Postgraduate School Monterey, California 93940	1
5.	LT Leo James Michael Baird, USN (student) 115 Morau Circle Monterey, California 93940	1

Security Classification

DOCUMENT CONTROL DATA - R & D

(Security classification of title, body of abstract and indexing annotation must be entered when the overall report is classified)

1. ORIGINATING ACTIVITY (Corporate author)

Naval Postgraduate School
Monterey, California 93940

2a. REPORT SECURITY CLASSIFICATION

Unclassified

2b. GROUP

3. REPORT TITLE

The Coanda Effect with Jet Displacement Over Planar, Concave, and Convex Walls

4. DESCRIPTIVE NOTES (Type of report and inclusive dates)

Engineer's Thesis; December 1973

5. AUTHOR(S) (First name, middle initial, last name)

Leo James Michael Baird

6. REPORT DATE	7a. TOTAL NO. OF PAGES	7b. NO. OF REFS
December 1973	161	7

8a. CONTRACT OR GRANT NO.	9a. ORIGINATOR'S REPORT NUMBER(S)
b. PROJECT NO.	
c.	9b. OTHER REPORT NO(S) (Any other numbers that may be assigned this report)
d.	

10. DISTRIBUTION STATEMENT

Approved for public release; distribution unlimited.

11. SUPPLEMENTARY NOTES	12. SPONSORING MILITARY ACTIVITY
	Naval Postgraduate School Monterey, California 93940

13. ABSTRACT

Bourque and Newman presented an extensive paper analyzing the separate effects of deflection angle and offset distance on the reattachment of flow issuing from a two-dimensional incompressible turbulent jet to an adjacent inclined flat plate. Levin and Manion combined the effects of offset distance and vertical wall incidence and derived a set of parametric equations to solve for the attachment distance at a given offset distance and deflection angle. Subsequently Perry extended the control volume model to account for inaccuracies in defining a base pressure. As part of a general investigation of the Coanda effect, the work of Levin and Manion has been expanded herein to encompass concave and convex surfaces of arbitrary planform. Two methods are outlined for determining the attachment distance for these additional planforms. On the concave wall, agreement averaged within 20% of the experimental data for the range of spread parameters used, and agreement between the two methods as outlined for this surface averaged within 12%. The two methods agree within 10% on the convex wall, and agree within 15% and 12% respectively with the convex wall experimental data, in the range of values of spread parameter used. The planar wall data agree within an average of 12% of theoretical solutions.

The hysteresis of flow attachment is viewed with particular attention focused on the intermediate region in which the flow divides and one portion attaches to the wall, while the remaining portion acts as if issuing from a free jet.

DD FORM 1 NOV 68 1473 (PAGE 1)

S/N 0101-807-6811

Security Classification

A-31408

KEY WORDS	LINK A		LINK B		LINK C	
	ROLE	WT	ROLE	WT	ROLE	WT
Fluidics						
Jet Attachment						
Coanda Effect						

Thesis
B1495 Baird
c.1

143436

The Coanda effect with jet displacement over planar, concave, and convex walls.

Thesis
B1495 Baird
c.1

143436

The Coanda effect with jet displacement over planar, concave, and convex walls.

thesB1495
The Coanda effect with jet displacement
3 2768 001 91187 8
DUDLEY KNOX LIBRARY